Charged-particle distributions in $\sqrt{s}$=13 TeV pp-interactions measured for p_T>0.5 GeV and |η|<2.5 with ATLAS detector at the LHC

ATLAS-CONF-2015-028
ATLAS-COM-CONF-2015-046
ATLAS-COM-2015-313

Yuri Kulchitsky[1,2], Elena Plotnikova[1], Pavel Tsiareshka[1,2]
[1]JINR, Dubna, Russia
[2]Institute of Physics, National Academy of Sciences, Minsk, Belarus

Russian ATLAS workshop, 22-23 September, Dubna

The ATLAS Detector

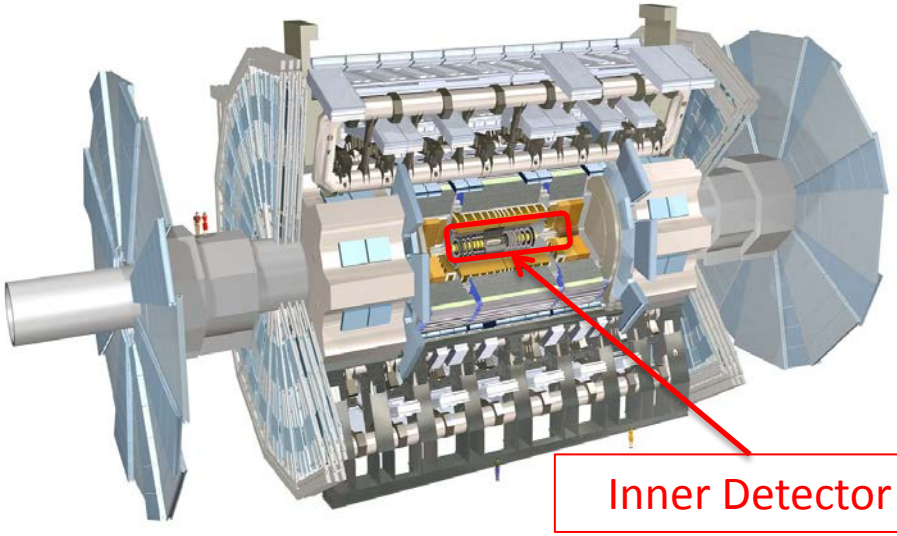

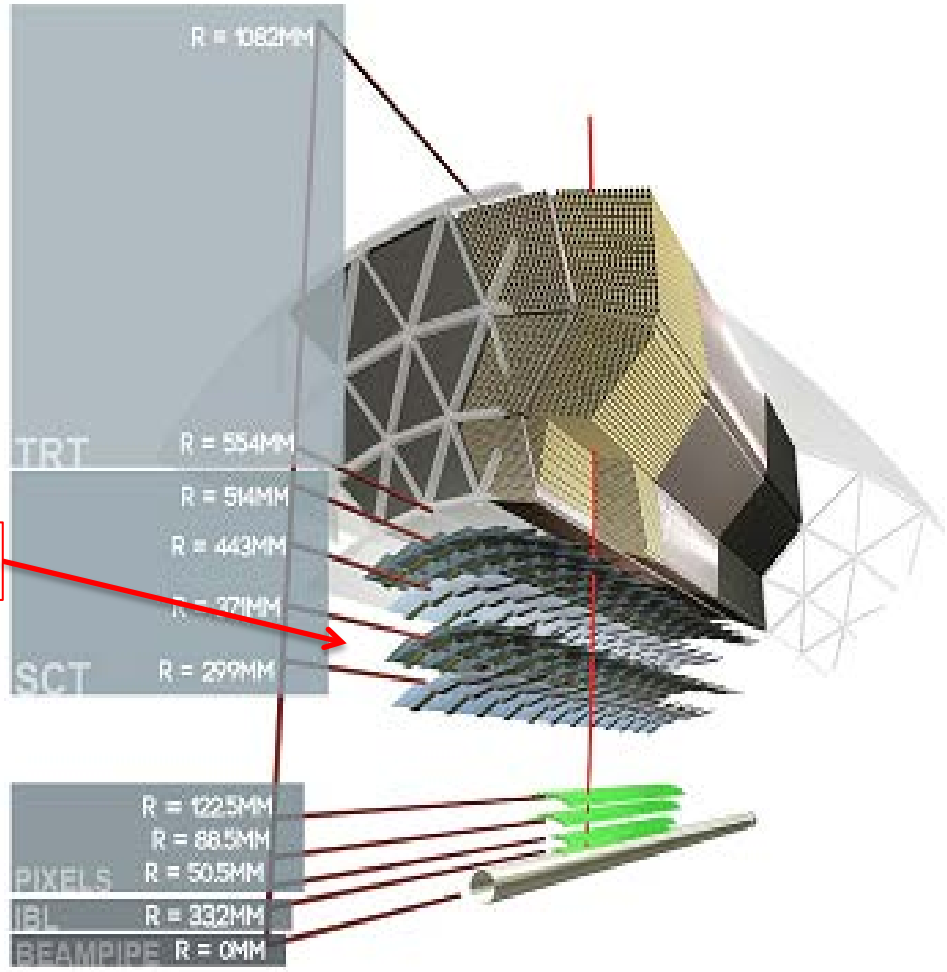

Inner Detector

$$\frac{\sigma(p_T)}{p_T} = 0.05\% \cdot p_T[\mathrm{GeV}] \oplus 1\%$$

$$\sigma(d_0) = 24[\mu m] \oplus \frac{50[\mu m GeV]}{p_T[\mathrm{GeV}]\sqrt{\sin\Theta}}$$

$$\sigma(z_0 \sin\vartheta) = 72.5[\mu m] \oplus \frac{71.5[\mu m GeV]}{p_T[\mathrm{GeV}]\sqrt{\sin\Theta}}$$

ATLAS Inner Detector (ID) main tracking device of ATLAS

- **consists of Pixel, Silicon strip (SCT) and drift tube (TRT) detectors**
- **single hit resolution between 10 μm (Pixel) and 130 μm (TRT)**

Minimum Bias events

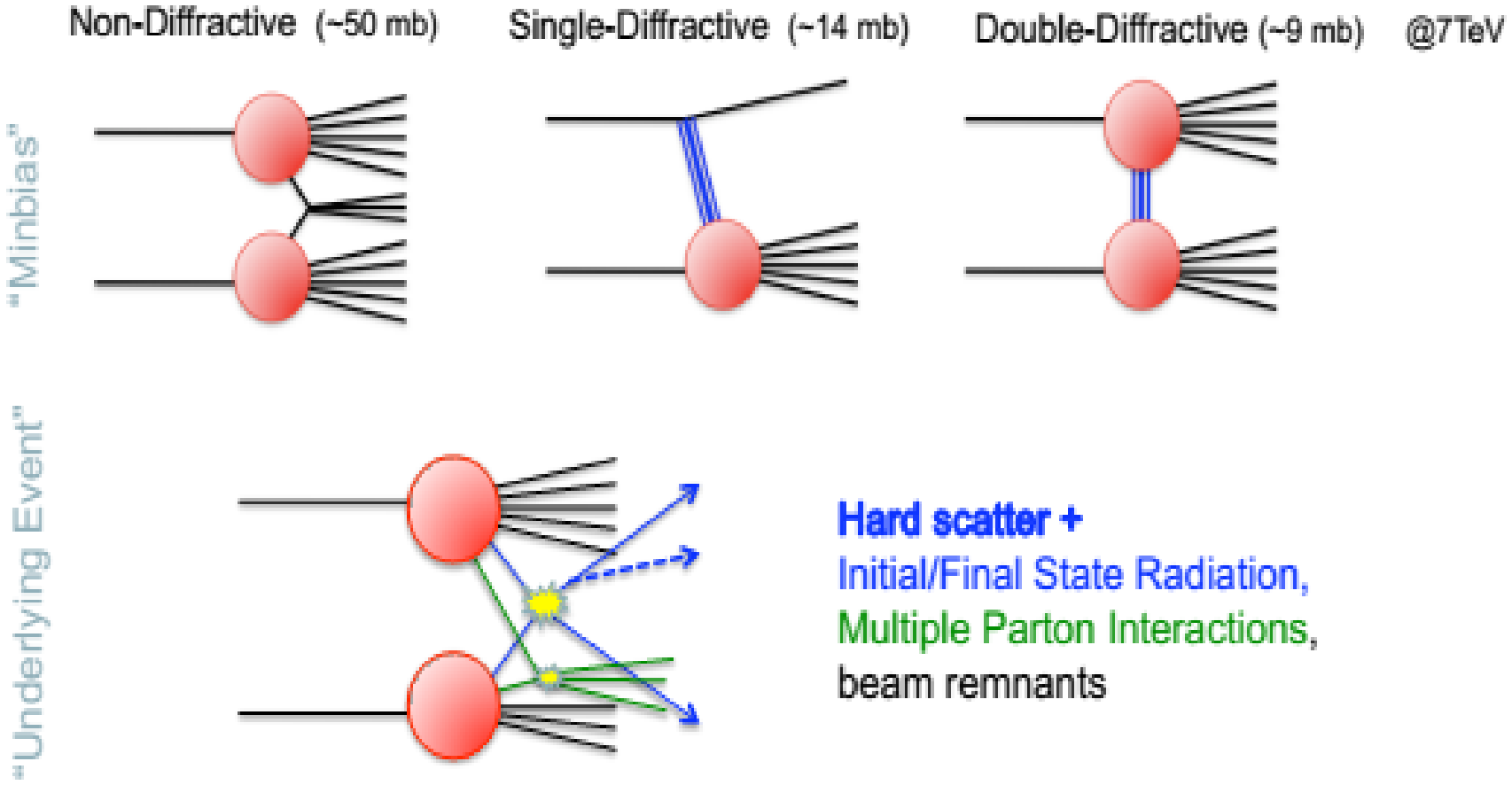

- Low energy QCD, requires MC models tuned to data
- A good MC description is essential for hadron collider physics!
- UE and pileup affect jets, E_T^{miss}, rapidity gaps, lepton ID, …

Charged particle distributions

Multiplicity versus η

$$\frac{1}{N_{ev}} \cdot \frac{dN_{ch}}{d\eta},$$

Multiplicity versus p_T

$$\frac{1}{N_{ev}} \cdot \frac{1}{2\pi p_T} \cdot \frac{d^2 N_{ch}}{d\eta dp_T},$$

Multiplicity distribution

$$\frac{1}{N_{ev}} \cdot \frac{dN_{ev}}{dn_{ch}}$$

and $\langle p_T \rangle$ versus n_{ch}

Also quote the value at $\eta=0$ and compare to measurements at lower $\sqrt{s}$

For primary charged particles with $p_T > 500$ MeV and $|\eta| < 2.5$ in events with $n_{ch} \geq 1$

Primary charged particles are defined as charged particles with a mean lifetime $\tau > 3 \times 10^{-10}$ s, either directly produced in pp interactions or from decays of directly produced particles with $\tau < 0.3 \times 10^{-10}$ s; particles produced from decays of particles with $\tau > 0.3 \times 10^{-10}$ s are denoted secondary particles and are excluded.[1]

[1]This definition differs from earlier analyses in that charged particles with a mean lifetime $0.3 \times 10^{-10} < \tau < 3 \times 10^{-10}$ s were previously included. These are charged strange baryons and have been removed due to the low efficiency of reconstructing them.

Analysis overview

- Select events
- Check for event backgrounds (negligible)
- Check for pileup effects (negligible)
- Check for split vertex effects (negligible: 0.02% of events from MC)
- Correct for tracks from non-primary particles:
  - Tracks from secondary particles
  - Tracks from strange baryons
  - Check for contribution from fake tracks (negligible: 0.1% from MC)
- Correct for detector inefficiencies and unfold distributions
  - Trigger and vertex inefficiencies (data driven)
  - Track reconstruction inefficiency (MC driven, checks with data for systematics)
  - Unfold distributions
- Compare particle-level results with MC predictions

Event Selection

- Accepted on single-arm Minimum Bias Trigger Scintillator (MBTS)
- Primary vertex (2 tracks with $p_T > 100$ MeV)
- Veto on any additional vertices with ≥ 4 tracks
- At least one selected track:
  - $p_T > 500$ MeV and $|\eta| < 2.5$ (note track reconstruction run with 100 MeV)
  - At least 1 pixel hit and at least 6 SCT hits
  - IBL hit required if expected (if not expected, next to innermost hit required if expected)
  - $|d_0^{BL}| < 1.5$ mm (transverse impact parameter w.r.t. beam line)
  - $|\Delta z_0 \cdot \sin\theta| < 1.5$ mm (Δz_0 is difference between track z_0 and vertex z position)
  - Track fit χ^2 probability > 0.01 for tracks with $p_T > 10$ GeV

8,870,790 events with 106,353,390 selected tracks

Distributions of d_0 and Track Fractions for η-region

Run2: Track Fractions for d_0 distribution for $|\eta| \approx 2.5$

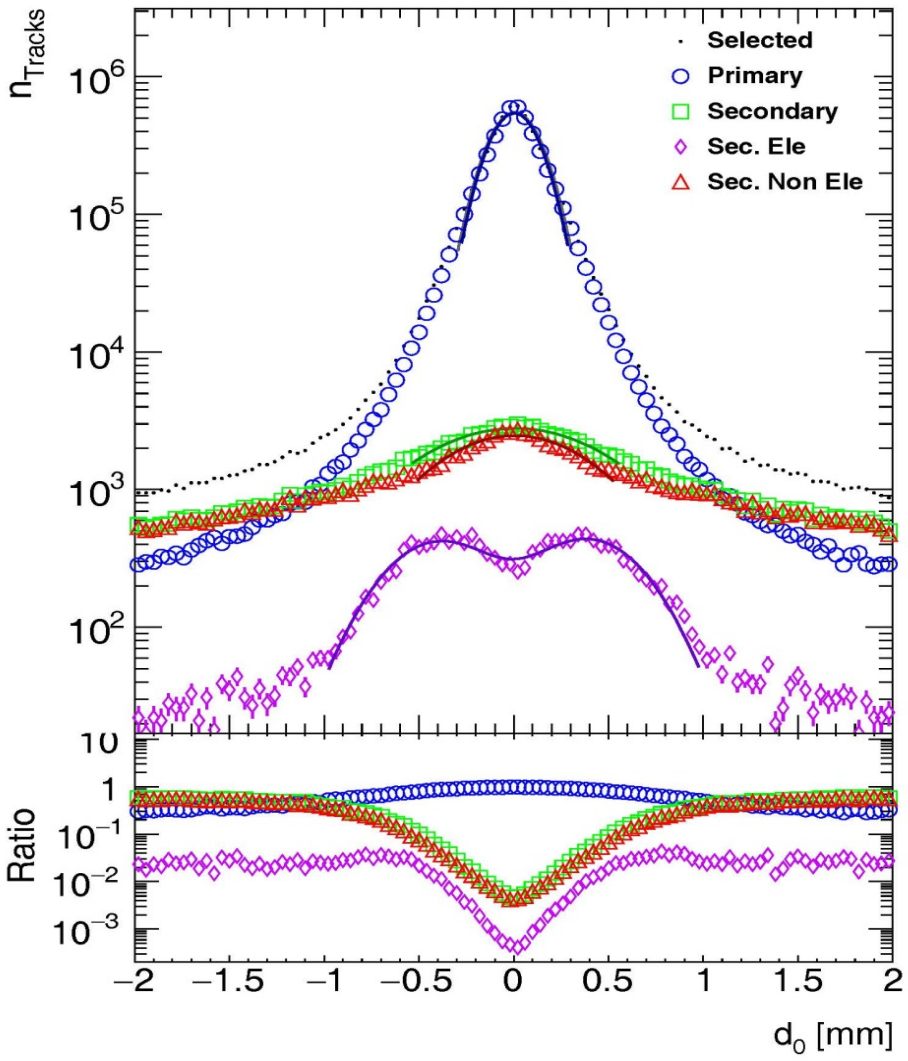

Run1: Track Fractions for d_0 distribution for $|\eta| \approx 2.5$

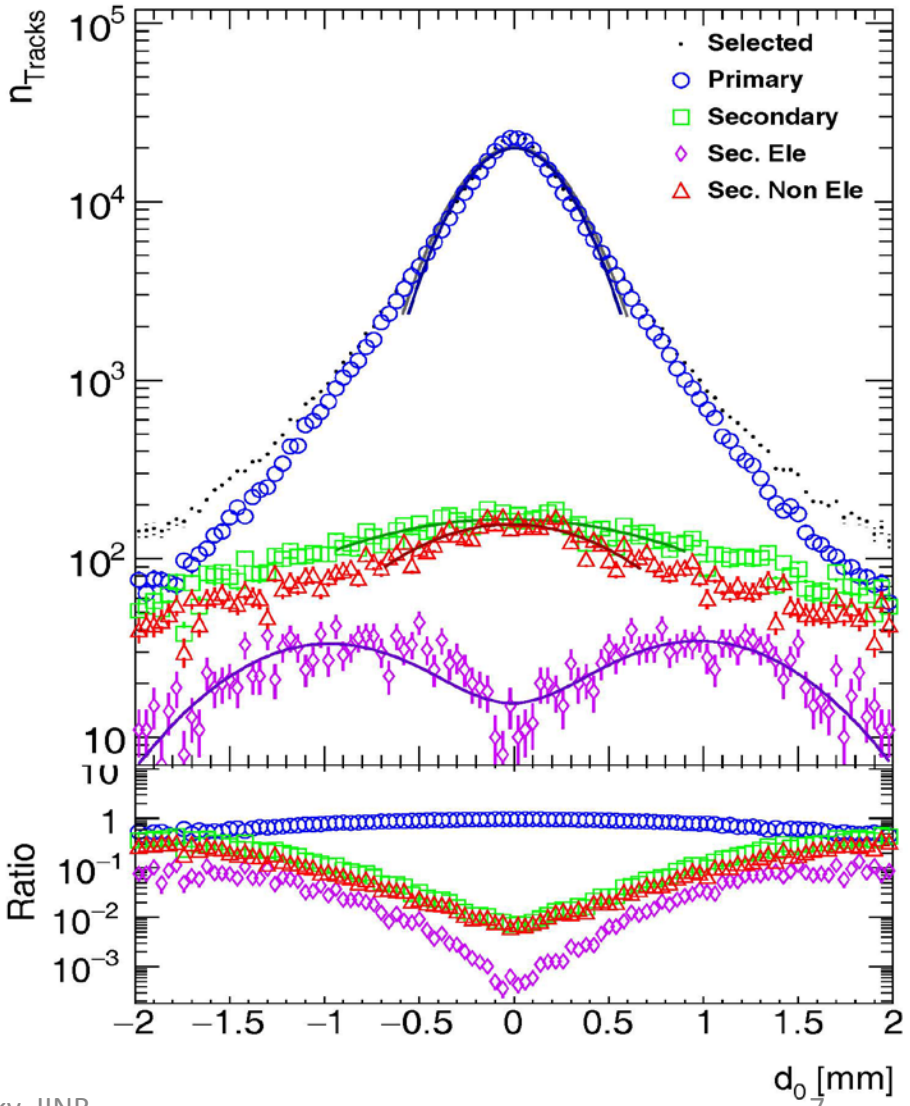

Fraction of Secondary tracks for $|d_0|<1.5$ mm and $|z_0 \sin\Theta|<1.5$ mm vs η

Run2: Secondary tracks Fractions vs η

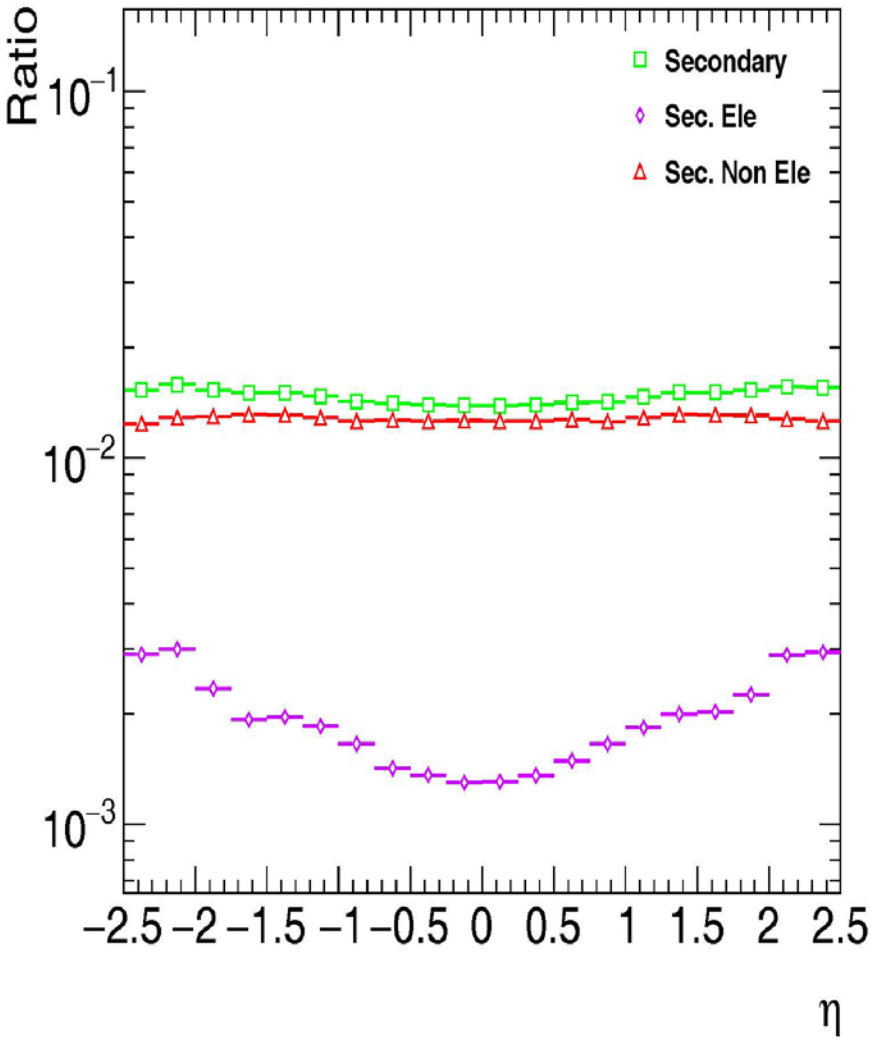

Run1: Secondary tracks Fractions vs η

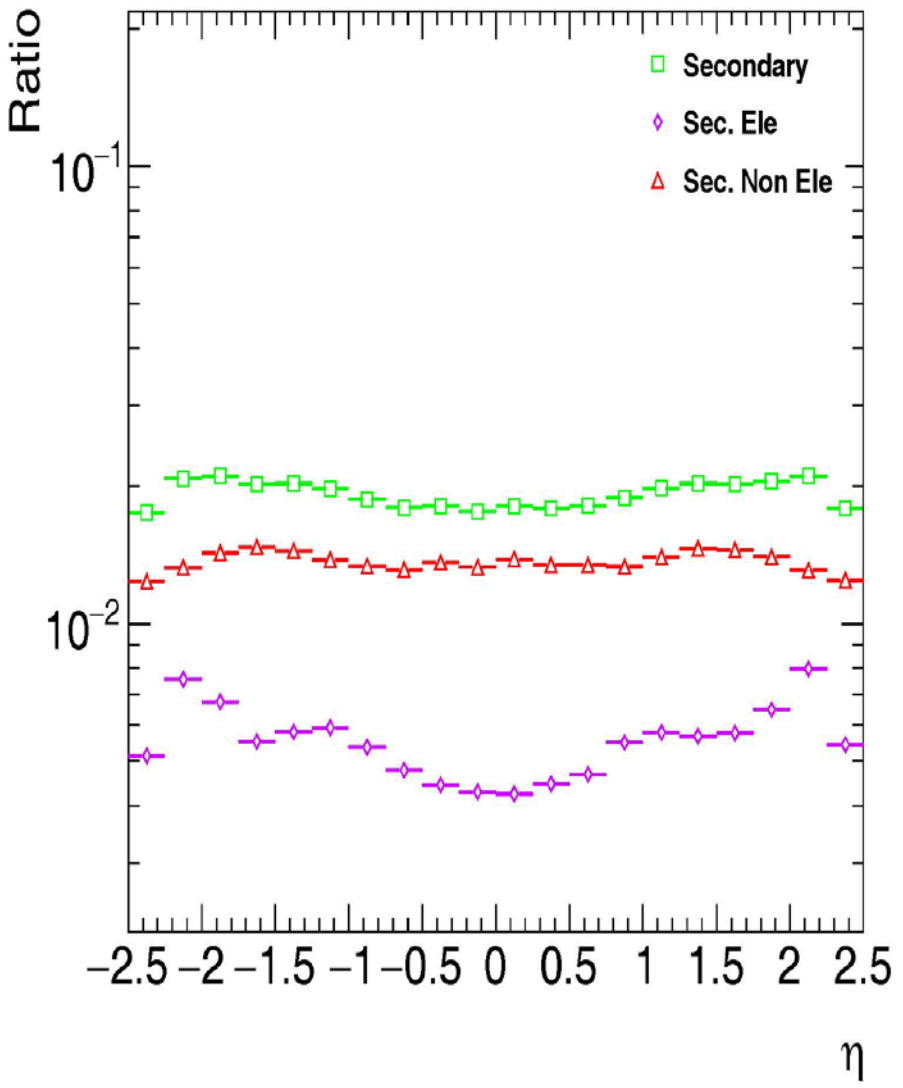

Reprocessing. Selected tracks. Resolution of IP d_0 vs η

Deconvolution. Resolution of IP d_0 vs η

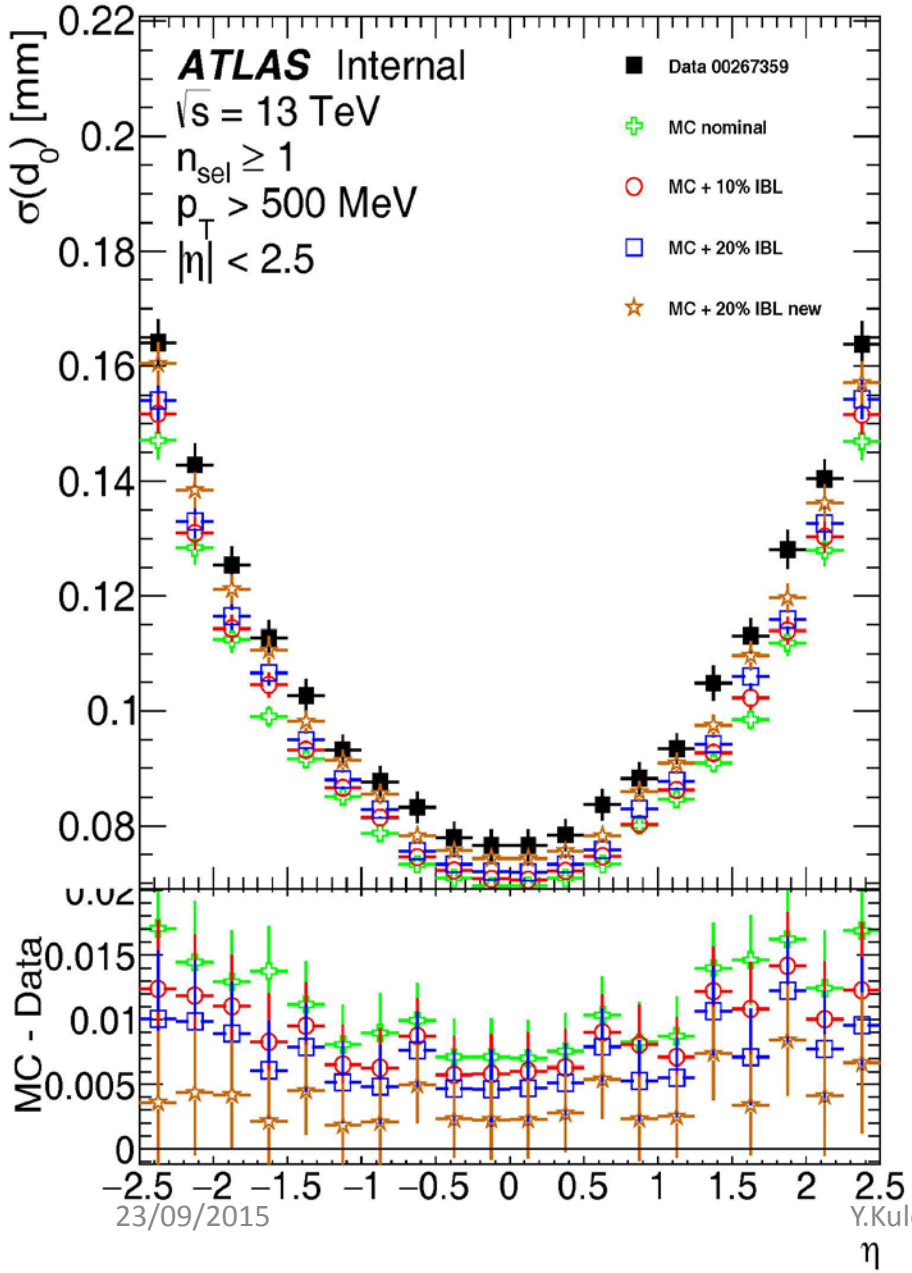

Resolution of IP d_0 vs η

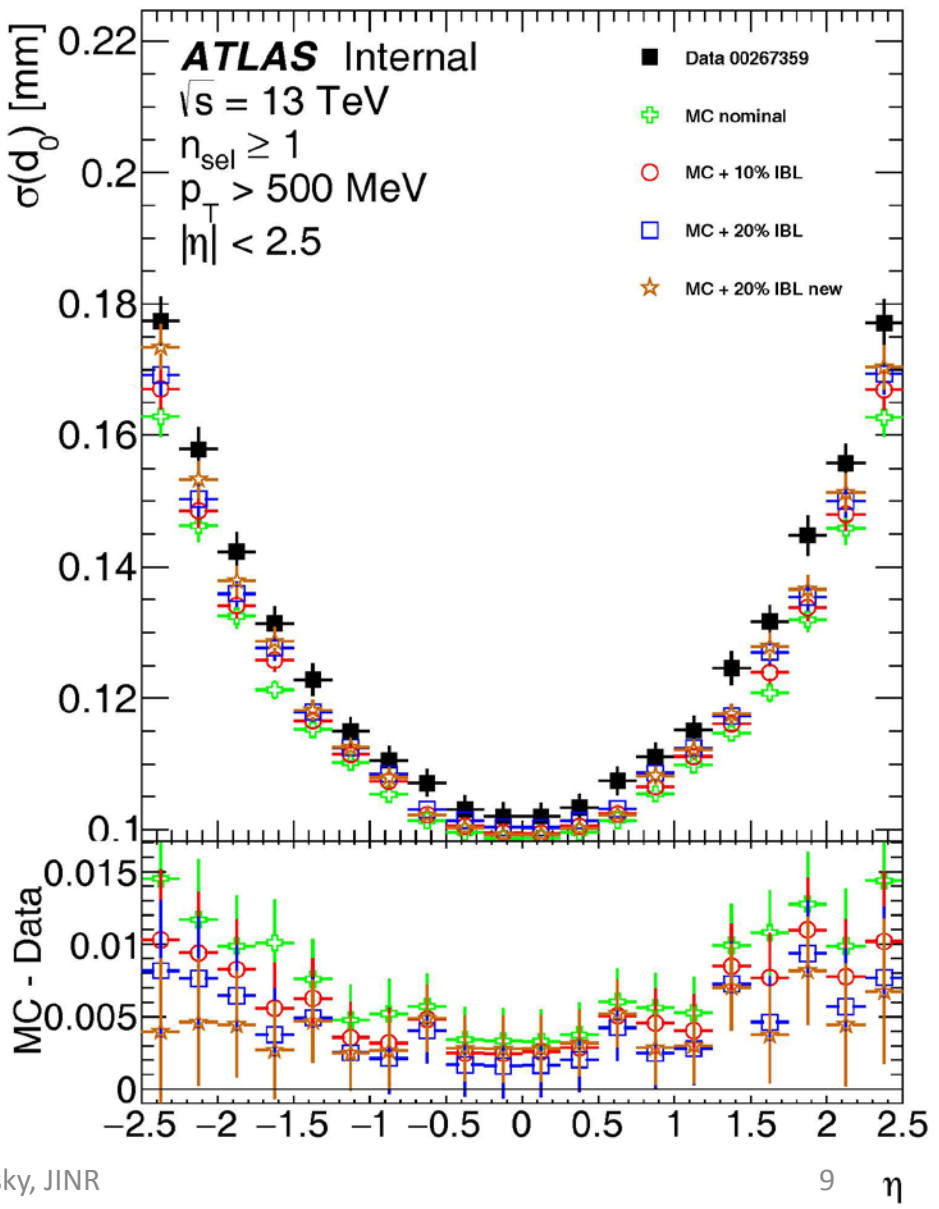

Analysis of K_s^0 vs R

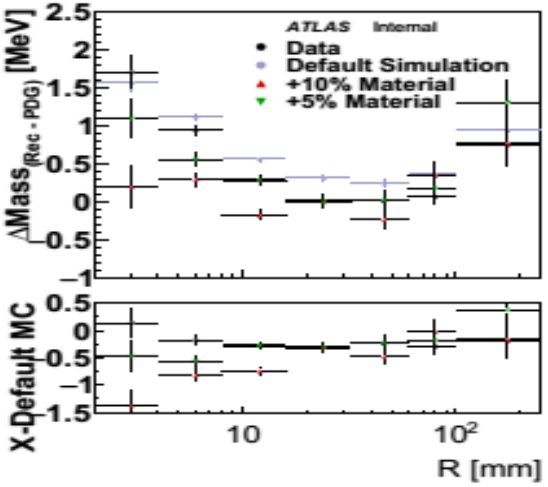

(a) $-2.5 < \eta < -1.5$

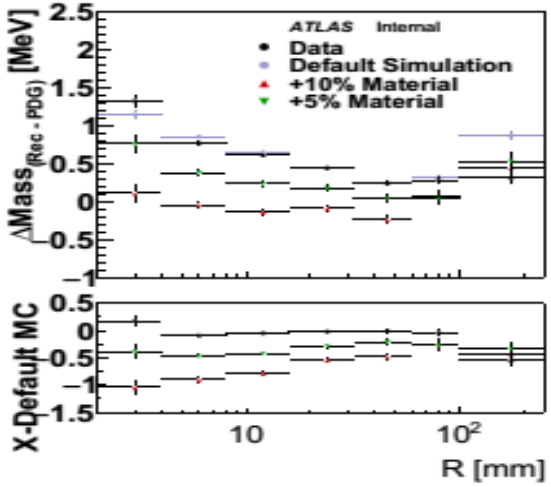

(b) $-1.5 < \eta < -0.5$

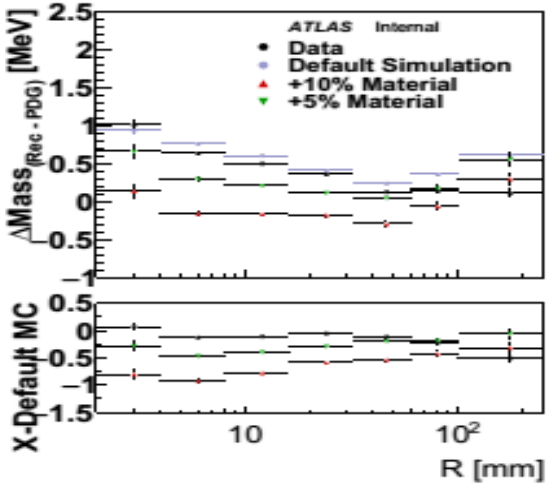

(c) $-0.5 < \eta < 0.5$

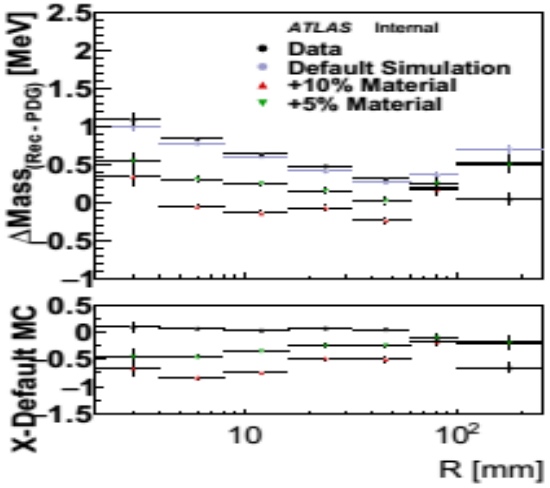

(d) $0.5 < \eta < 1.5$

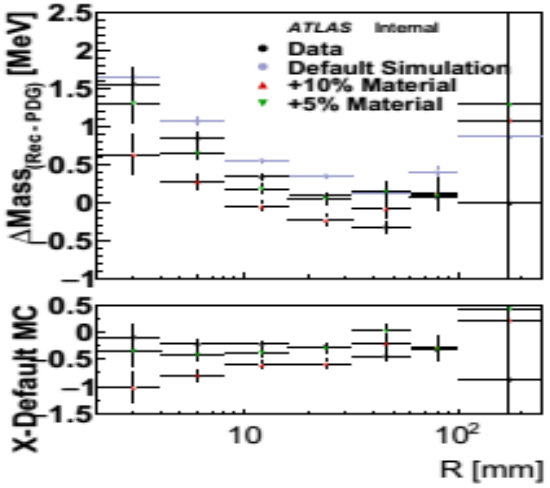

(e) $1.5 < \eta < 2.5$

Figure 110: Reconstructed K_s^0 mass a function of decay radius in data and various MC samples. The directions are defined by the momentum vector of the K_s^0 candidate. The K_s^0 candidates are required to have a reconstructed decay radius of greater than 2 mm and $\cos\theta > 0.999$. Only statistical fit uncertainties are shown.

Corrections

Reweight events by: $$w_{ev}(n_{sel}^{BL},\eta) = \frac{1}{\varepsilon_{trig}(n_{sel}^{BL})} \cdot \frac{1}{\varepsilon_{vtx}(n_{sel}^{BL},\eta)}$$

- For η and p_T distributions, reweight tracks by:

$$w_{trk}(p_T,\eta) = \frac{1}{\varepsilon_{trk}(p_T,\eta)} \cdot (1 - f_{sec}(p_T,\eta) - f_{sb}(p_T,\eta) - f_{okr}(p_T,\eta))$$

  - Then (Bayesian) unfold the p_T spectrum to account for momentum smearing

- For multiplicity distribution (Bayesian) unfold with matrix from MC

- For $\langle p_T \rangle$ versus multiplicity unfold the numerator: Σp_T of all tracks in all events and denominator: total number of tracks in all events then take the ratio

Trigger and vertex efficiency

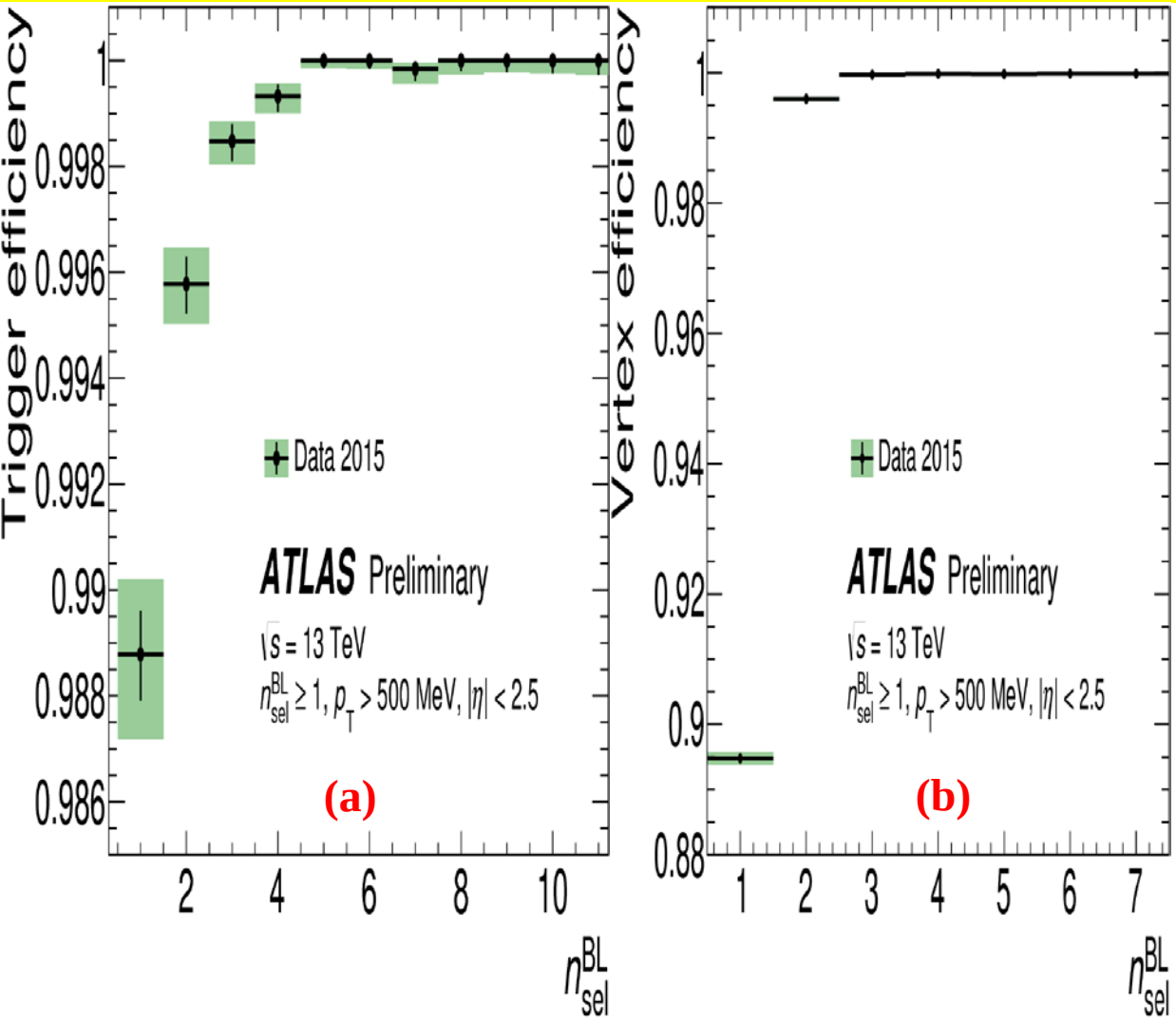

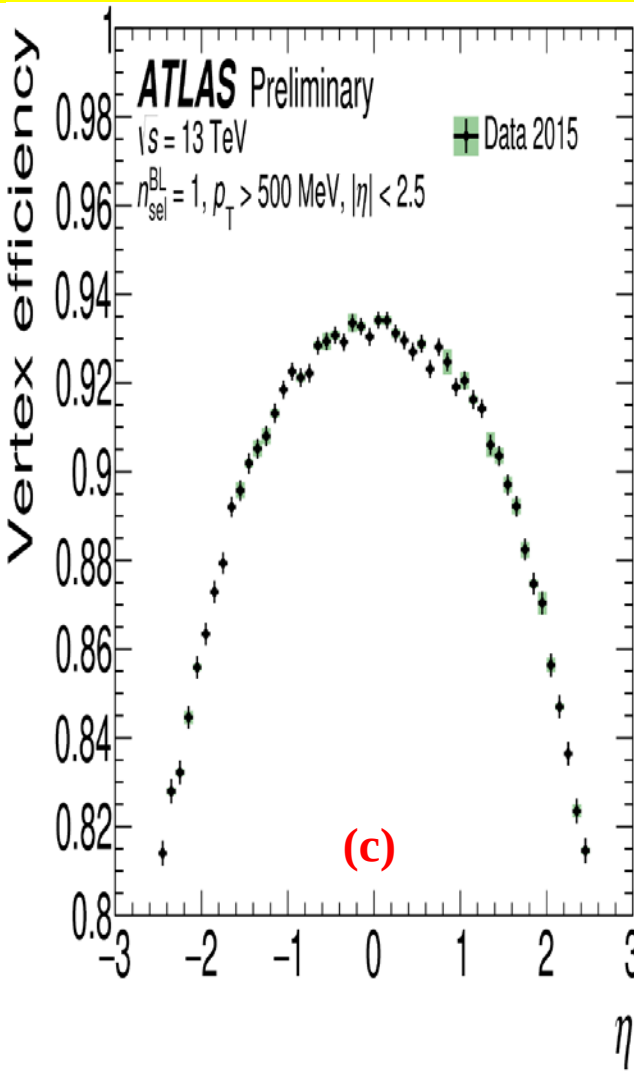

(a) Trigger efficiency and (b) vertex reconstruction efficiency with respect to the event selection, as a function of the number of reconstructed tracks without the $\Delta z_0 \sin\theta$ constraint (n_{sel}^{BL}).
(c) Vertex efficiency in data with respect to the event selection for events with exactly one selected track as a function of η. The statistical uncertainties are shown as black lines and the

Tracking efficiency

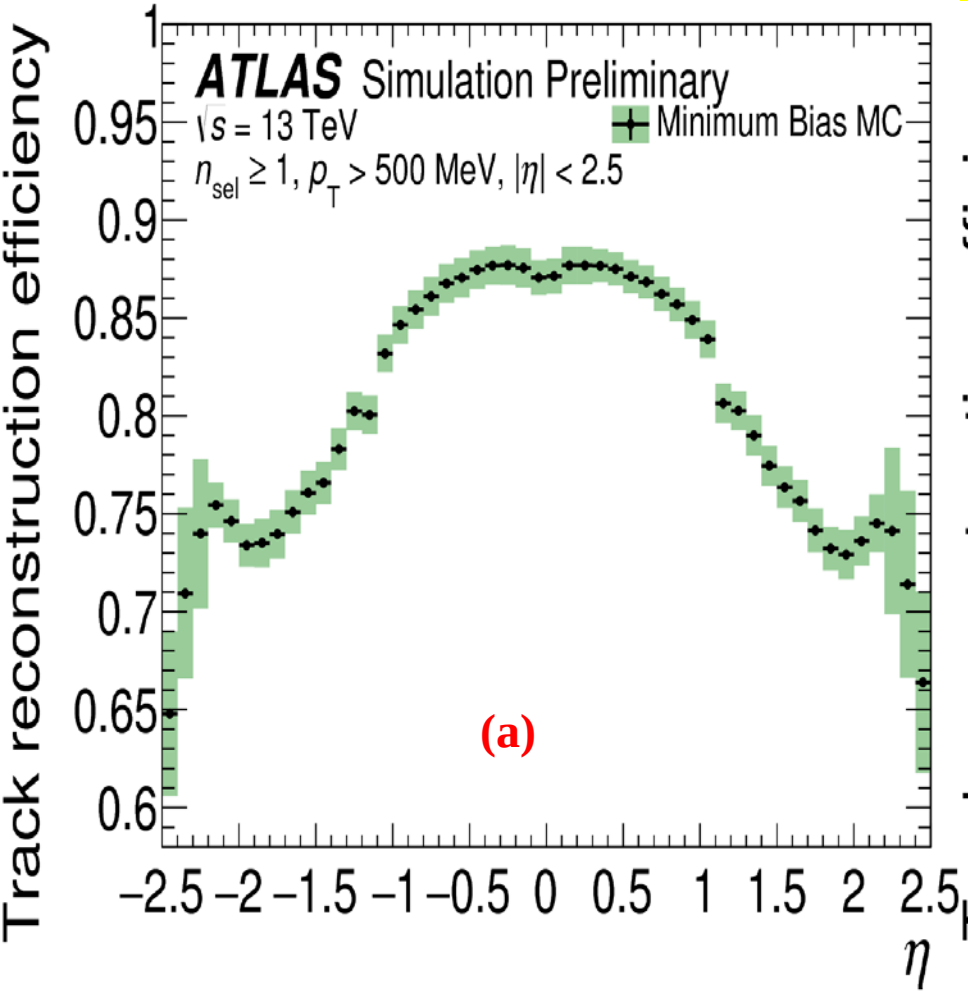

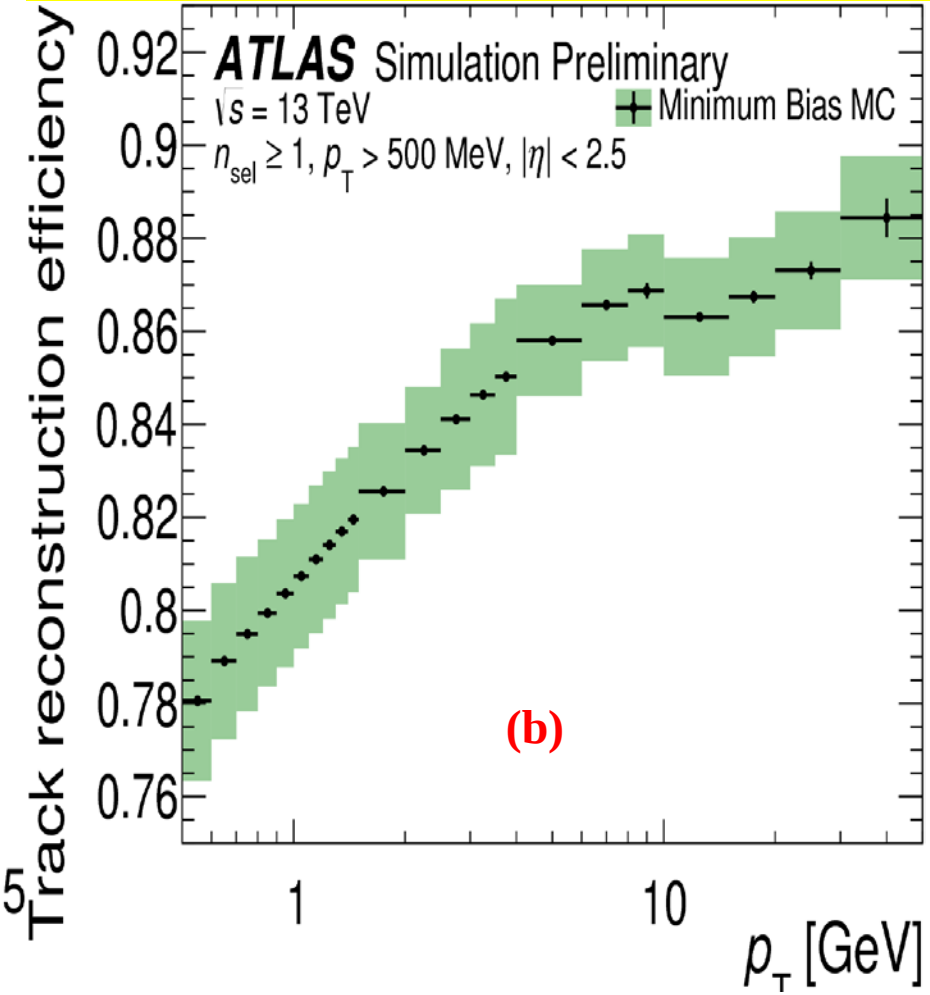

The track reconstruction efficiency as a function of (a) pseudorapidity, η, and (b) transverse momentum, p_T as predicted by Pythia8 A2 simulation. The statistical uncertainties are shown as black lines, the total uncertainties as green shaded areas.

MC models. I

The MC models used to correct the data for detector effects and to compare with particle-level corrected data. The **PYTHIA 8, HERWIG++, EPOS** and **QGSJET-II** generators are used.

In **PYTHIA 8** inclusive hadron–hadron interactions are described by a model that splits the total inelastic cross-section into non-diffractive (ND) processes, dominated by *t*-channel gluon exchange, and diffractive processes involving a colour-singlet exchange. The simulation of ND processes includes multiple parton-parton interactions (MPI). The diffractive processes are further divided into single-diffractive dissociation (SD), where one of the initial hadrons remains intact and the other is diffractively excited and dissociates, and double-diffractive dissociation (DD) where both hadrons dissociate.

In **HERWIG++** inclusive hadron–hadron collisions are simulated by applying an MPI model for the ND process to events with no hard scattering. It is therefore possible to generate an event with zero $2 \rightarrow 2$ partonic scatters, in which only beam remnants are produced, with nothing in between them. While **HERWIG++** has no explicit model for diffractive processes in the simulation of inclusive hadron–hadron collisions, the zero-scatter events will look similar to double-diffractive dissociation.

EPOS provides an implementation of a parton-based Gribov-Regge theory which is an effective QCD-inspired field theory describing hard and soft scattering simultaneously.

QGSJET-II provides a phenomenological treatment of hadronic and nuclear interactions in the Reggeon field theory framework. The soft and semihard parton processes are included in the model within the “semihard Pomeron” approach.

EPOS and **QGSJET-II** calculations do not rely on the standard parton distribution functions (PDFs) as used in generators like **PYTHIA 8** and **HERWIG++.**

MC models. II

Different settings of model parameters optimised to reproduce the existing experimental data have been used in the simulation. These settings are referred to as tunes.

For **PYTHIA 8** two tunes are used (A2 and MONASH), for **HERWIG++** and **EPOS** the UE-EE-5-CTEQ6L1 and LHC tunes are respectively used. **QGSJET-II** uses the default tune from the generator.

Each tune incorporates 7 TeV underlying event and/or minimum-bias data, with this **HERWIG++** tune being the only one that does not incorporate minimum-bias data. Each tune is summarised in Table 1, together with the version of each generator used to produce the samples. The **A2 PYTHIA 8** (with MSTW2008LO PDF) sample is used to derive the detector corrections for these measurements.

Generator	Version	Tune	PDF	7 TeV data	
				MB	UE
PYTHIA 8	8.185	A2	MSTW2008LO [19]	yes	no
PYTHIA 8	8.186	MONASH	NNPDF2.3LO [20]	yes	yes
HERWIG++	2.7.1	UE-EE-5-CTEQ6L1	CTEQ6L1 [21]	no	yes
EPOS	3.1	LHC	N/A	yes	no
QGSJET-II	II-04	default	N/A	yes	no

Table 1: Summary of MC tunes used to compare to the corrected data. The generator and its version are given in the first two columns, the tune name and the PDF used are given in the next two columns and the last two columns indicate whether the data used in the tune included 7 TeV minimum bias (MB) and/or underlying event (UE) data.

All the events are processed through the ATLAS detector simulation program, which is based on GEANT4. They are then reconstructed and analysed by the same program chain used for the data.

η distribution

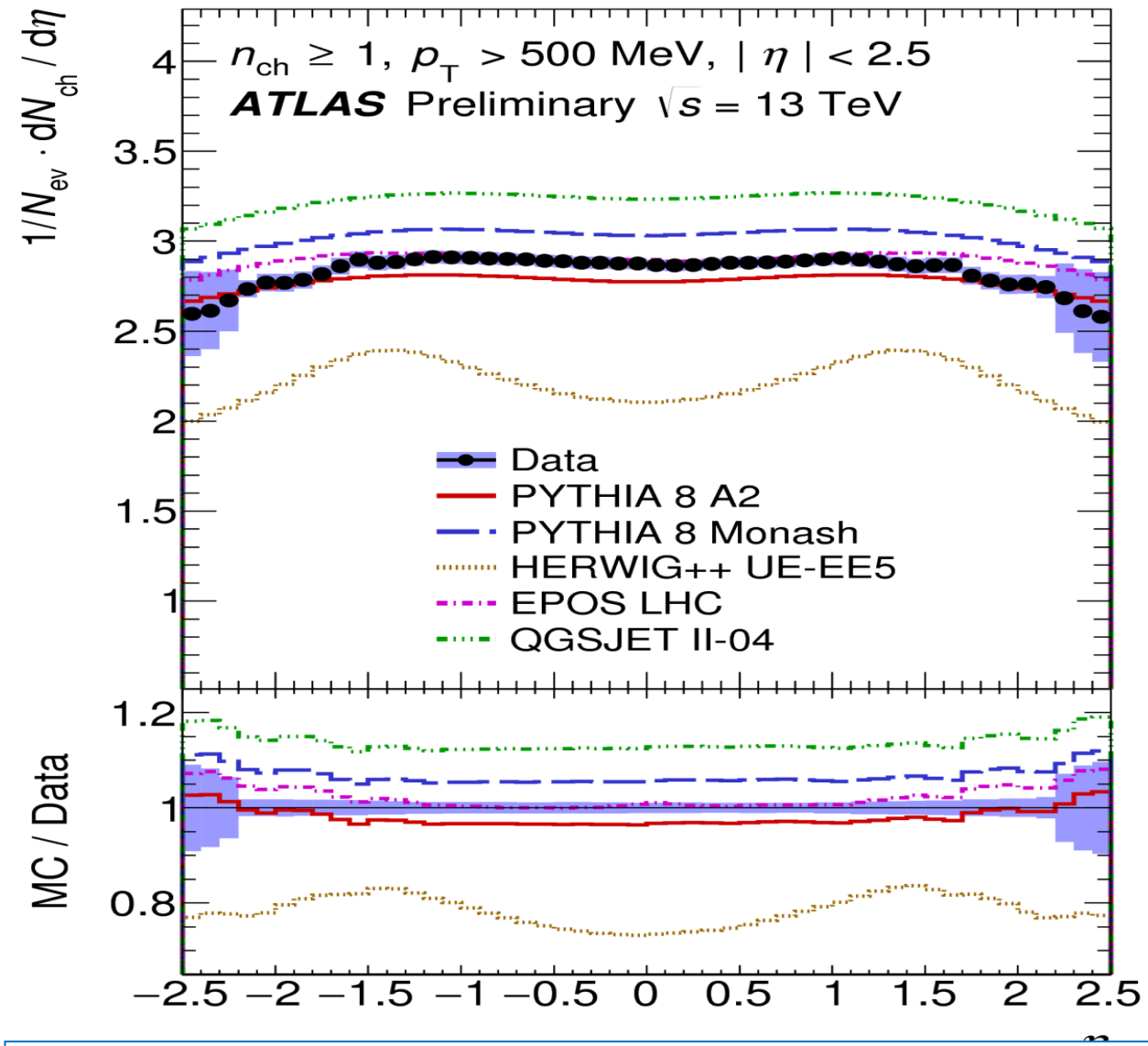

Charged-particle multiplicity as a function of the pseudorapidity for events with $n_{ch} \geq 1$, $p_T > 500$ MeV and $|\eta| < 2.5$. The dots represent the data and the curves the predictions from different MC models. The x-value in each bin corresponds to the bin centroid. The vertical bars represent the statistical uncertainties, while the shaded areas show statistical and systematic uncertainties added in quadrature. The bottom inserts show the ratio of the MC over the data. The values of the ratio correspond to the averages of the bin content.

The same shape in Models but different normalisation. Except **HERWIG** which is tuned entirely on UE. **EPOS** and **Pythia 8 A2** give remarkably good predictions.

p_T distribution

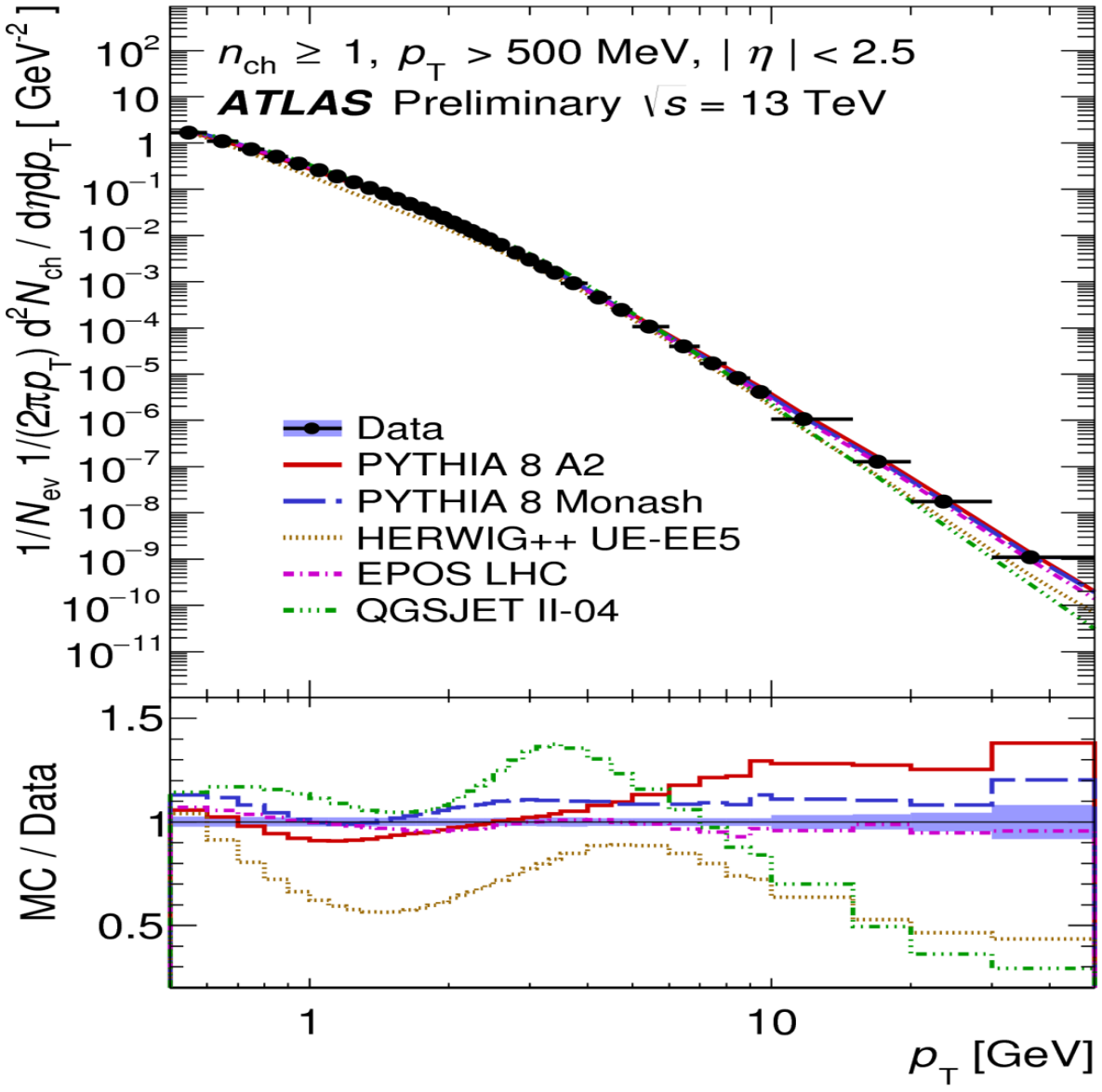

Charged-particle multiplicity as a function of the transverse momentum for events with $n_{ch} \geq 1$, $p_T > 500$ MeV and $|\eta| < 2.5$. The dots represent the data and the curves the predictions from different MC models. The x-value in each bin corresponds to the bin centroid. The vertical bars represent the statistical uncertainties, while the shaded areas show statistical and systematic uncertainties added in quadrature. The bottom inserts show the ratio of the MC over the data. The values of the ratio correspond to the averages of the bin content.

Measurement spans 10 orders of magnitude. **EPOS** and **Pythia 8 Monash** give remarkably good predictions.

Multiplicity distribution

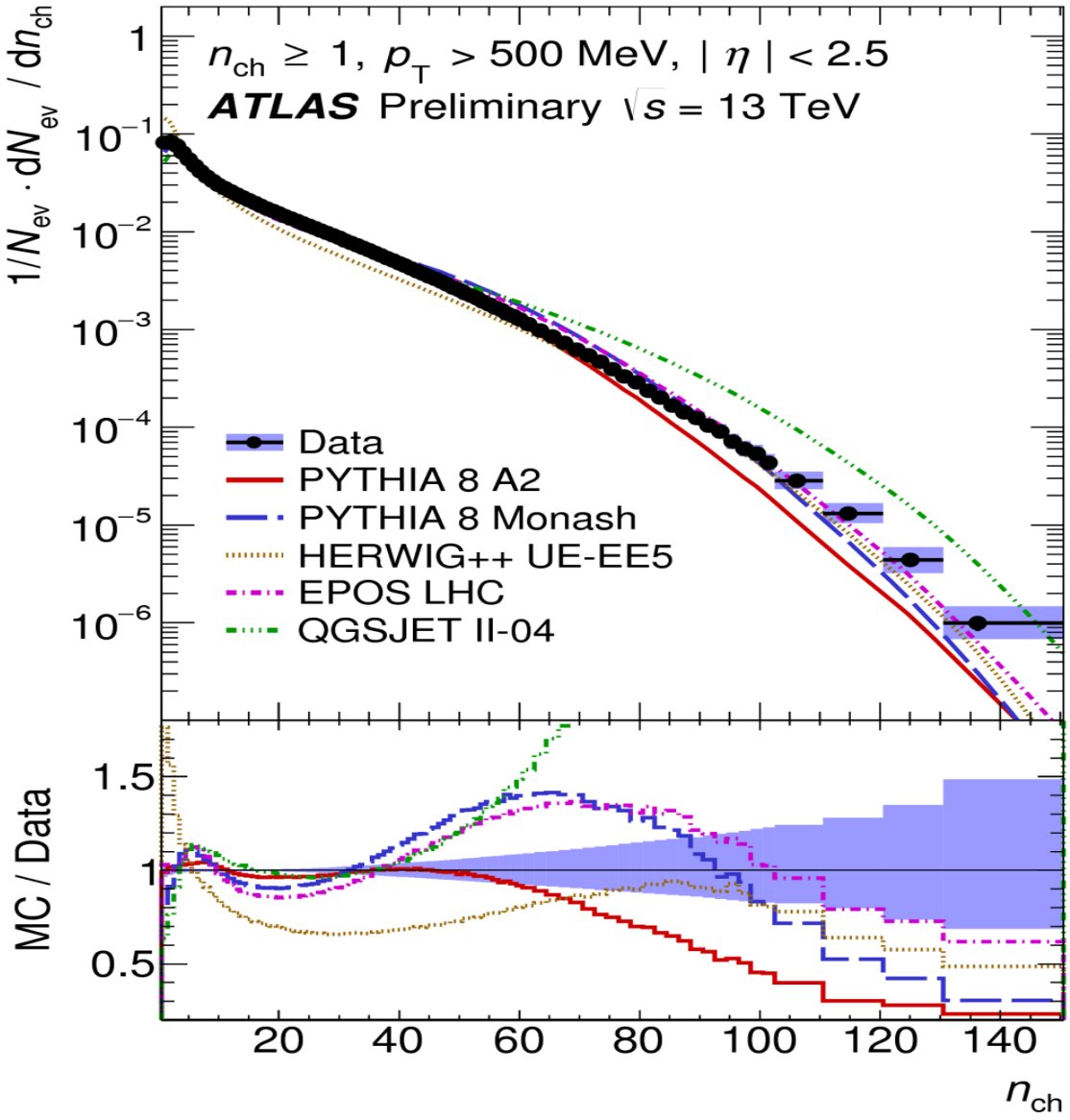

Charged-particle events as a function of the multiplicity for events with $n_{ch} \geq 1$, $p_T > 500$ MeV and $|\eta| < 2.5$. The dots represent the data and the curves the predictions from different MC models. The x-value in each bin corresponds to the bin centroid. The vertical bars represent the statistical uncertainties, while the shaded areas show statistical and systematic uncertainties added in quadrature. The bottom inserts show the ratio of the MC over the data. The values of the ratio correspond to the averages of the bin content.

Low n_{ch} not well modelled by any MC; because of large contribution from diffraction.

Average transverse momentum distribution

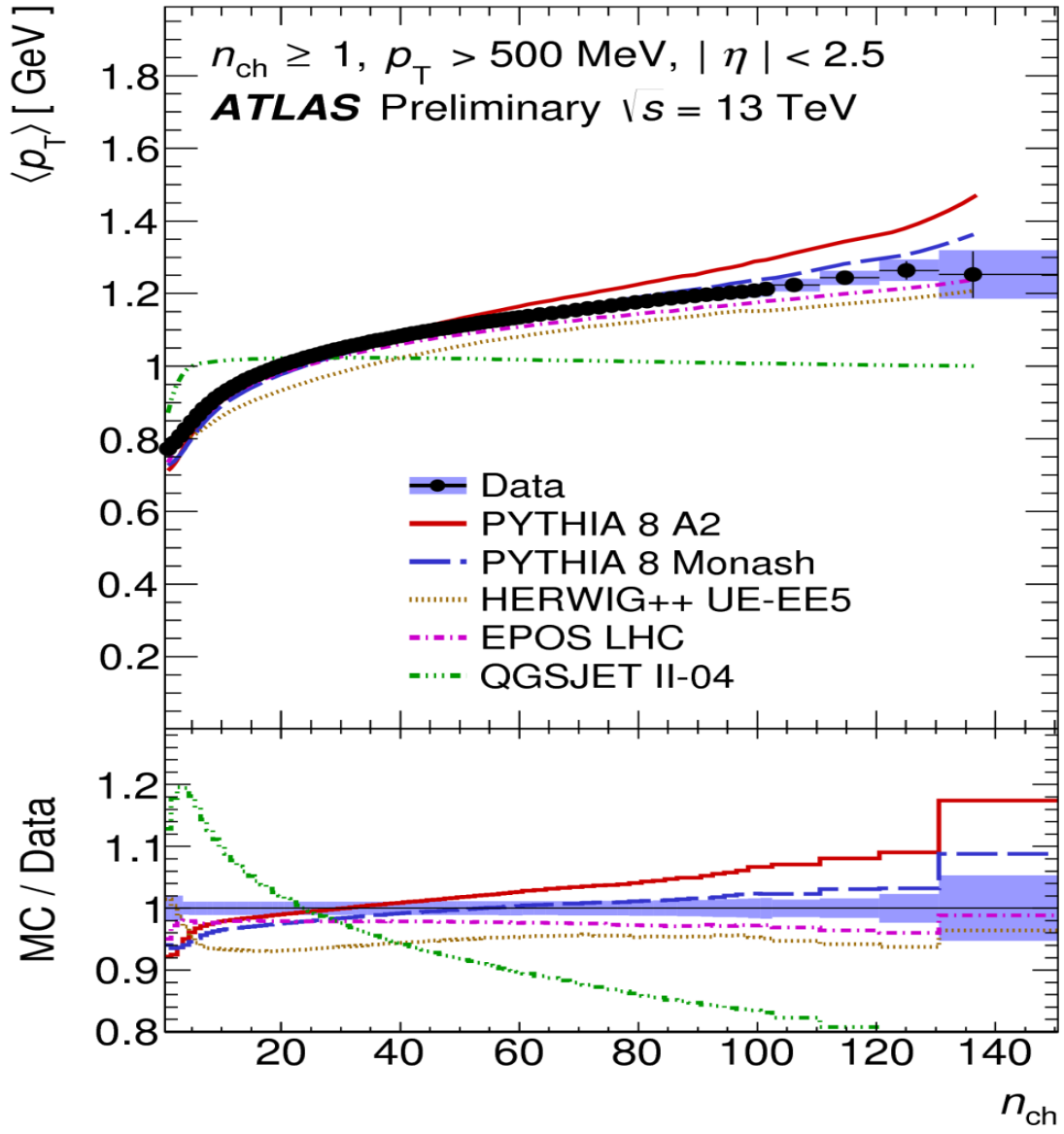

Mean transverse momentum versus the charged-particle multiplicity distribution for events with $n_{ch} \geq 1$, $p_T > 500$ MeV and $|\eta|<2.5$. The dots represent the data and the curves the predictions from different MC models. The x-value in each bin corresponds to the bin centroid. The vertical bars represent the statistical uncertainties, while the shaded areas show statistical and systematic uncertainties added in quadrature. The bottom inserts show the ratio of the MC over the data. The values of the ratio correspond to the averages of the bin content.

Models without colour reconnection, **QGSJET,** fail to model scaling with n_{ch} very well.

Mean charged-particle multiplicity per 1η for η=0

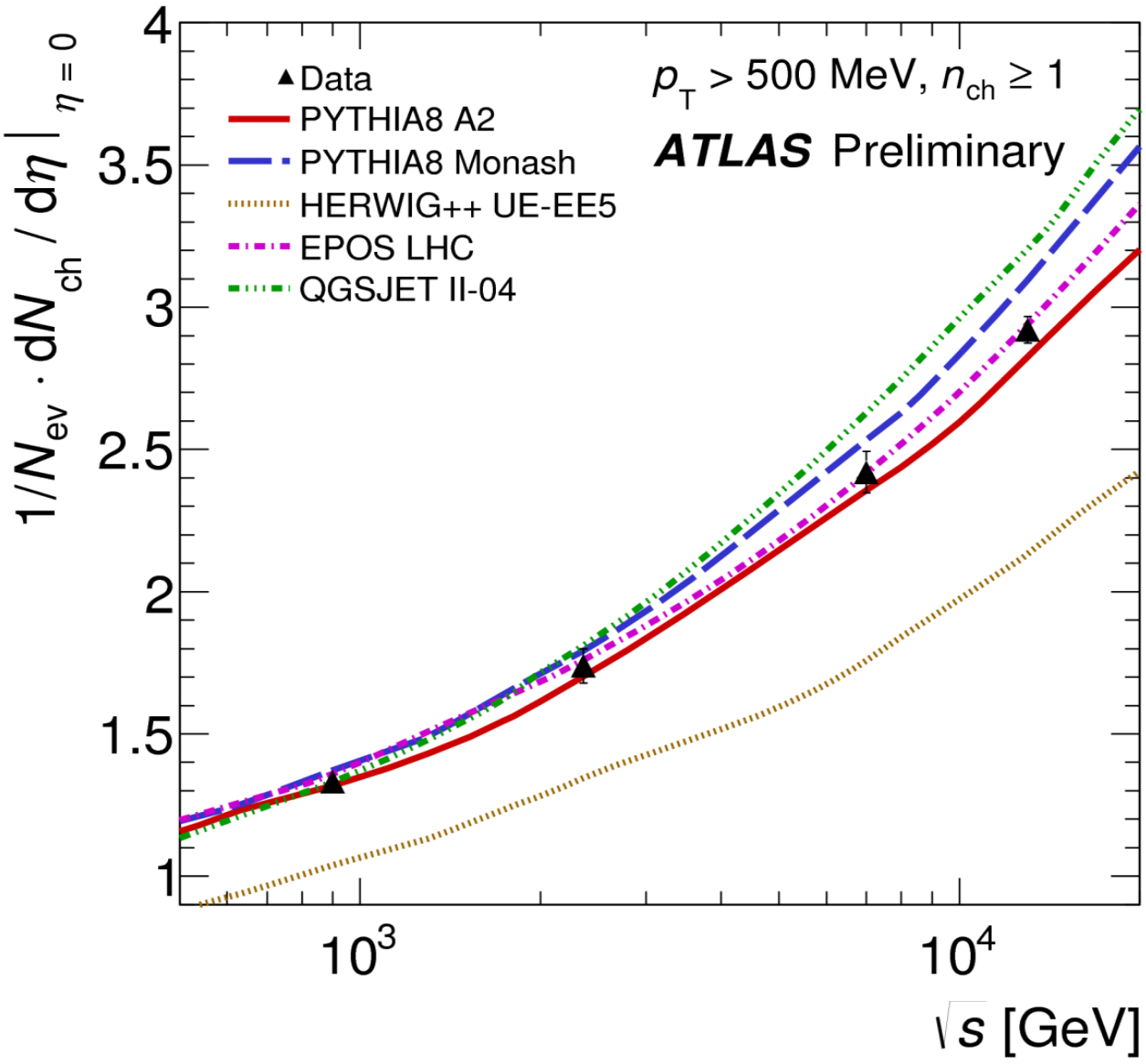

The average charged-particle multiplicity per unit of rapidity for η=0 as a function of the centre-of-mass energy. The definition of charged-particle includes charged strange baryons. The data are compared to various particle level MC predictions. The vertical error bars on the data represent the total uncertainty.

Conclusion

- Charged-particle multiplicity measurements with the ATLAS detector using pp-collisions for p_T>0.5 GeV, |η|<2.5 delivered by the LHC at $\sqrt{s}$=13 TeV during 2015 are presented.
- The result based on nearly 9 million inelastic interactions the properties of events were studied.
- The data were corrected with minimal model dependence to obtain inclusive distributions.
- The selected kinematic range (p_T>0.5 GeV, |η|<2.5, n_{sel}>1) and the precision of this analysis highlight clear differences between MC models and the measured distributions.
- Of the models considered EPOS reproduces the data the best, PYTHIA 8 A2 and MONASH give reasonable descriptions of the data and HERWIG++ and QGSJET-ii provide the worst descriptions of the data.

BACKUP SLIDES

ATLAS Publications

1. 0.9 TeV data

1. Charged-particle multiplicities in pp interactions at $\sqrt{s}$=900 GeV measured with the ATLAS detector at the LHC. ATLAS Collaboration arXiv:1003.3124 [hep-ex]. **Phys.Lett. B688 (2010) 21-42.**

2. 2.36 and 7 TeV data

1. Charged-particle multiplicities in pp interactions measured with the ATLAS detector at the LHC. ATLAS Collaboration, arXiv:1012.5104 [hep-ex]. **New J.Phys. 13 (2011) 053033.**
2. Central charged-particle multiplicities in pp interactions with $|\eta|<0.8$ and $p_t>0.5$ and 1 GeV measured with the ATLAS detector at the LHC; ATLAS Collaboration. **ATLAS-CONF-2010-113.**

3. 8 TeV data

Charged-particle multiplicities in *pp* interactions at $\sqrt{s}$=8 TeV measured with the ATLAS detector at the LHC. **ATL-COM-PHYS-2014-449**

4. 13 TeV data

Charged-particle multiplicities in $\sqrt{s}$=13 TeV pp interactions measured with ATLAS at the LHC

1. **Paper: ATL-COM-PHYS-2015-346**
2. **Support note: ATL-COM-PHYS-2015-313**
3. **Editorial board: STDM-2015-02**
4. **Will be published in July 2015**

Introduction

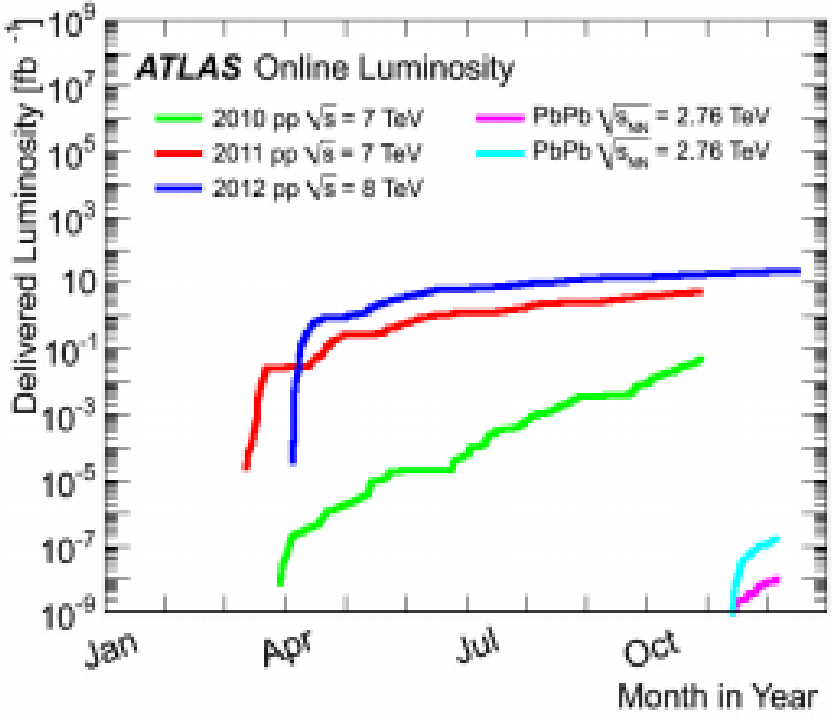

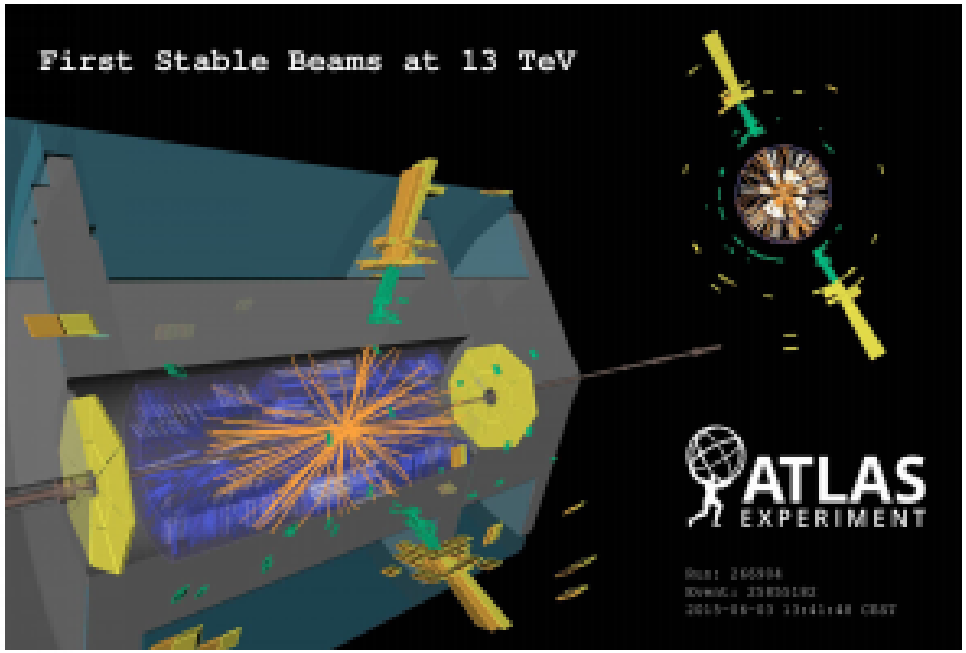

- Tracking system ideal for the measurement of track based particles properties
- Multi purpose detector:
  - Can measure events with different detector technologies
  - Possibility to measure soft-QCD with complementary methods
  - First comparisons with 13 TeV data will be shown in the talk

Inner Detector

- The ATLAS Inner Detector tracker is composed of three sub-detectors:
  - The *Pixel Detector* made of silicon pixels (3 hits/track)
  - The *Semi-Conductor Tracker* (SCT) made of silicon micro-strips (8 hits/track)
  - The *Transition Radiation Tracker* (TRT) made of proportional drift tubes (~30 hits/track)

	Channels	Element Size (X * Y)	Resolution (X * Y) μm
Pixel	80×10^6	50 μm x 400 μm	10 x 115
SCT	6.3×10^6	80 μm x 12 cm	17 x 580
TRT	3.5×10^5	4 mm (diam.)	130

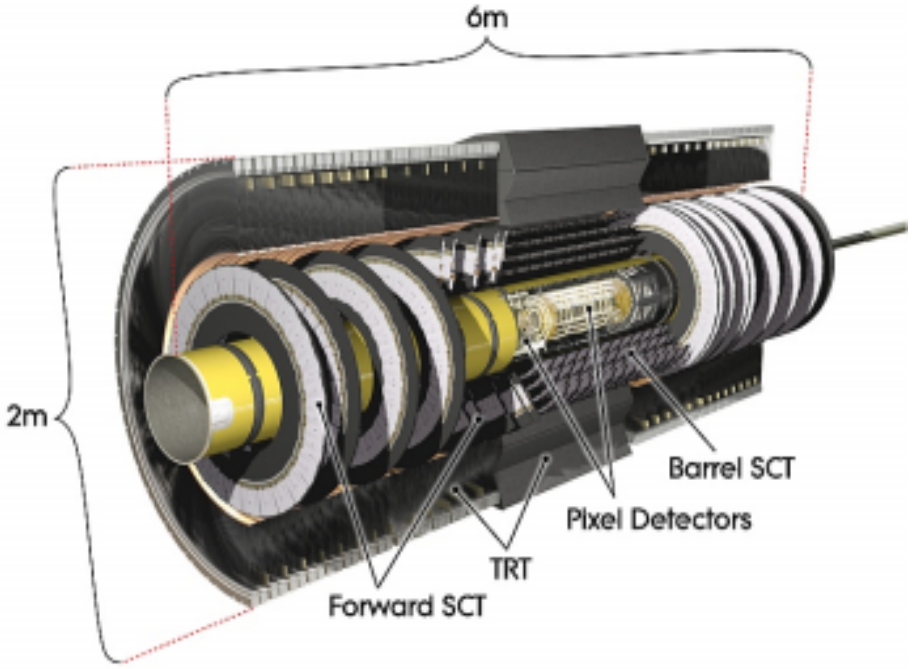

- All these sub-detectors allow precision measurement of charged particle trajectories in the high-multiplicity LHC environment.
- Each detector consists of barrel and two end-cap regions in order to minimize the material traversed by particles coming from the interaction vertex.

Pseudorapidity coverage of the Inner Detector

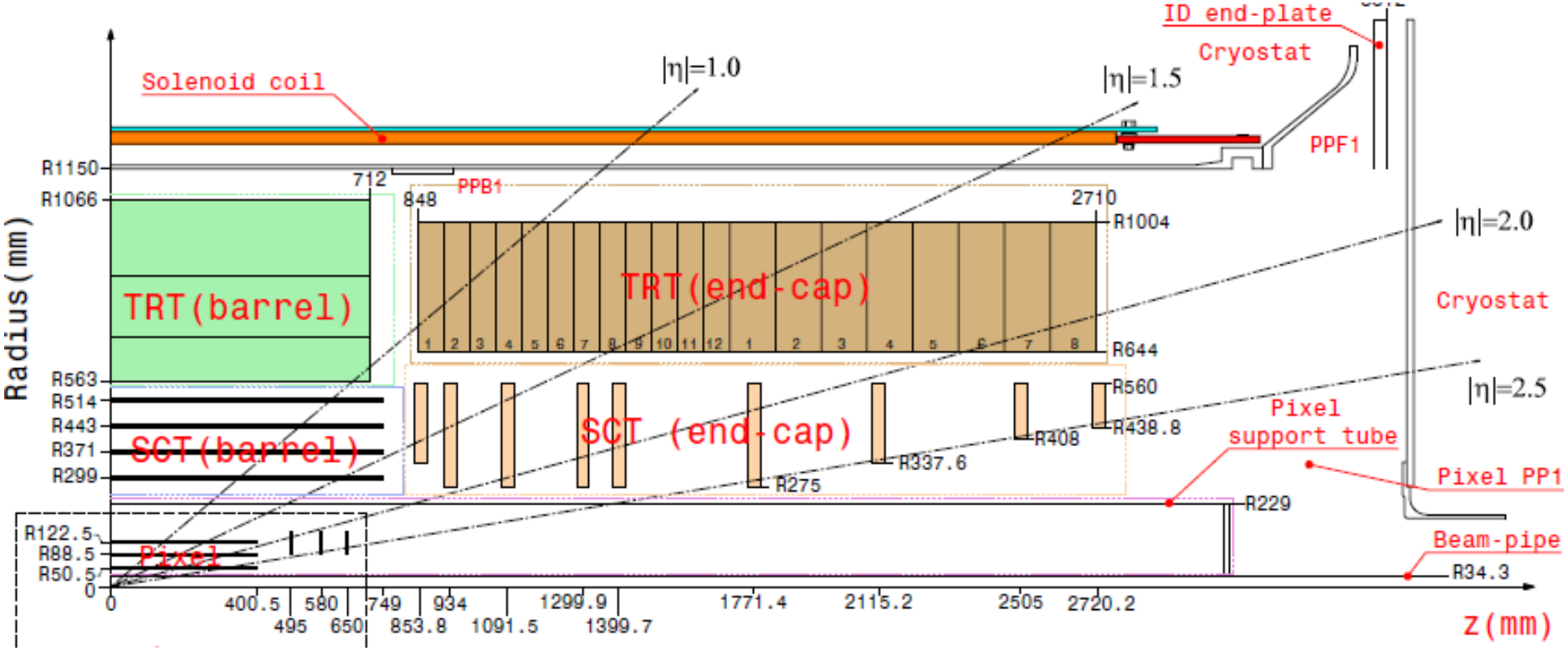

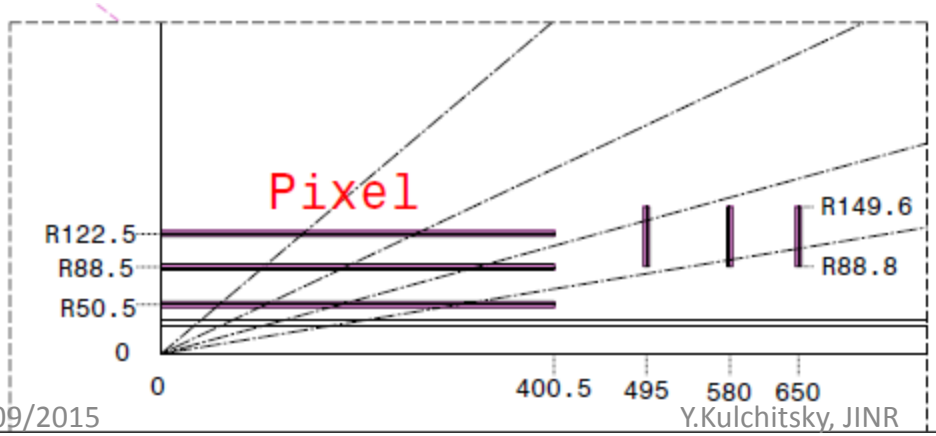

Envelopes

Pixel		45.5<R<242mm |z|<3092mm
SCT barrel		255<R<549mm |z|<805mm
SCT end-cap		251<R<610mm 810<|z|<2797mm
TRT barrel		554<R<1082mm |z|<780mm
TRT end-cap		617<R<1106mm 827<|z|<2744mm

NEW in Run2: Insertable B-layer

Motivation

- Excellent vertex detector performance
- Improve heavy flavor tagging, primary and secondary vertex reconstruction/ separation
- Add additional redundancy of the detector in case of radiation damage

Detector overview

- Length: ~64cm (~7m when integrated with services in both sides)
- 14 local support structures (stave) at 3.27 cm overlapped in phi
- 32 R/O chips per stave
- New R/O chip: FE-I4 in IBM 130 nm CMOS
  - Cell size (50 x 250) μm^2
  - 80 columns x 336 rows = 26880 channels / FE
- Data transfer at 160 MHz
- CO_2 cooling integrated into the staves

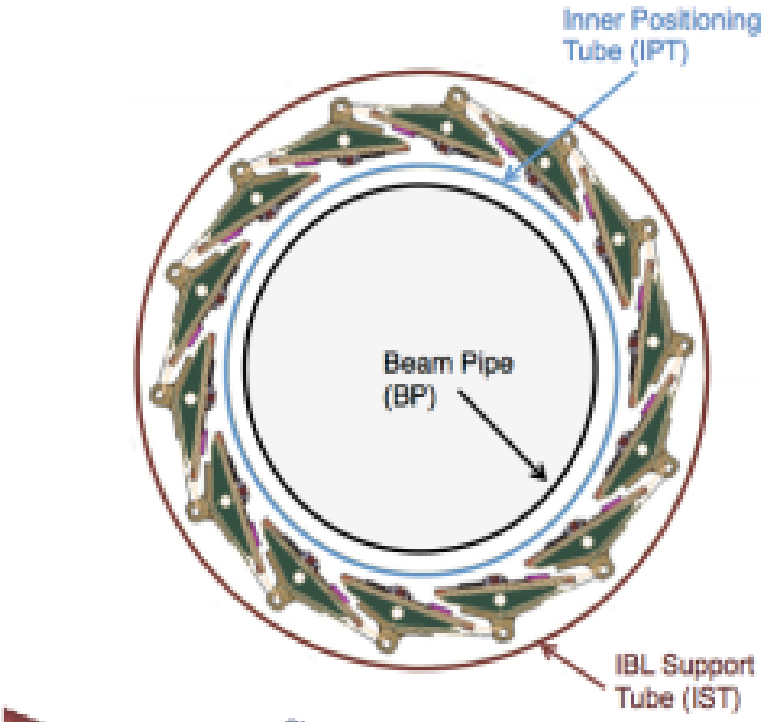

Minim bias distributions

Charged particle distributions

1. multiplicity
2. p_T distribution
3. η distribution
4. Mean p_T vs multiplicity

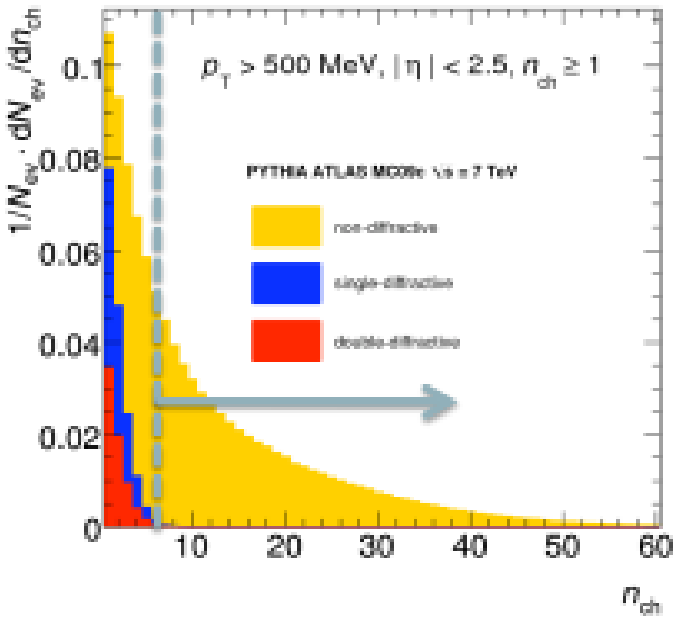

- Define a *diffraction suppressed* sample for MC tuning : $n_{ch} \geq 6$ {p_T > 500 MeV, |η| < 2.5}

√s	lumi.	N_{ev}
0.9 TeV	9 μb^{-1}	157,896
7 TeV	6.8 μb^{-1}	231,665

- Define a *diffraction enhanced* sample :
  - $n_{ch} \geq 1$ {p_T > 500 MeV, |η| < 2.5}
  - veto activity in *one* forward scintillator disk

√s	lumi.	N_{ev}
7 TeV	23 μb^{-1}	52,801

Our Philosophy:

- **Results presented in a well defined phase space.**
- **Do not extrapolate to full coverage with some MC model.**
- **Do not correct data for "diffractive background".**

Tracking performance plots

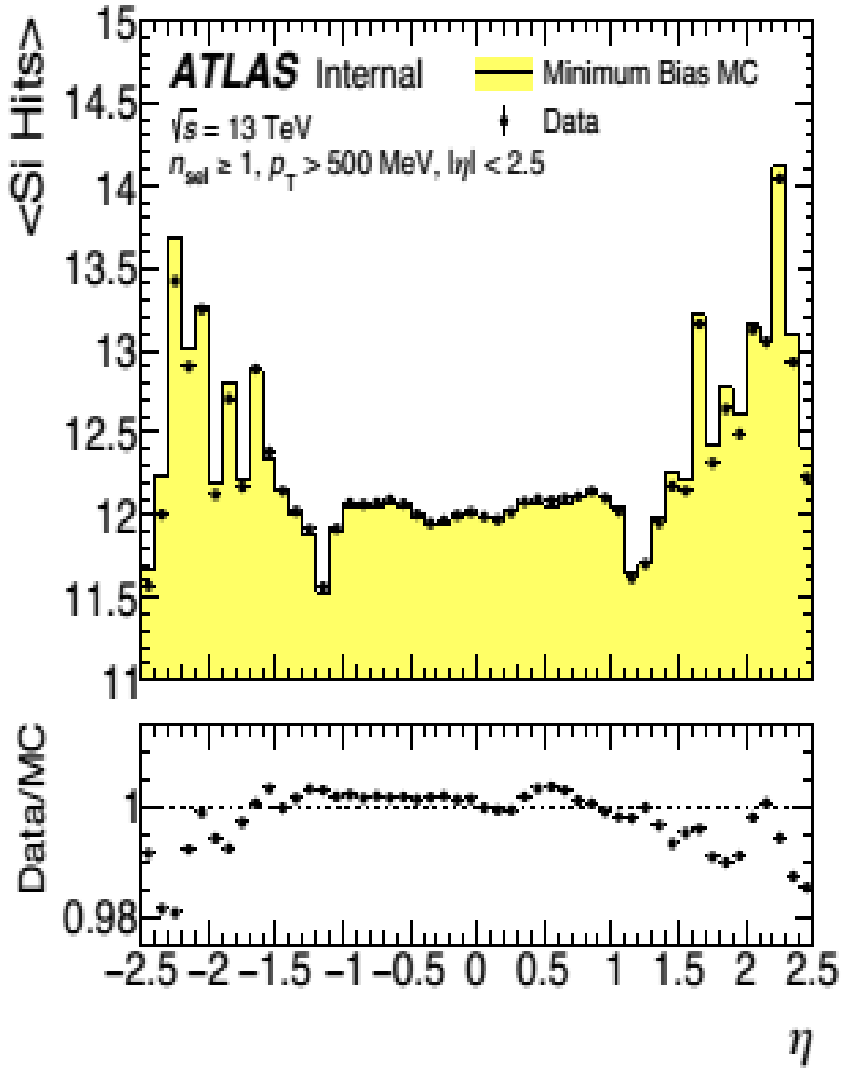

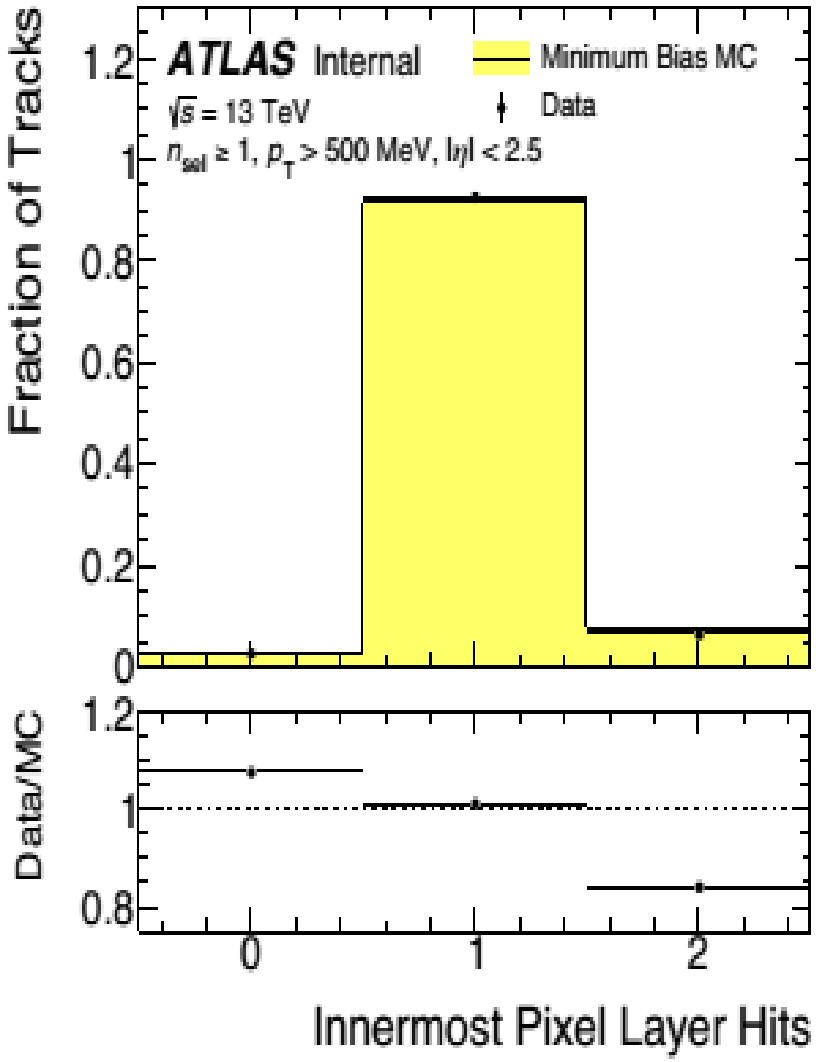

Tracking performance plots

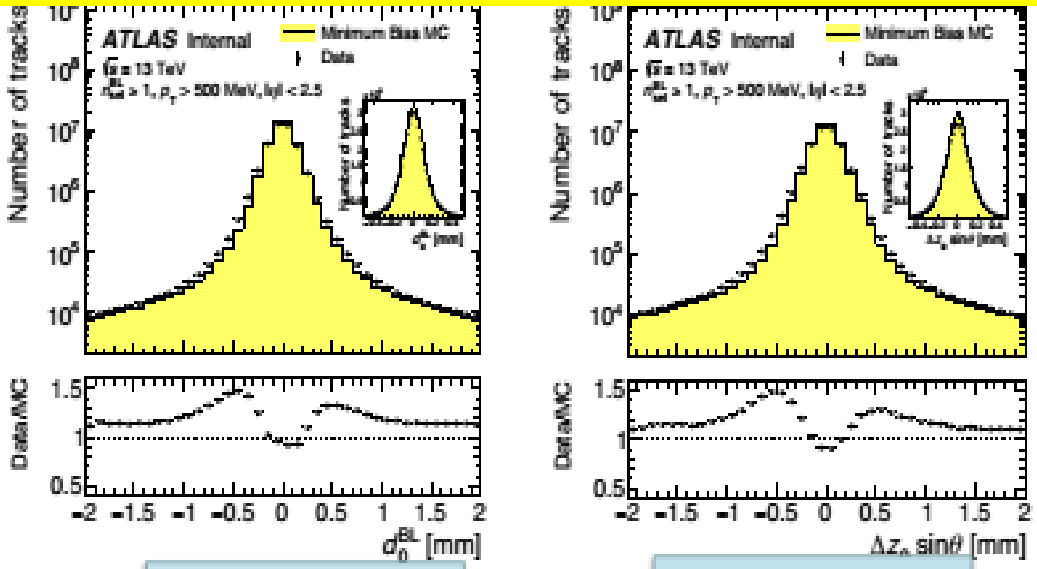

Gaussian smearing σ=70 μm

Gaussian smearing σ=90 μm

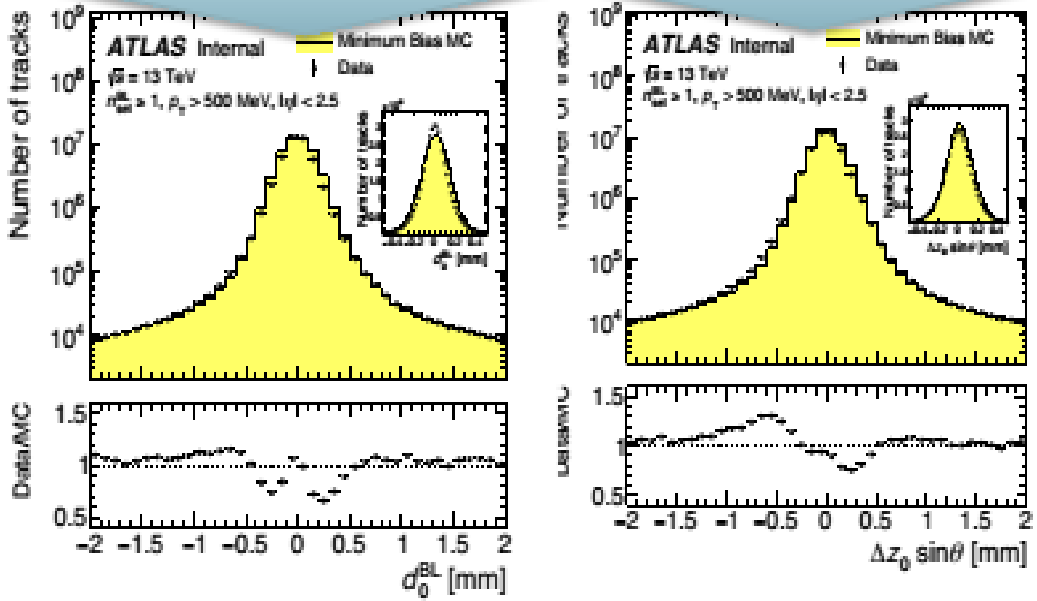

0.003% change in selected tracks

- We propose to use the unsmeared versions and update the entire analysis once we have a proper η/p_T dependent smearing (in time for the Paper).
- Might be best not to make these plots public as they raise more questions then they answer? We could instead reference the tracking performance PUB note(where the resolution is measured) https://cds.cern.ch/record/2029600/

Motivation

Analysis of transverse Impact Parameter distributions (d_0, z_0) within the ID for selected, primaries and secondary tracks with the aim of characterizing the resolution, misalignment, material budget.

MC samples used for Run2. *Non-Diffractive sample (ND):* group.det-indet.207000.Pythia8_Monash_MinBias_ND.merge.HITS.e3385_s1982_s2008_R20132_v008/ (10 millions events)

MC samples used for Run1: group.det-indet.Mon_ND.v3.Run1.s1982_Rec20_0n_EXT2

OLD datasets

MC samples used for Run2. *Non-Diffractive sample (ND):* mc14_13TeV.207000.Pythia8_Monash_MinBias_ND.merge.AOD.e3385_s1982_s2008_r5995_r5853 (150000 events in 30 files)

Non-Diffractive w/ 2.5% extra material sample: mc14_13TeV.207000.Pythia8_Monash_MinBias_ND.merge.AOD.e3385_s2095_s2008_r5995_r5853 (650000 events in 130 files)

Non-Diffractive w/ 5% extra material sample: mc14_13TeV.207000.Pythia8_Monash_MinBias_ND.merge.AOD.e3385_s2094_s2008_r5995_r5853 (500000 events in 100 files)

Selection cuts at 13 TeV

- **Select only well-defined tracks,**
- **Select a primary vertex to reduce error in IP.**

Cut parameter	Cut value
p_T	> 0.5 GeV/c
$\|\eta\|$	< 2.5
Number of Silicon hits	≥ 6
Number of Pixel hits	≥ 1
Number of b-layer hits	> 0
Number of tracks in PV	> 1
Number of PVs	= 1
Number tracks in PV	≥ 2
Track Probability for p_T>10 GeV	≥0.01

Impact parameters d_0 and $z_0 \sin\Theta$

A track in ATLAS is parametrized at the point of closest approach with the global Z-axis using five *perigee parameters*

- $\frac{q}{p}$: the charge of the particle divided by the momentum
- ϕ_0: the angle with the x-axis in the X-Y plane at the perigee point
- θ_0: the angle with the z-axis in the R-Z plane
- d_0: the signed distance to the z-axis. The sign of d_0 is positive, when $\phi - \phi_0 = \frac{\pi}{2} \mod (2\pi)$, where ϕ denotes the angle to the perigee position in the x-y plane, as shown in figure 6.4.
- z_0: the z-coordinate of the track at the point of closest approach to the global Z-axis.

$z_0 = z_{d0} + z_V - z_{PV}$
where $z_v = 0$ for MC

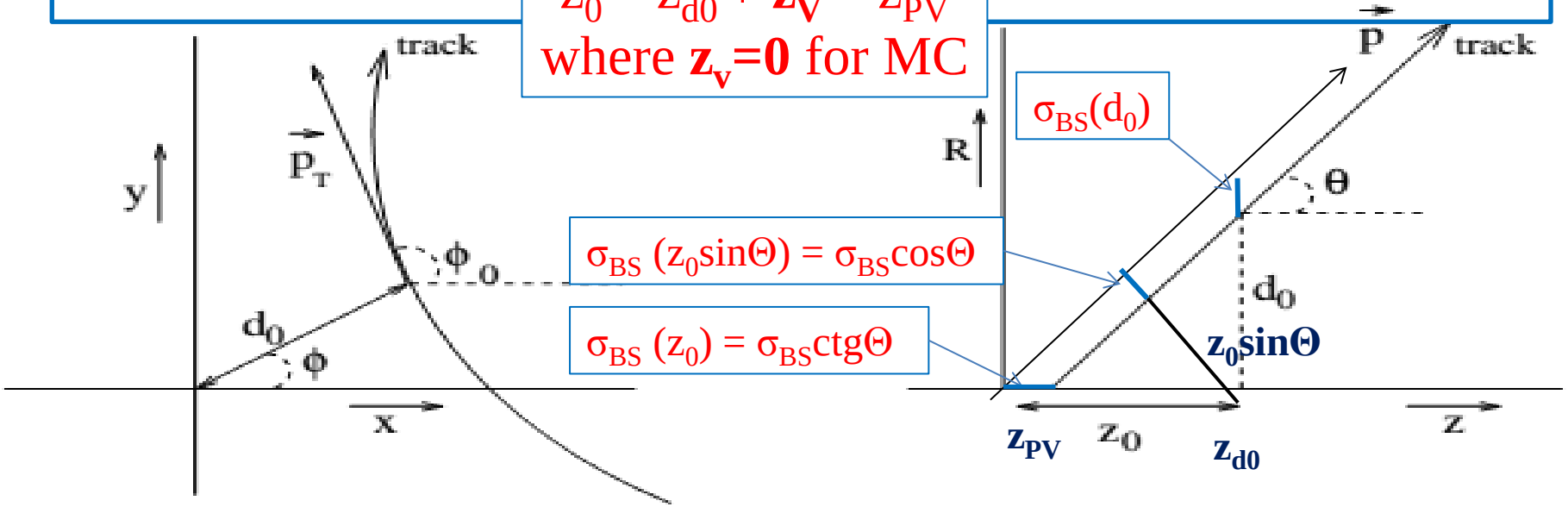

Figure 6.4: Illustration of the perigee parameters of a track in the transverse plane (left) and RZ-plane (right), as defined in the global ATLAS tracking frame.

Secondaries

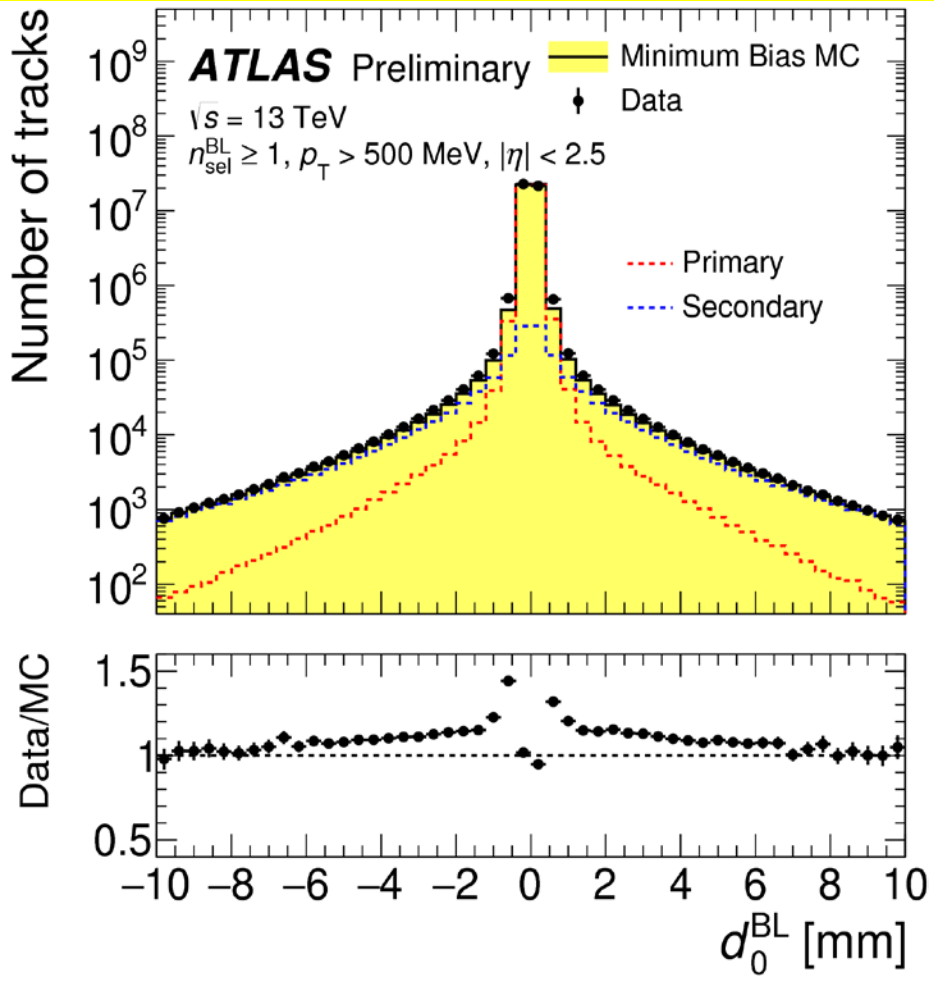

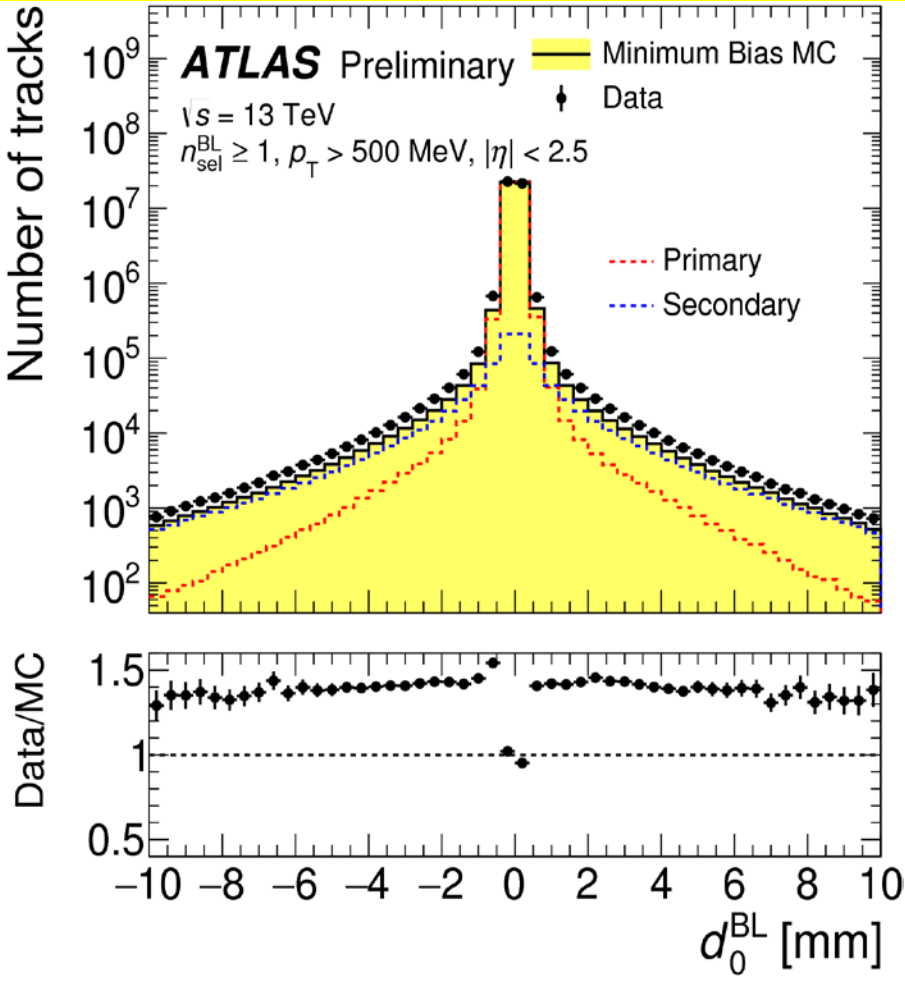

Comparisons between data and PYTHIA 8 A2 and MONASH simulations for the transverse impact parameter distribution of the reconstructed tracks. The separate contributions from tracks coming from primary and secondary particles are also shown and the fraction of secondary particles in the simulation is scaled to match that seen in the data, with the final simulation distributions normalised to the number of

2.2 ± 0.6 % of tracks are from secondary particles: dominant systematic from the interpolation of the number of tracks in the fit region $5 < |d_0^{BL}| < 9.5$ mm to the analysis region $|d_0^{BL}| < 1.5$ mm

Fraction of Secondary tracks for $|d_0|<1.5$ mm and $|z_0 \sin\Theta|<1.5$ mm vs p_T

Run2: Secondary tracks Fractions vs p_T

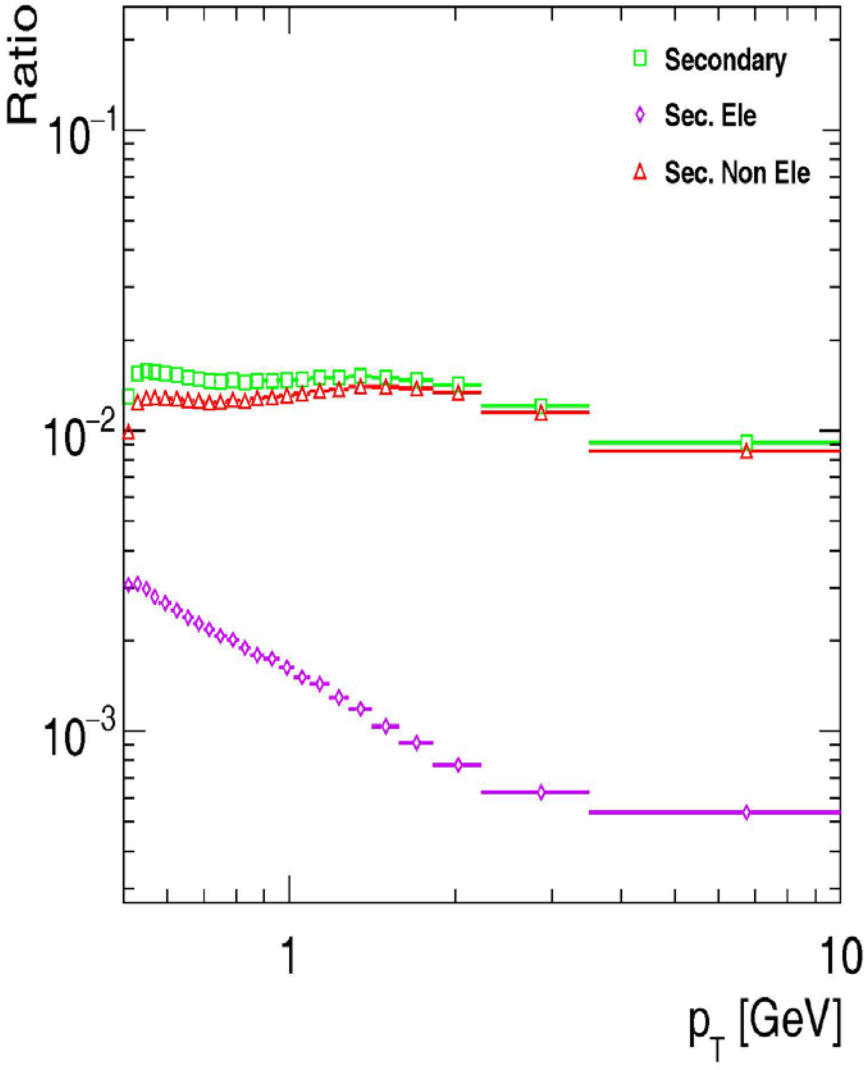

Run1: Secondary tracks Fractions vs p_T

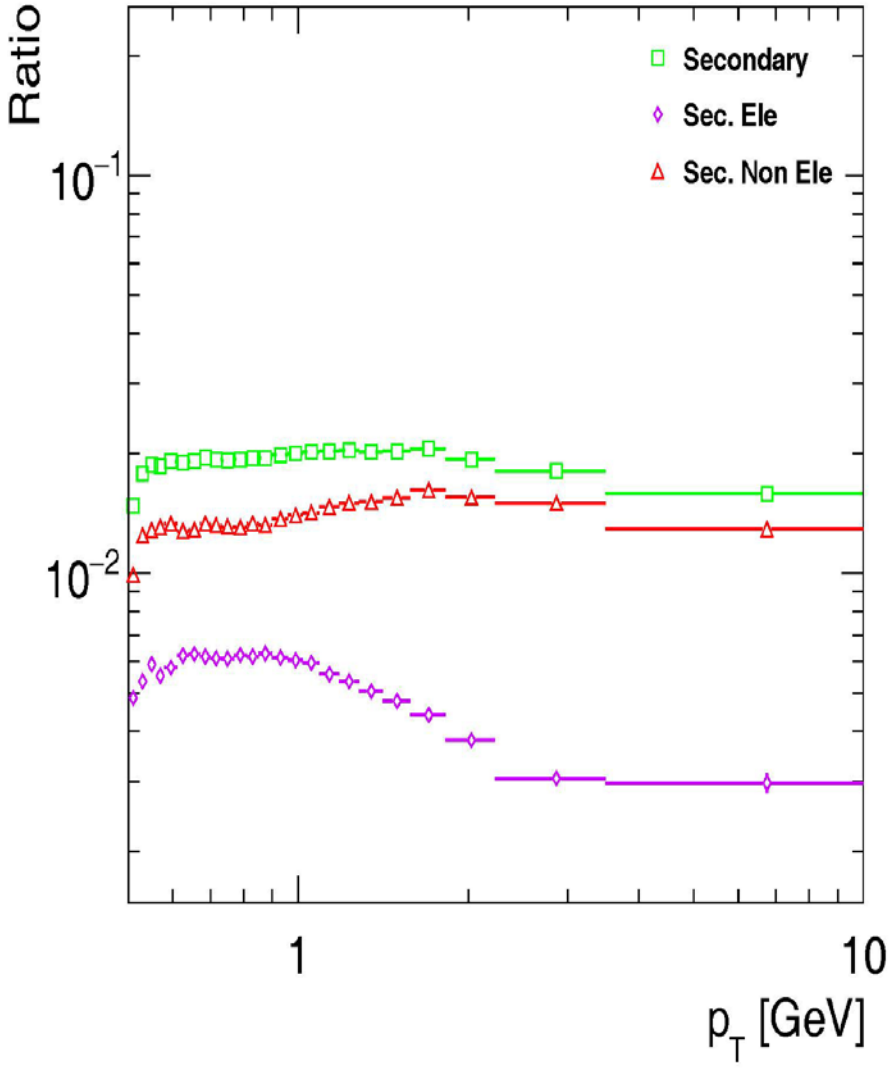

Fraction of Secondary tracks for $|d_0|<1.5$ mm and $|z_0 \sin\Theta|<1.5$ mm vs n_{sel}

Run2: Secondary tracks Fractions vs n_{sel}

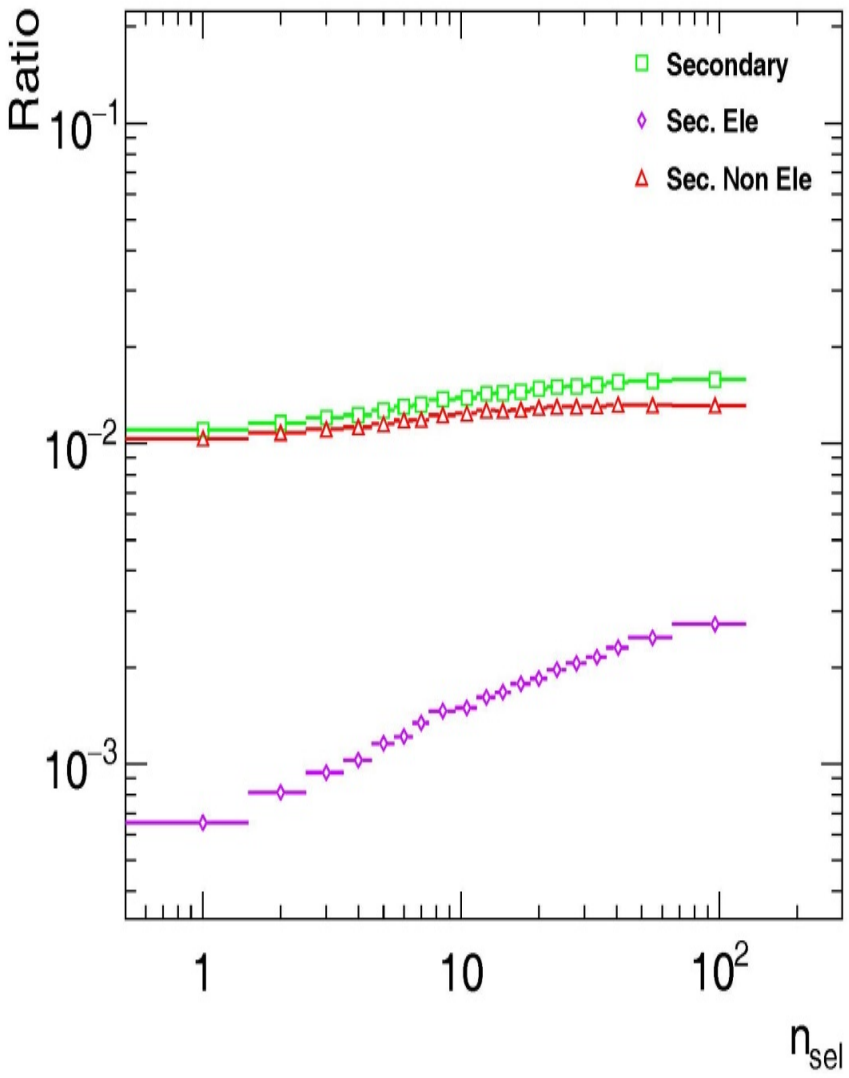

Run1: Secondary tracks Fractions vs n_{sel}

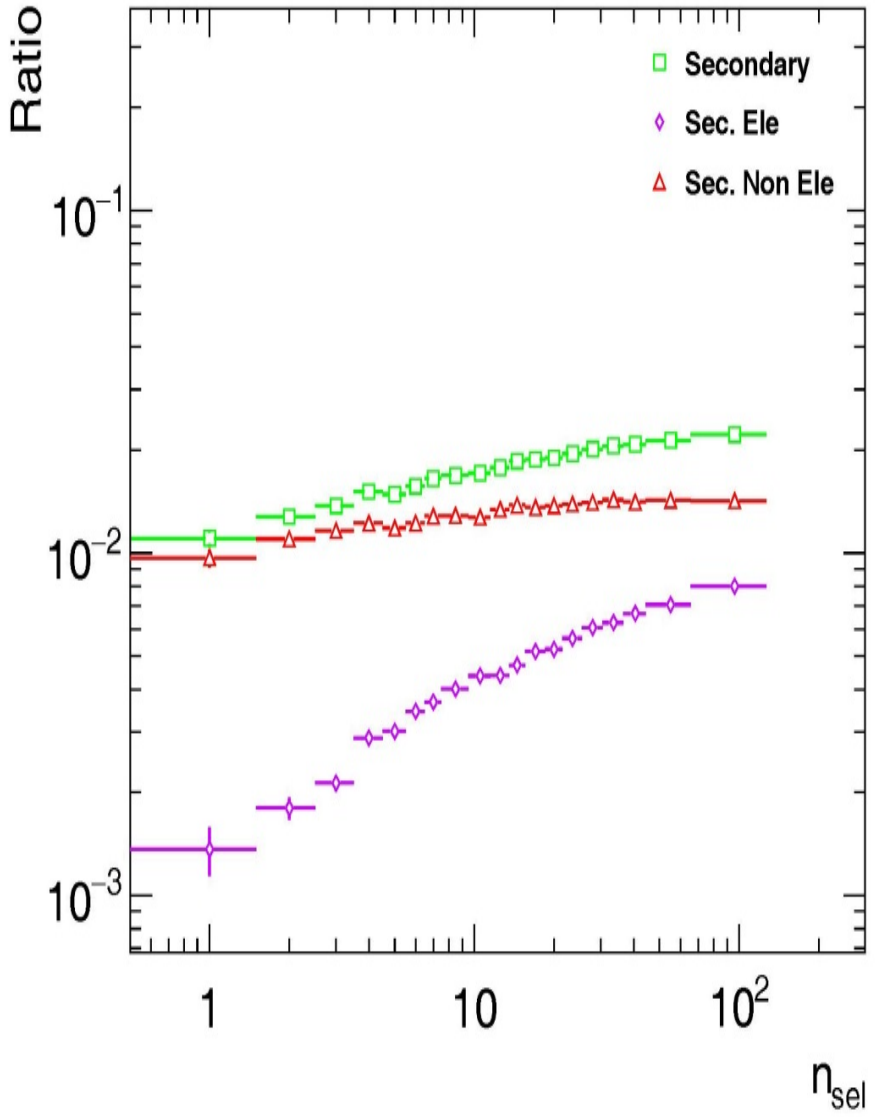

Convolution of Gaussian with Gaussian For $\sigma(d_0)$ and $\sigma(z_0 \sin\Theta)$

$$P_{IP \otimes BS} = \frac{C}{\sqrt{2\pi(\sigma_{IP}^2 + \sigma_{BS}^2)}} e^{-\frac{(x-(\mu_{IP}+\mu_{BS}))^2}{2(\sigma_{IP}^2+\sigma_{BS}^2)}}$$

1. The beam spot resolution for d_0:

$$\sigma_{BS}(d_0) = \sigma_{BS}.$$

2. The beam spot resolution for z_0:

$$\sigma_{BS}(z_0) = \sigma_{BS} ctg\Theta.$$

3. The beam spot resolution for $z_0 \sin\Theta$:

$$\sigma_{BS}(z_0 \sin\Theta) = \sigma_{BS} \cos\Theta.$$

Reprocessing. Selected tracks. Resolution of IP $d_0$vs p_T

Deconvolution. Resolution of IP d_0 vs p_T

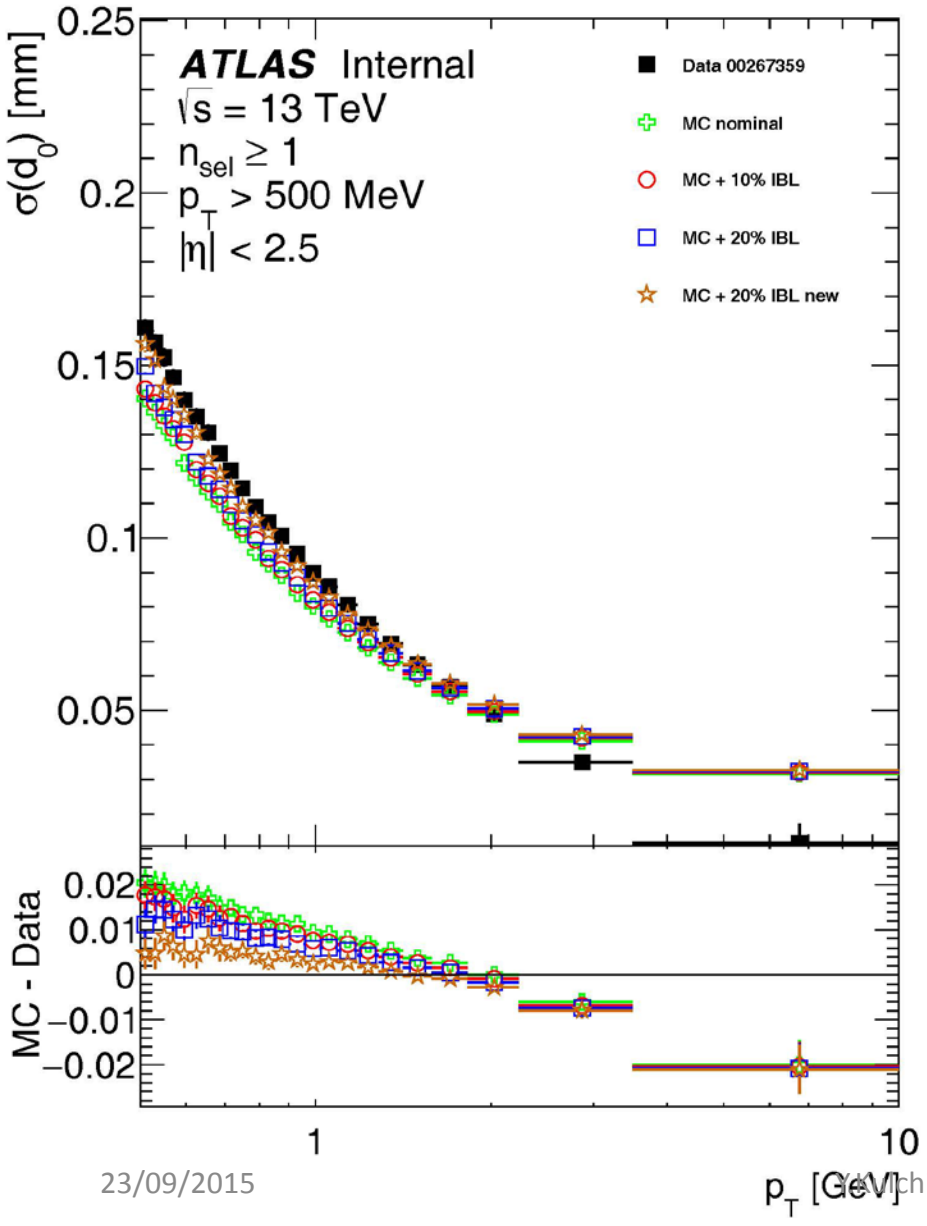

Resolution of IP d_0 vs p_T

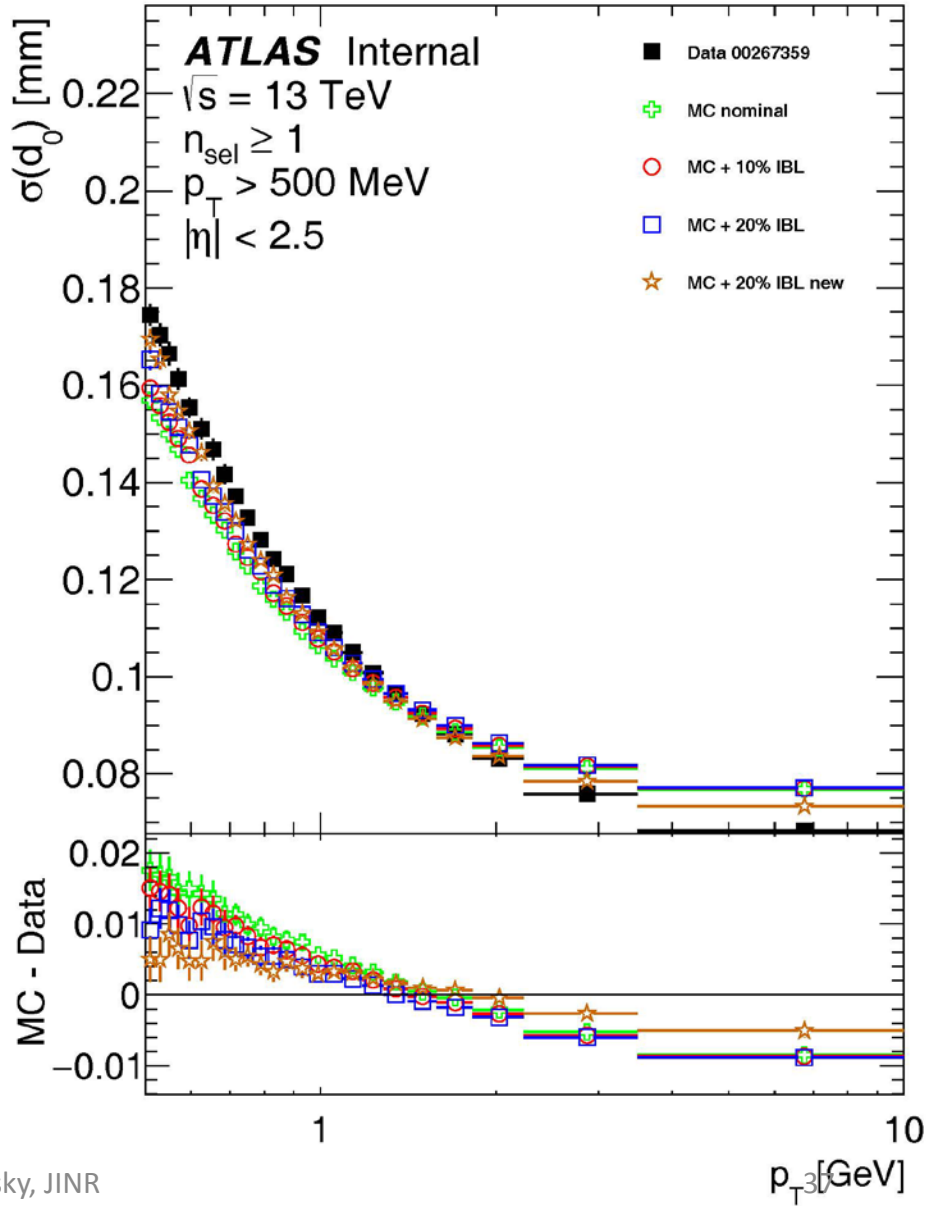

Reprocessing. Selected tracks. Resolution of IP d_0 vs n_{sel}

Deconvolution. Resolution of IP d_0 vs n_{sel}

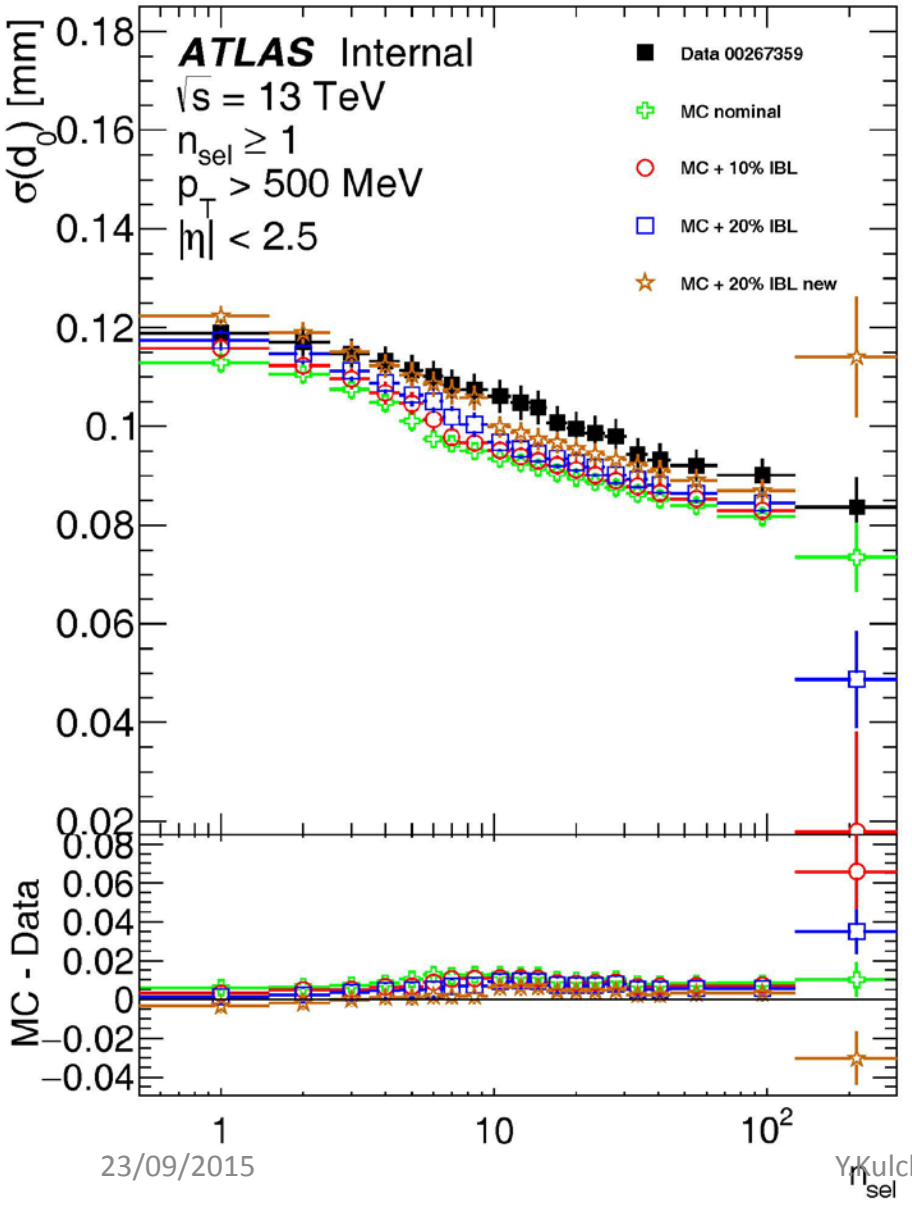

Resolution of IP d_0 vs n_{sel}

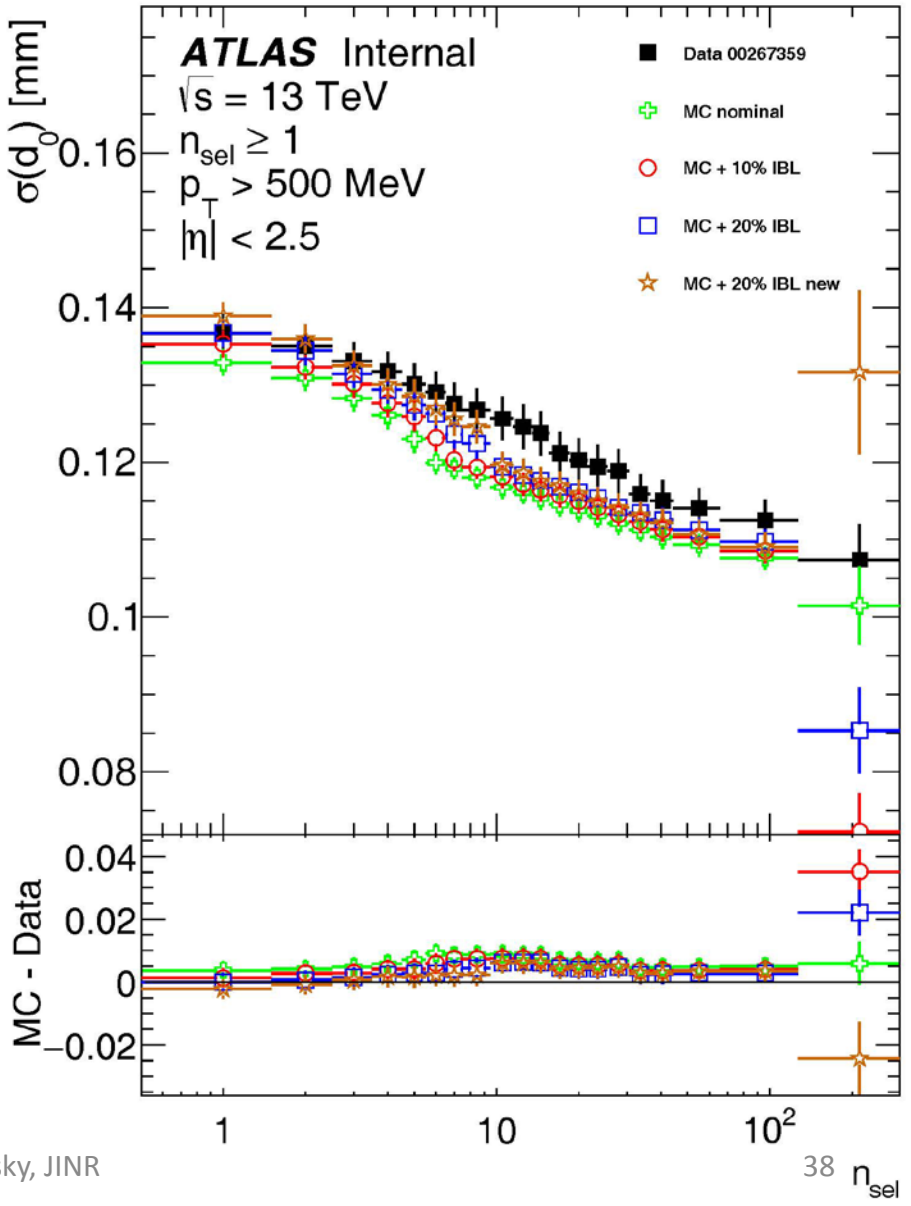

Reprocessing. Selected tracks. Resolution of IP d_0 vs $1/p_T^2 \sin\Theta$

Deconvolution. Resolution of IP d_0 vs $1/p_T^2 \sin\Theta$

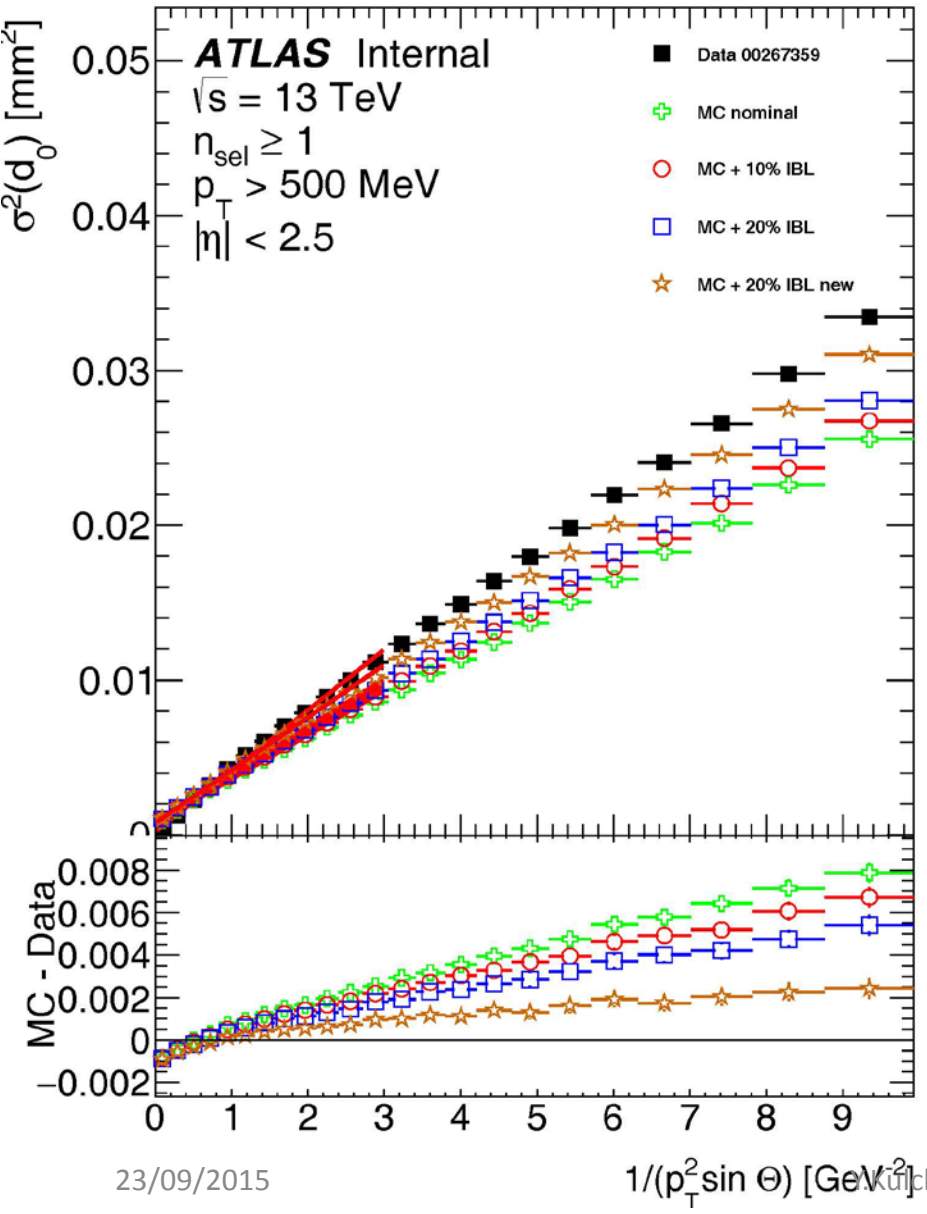

Resolution of IP d_0 vs $1/p_T^2 \sin\Theta$

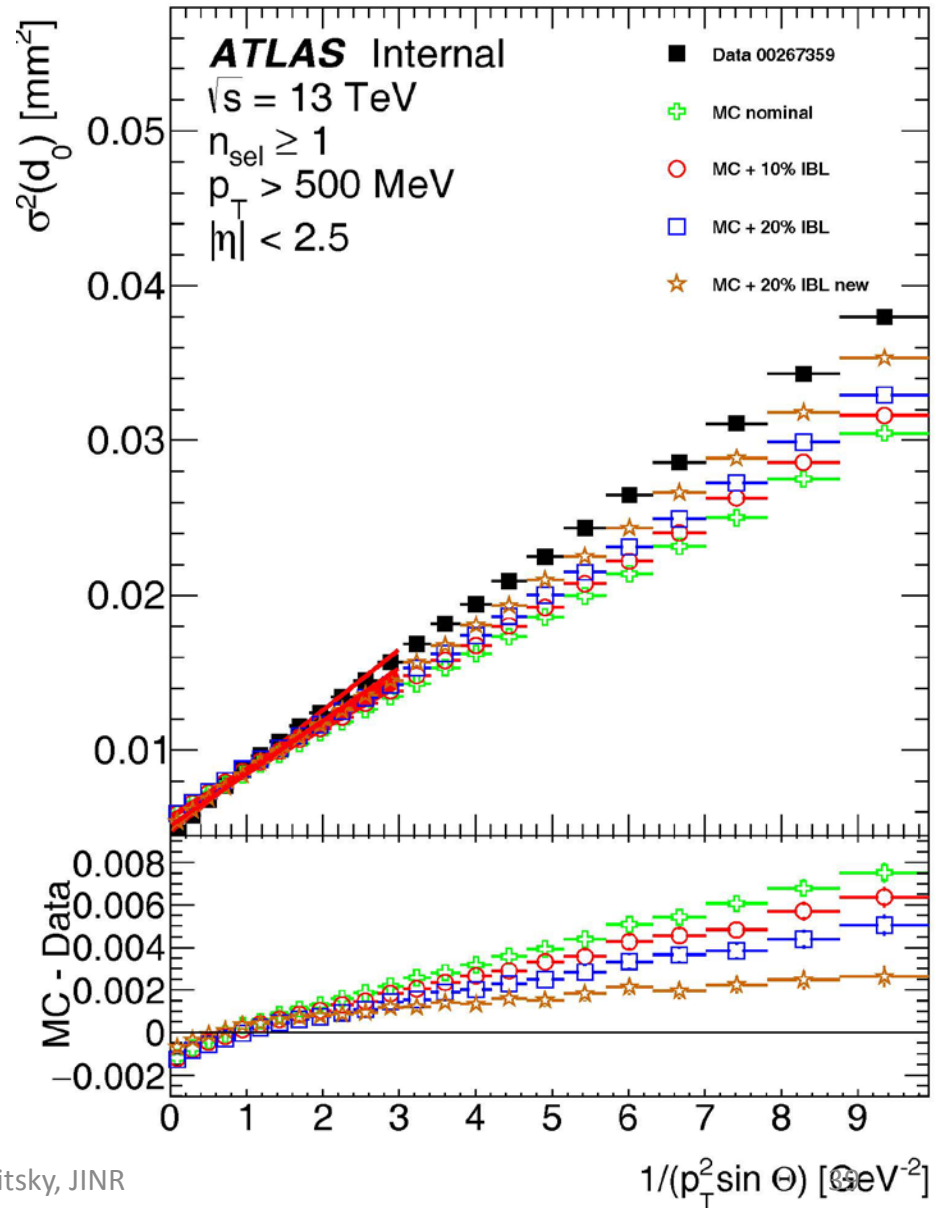

Distributions of $z_0 \sin\Theta$ and Track Fractions for η-region

Run2: Track Fractions for $z_0 \sin\Theta$ distribution for $|\eta| \approx 0$

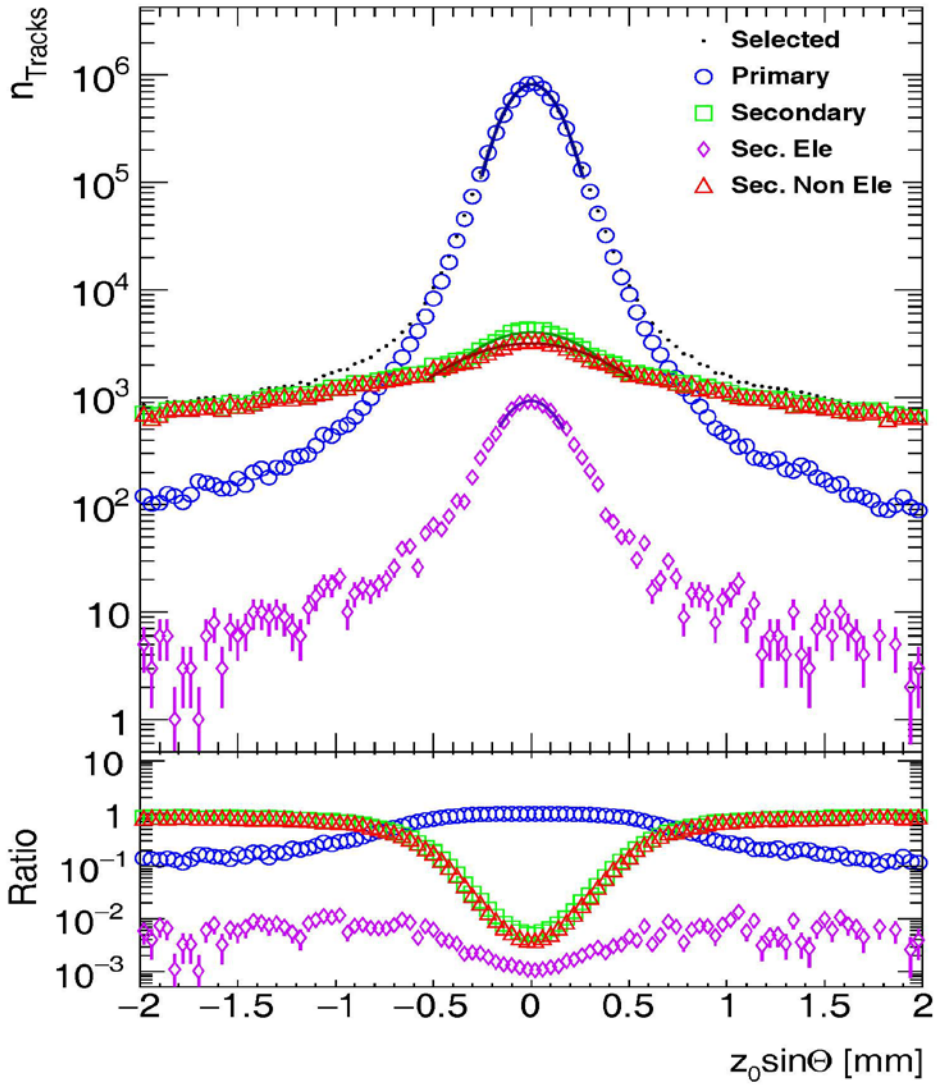

Run1: Track Fractions for $z_0 \sin\Theta$ distribution for $|\eta| \approx 0$

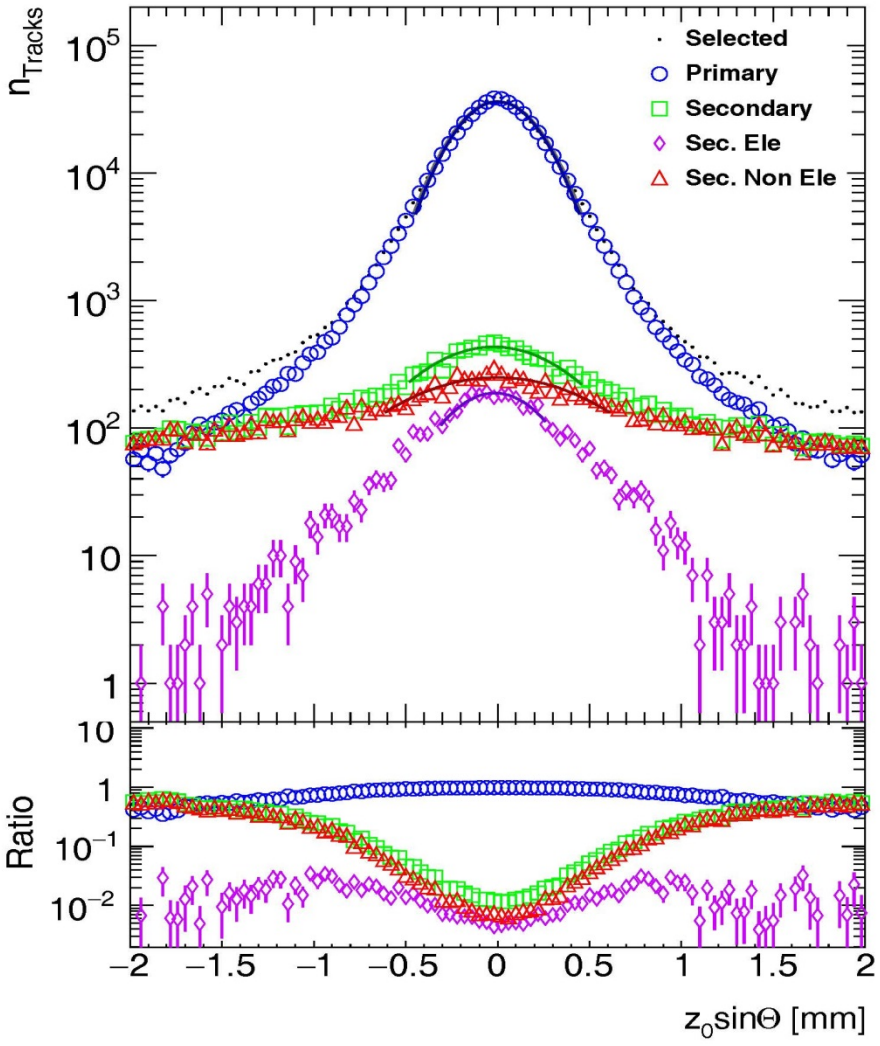

Reprocessing. Selected tracks. Resolution of IP $z_0 \sin\Theta$ vs η

Deconvolution. Resolution of IP $z_0 \sin\Theta$ vs η

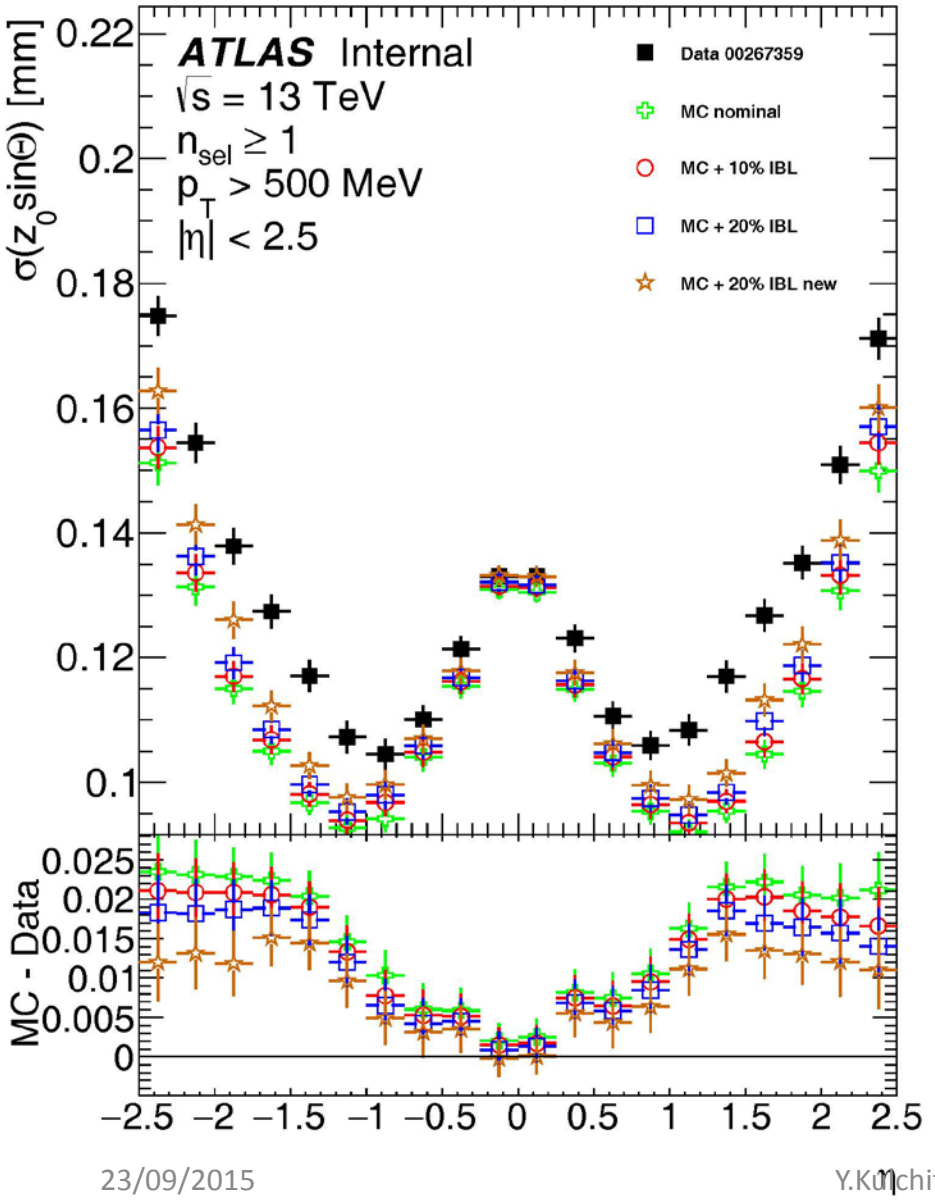

Resolution of IP $z_0 \sin\Theta$ vs η

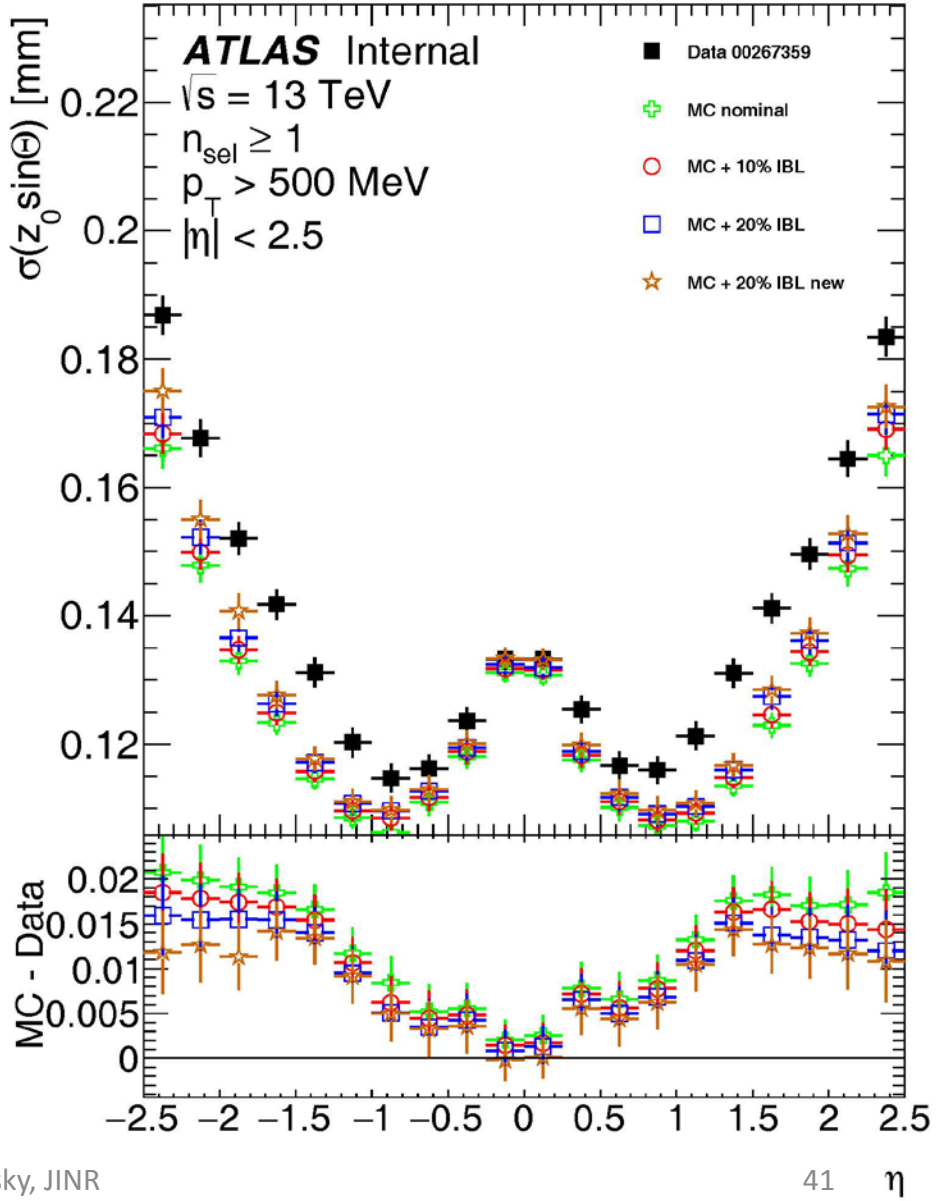

Reprocessing. Selected tracks. Resolution of IP $z_0 \sin\Theta$ vs p_T

Deconvolution. Resolution of IP $z_0 \sin\Theta$ vs p_T

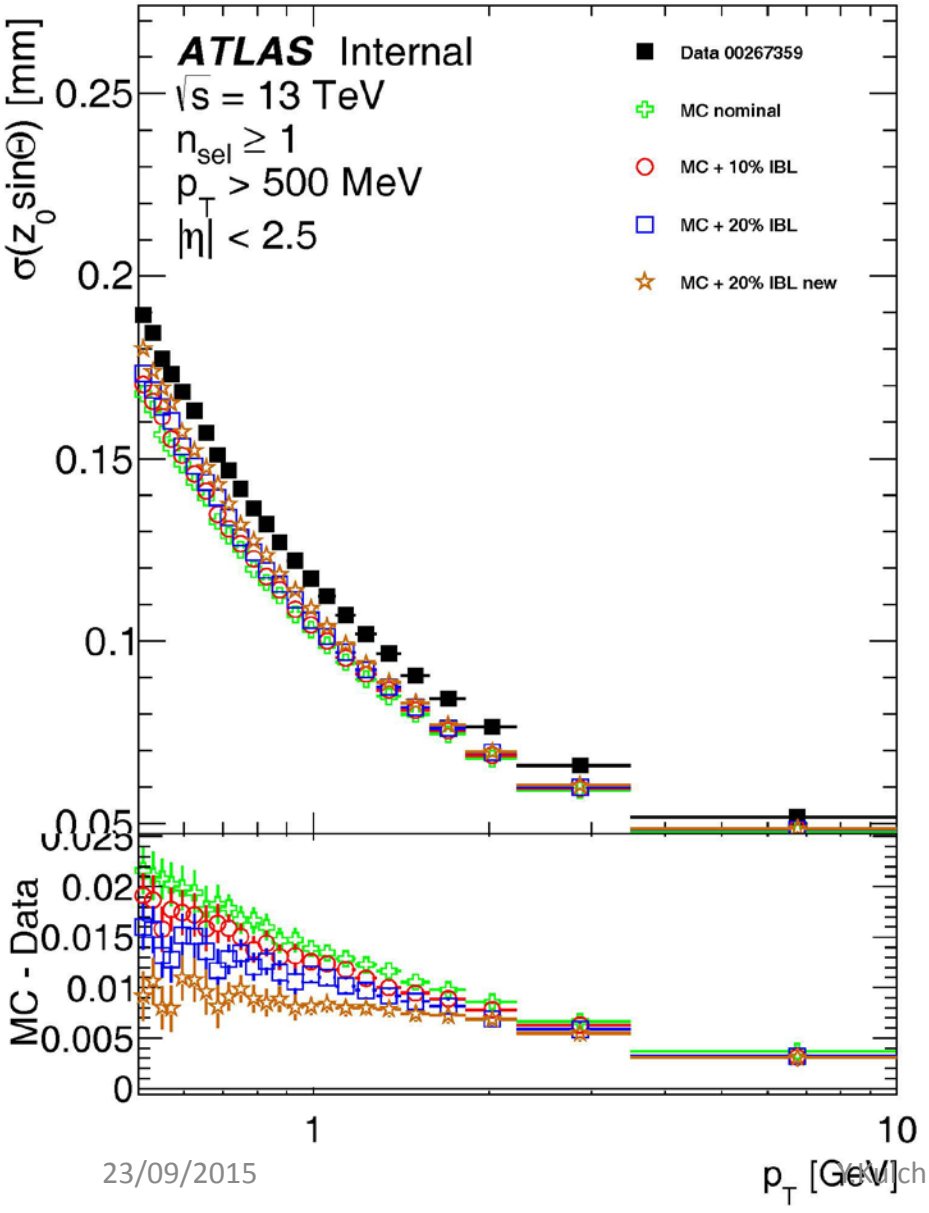

Reprocessing. Resolution of IP $z_0 \sin\Theta$ vs p_T

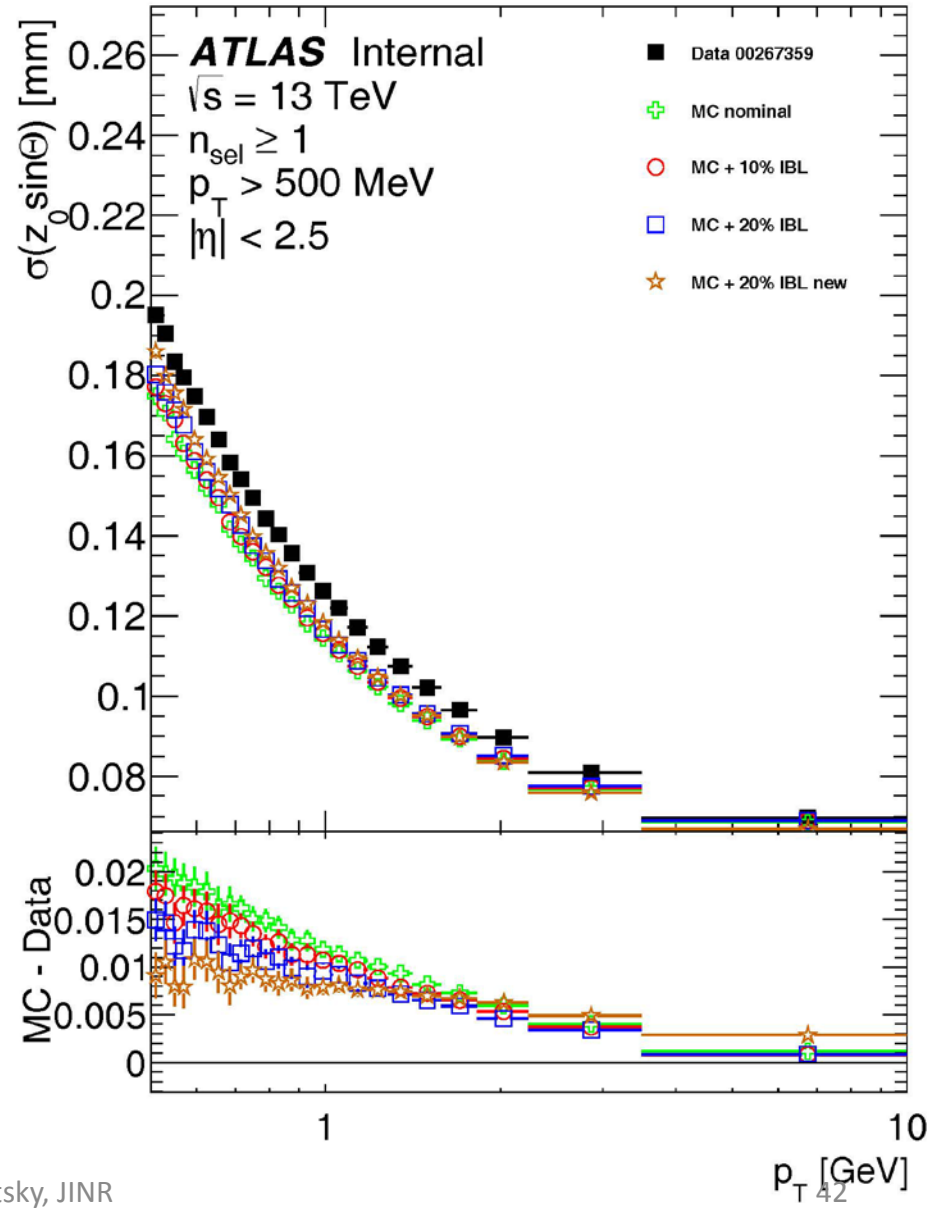

Reprocessing. Selected tracks. Resolution of IP $z_0 \sin\Theta$ vs n_{sel}

Deconvolution. Resolution of IP $z_0 \sin\Theta$ vs n_{sel}

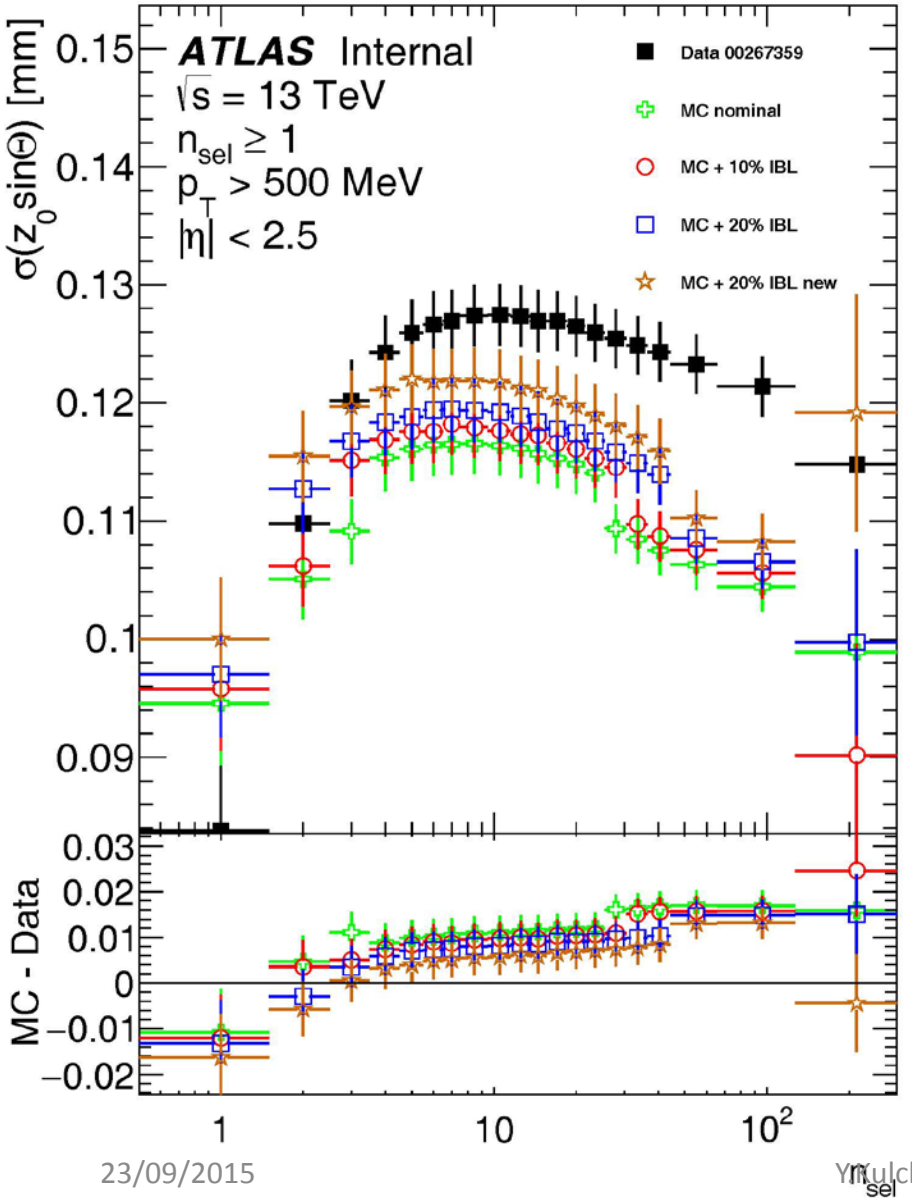

Resolution of IP $z_0 \sin\Theta$ vs n_{sel}

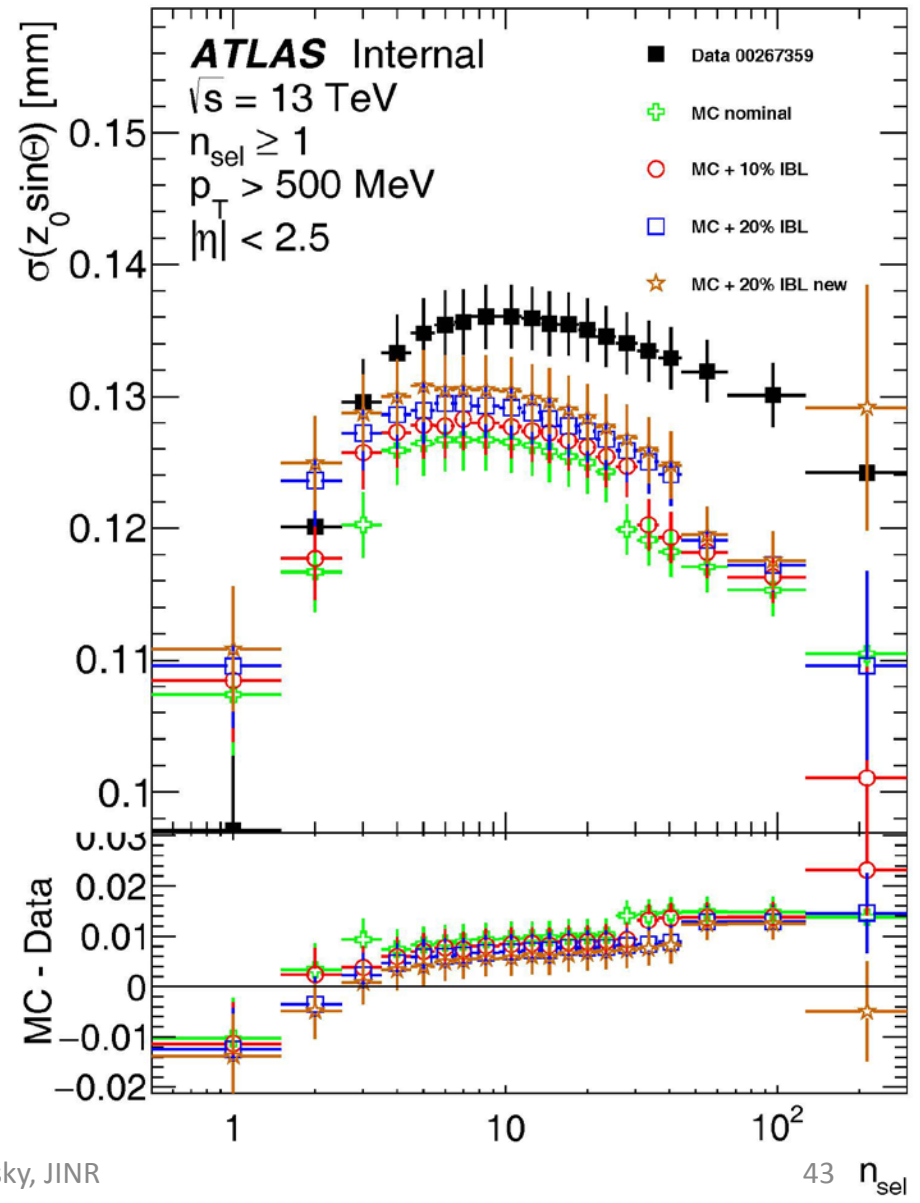

Reprocessing. Selected tracks. Resolution of IP $z_0 \sin\Theta$ vs $1/p_T^2 \sin\Theta$

Deconvolution. Resolution of IP $z_0 \sin\Theta$ vs $1/p_T^2 \sin\Theta$

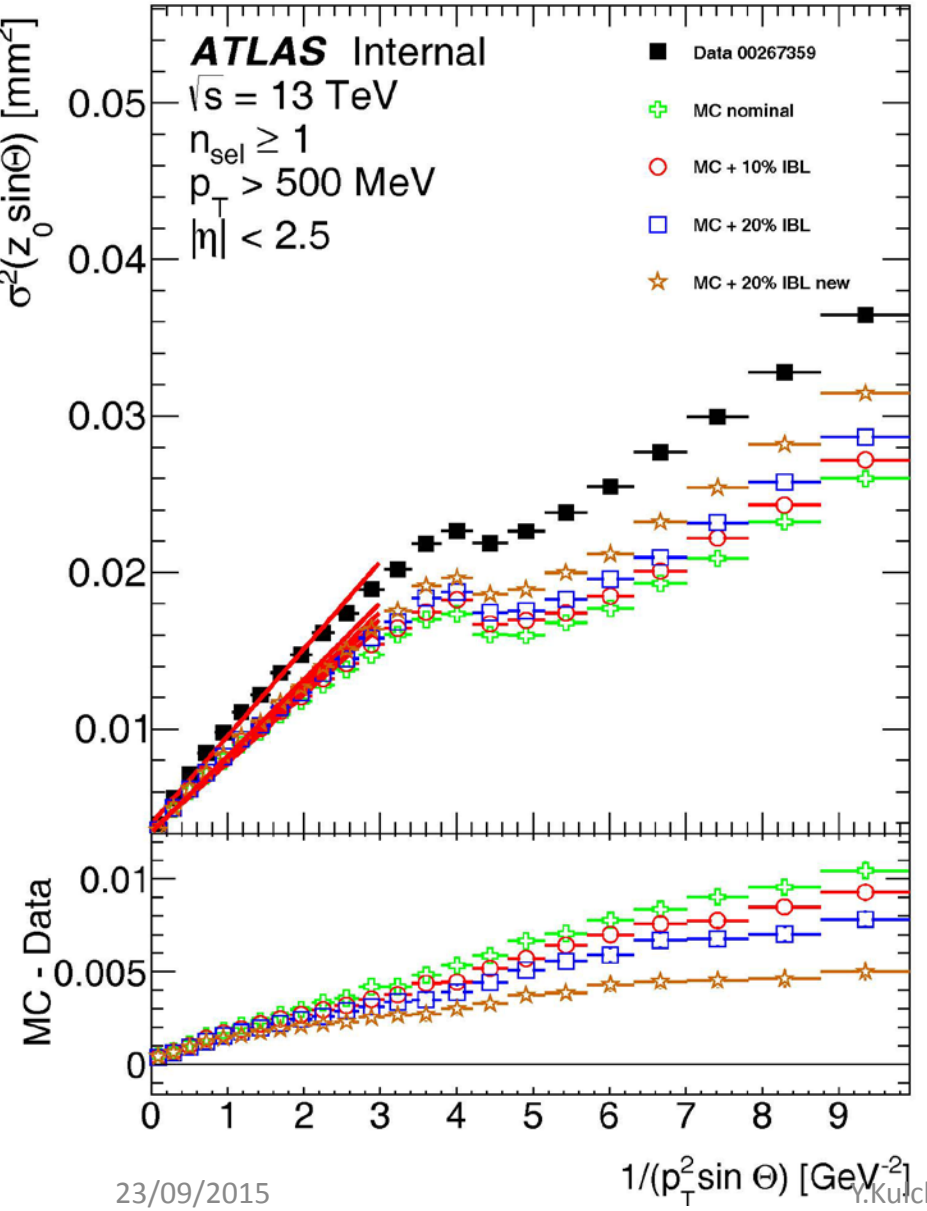

Reprocessing. Resolution of IP $z_0 \sin\Theta$ vs $1/p_T^2 \sin\Theta$

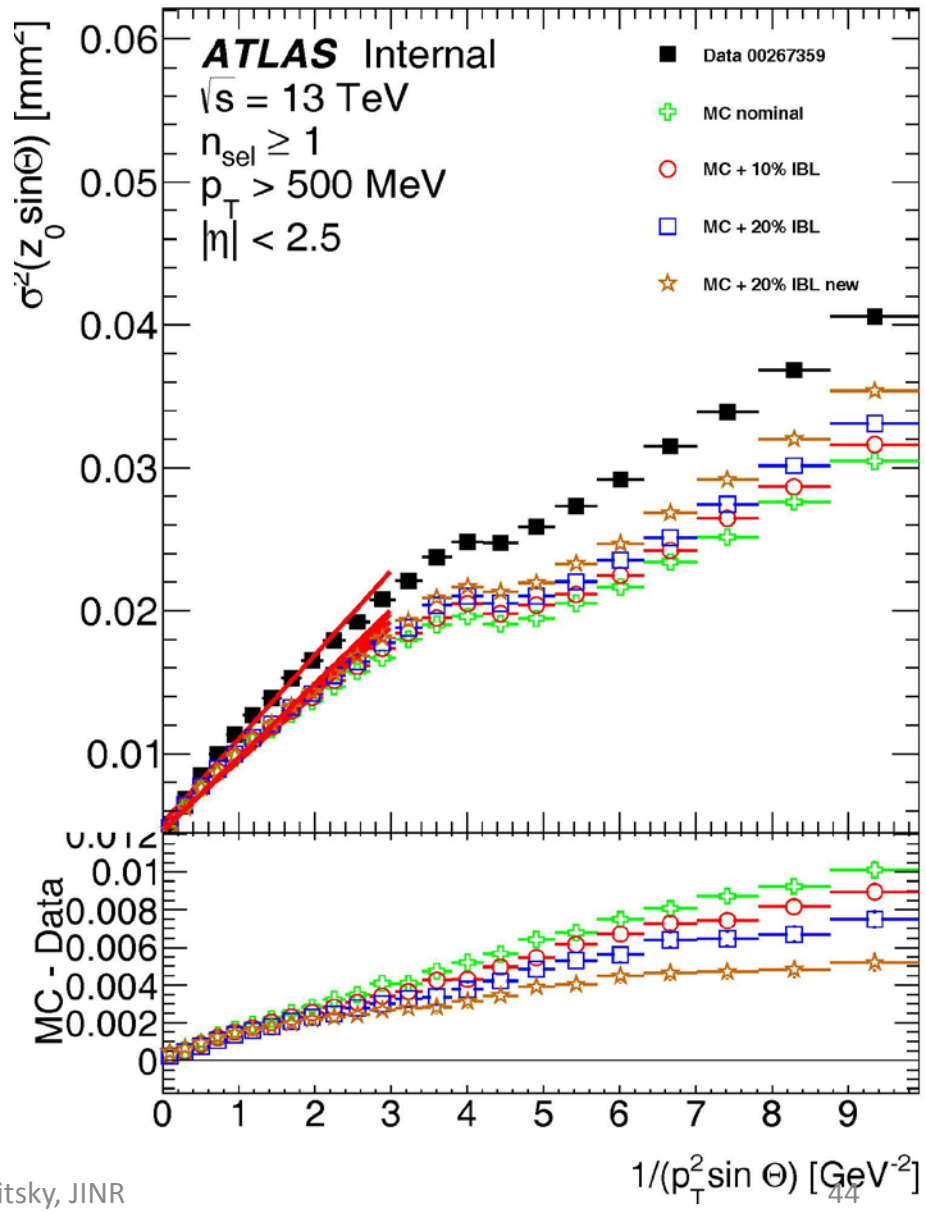

Study of Impact Parameters Resolution in the ATLAS Inner Detector
Motivation

Analysis of transverse Impact Parameter distributions (d_0, z_0) within the ATLAS Inner Detector for all, primary and secondary tracks with the aim of characterizing the

- IP Resolution vs. η, n_{ch} and p_T
- Misalignment vs. η
- Material budget vs. η (nominal, +2.5%, +5%, +10% additional materials)
- Fractions of secondary tracks (electrons and non-electrons)
- Comparison results for Run2 geometry with Run1 geometry

Finite single point resolution

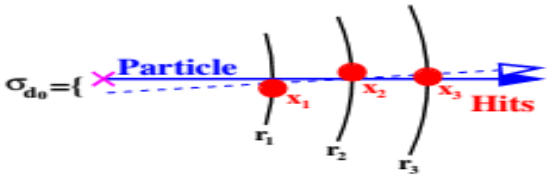

- Linear fit: $f(r) = r \cdot s + t$ (rz-plane or neglecting B)
- Error on the offset $t \longrightarrow$ impact parameter resolution

$$\sigma_{d_0} = \frac{\sqrt{\sum \left(\sum r_l^2 - r_i \sum r_k\right)^2}}{n \sum r_i^2 - \sum r_l \sum r_k} \sigma_{\mathrm{SP}} = \alpha$$

Multiple scattering

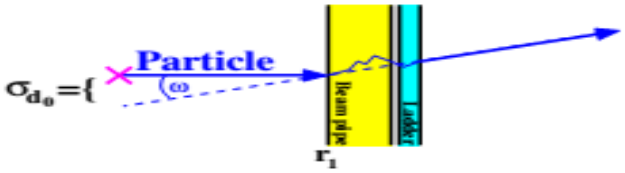

Scattering at thin layers:

$$\sigma_\theta = \frac{13.6\,\mathrm{MeV}}{\beta cp} z \sqrt{\frac{x}{X_0}} \left[1 + 0.038 \ln\left(\frac{x}{X_0}\right)\right]$$

R.M. Barnett et al., PDG, Phys. Rev. D54 (1996) 1

Impact parameter resolution:

$$\sigma_{d0} = \int \frac{r_1}{\sin\theta} \tan\omega$$

$$\simeq \frac{1}{cp \sin\theta \sqrt{\sin\theta}} \int \underbrace{r_1 13.6\,\mathrm{MeV} \sqrt{\frac{x}{X_0}} \left[1 + 0.038 \ln\left(\frac{x}{\sin\theta\, X_0}\right)\right]}_{\beta}$$

Impact Parameter resolutions $\sigma(d_0^{track}; z_0^{track})$

Divided Impact Parameter resolution into intrinsic detector resolution (including misalignment) and multiple scattering terms:

$$\sigma(d_0^{track}; z_0^{track}) = \sigma_{intrinsic} \oplus \sigma_{MS} \quad (1)$$

- Intrinsic detector resolution characterised the detector misalignment and primary vertex resolution. It is constant:

$$\sigma_{intrinsic} = \sigma_{misalignment} \oplus \sigma_{PV} \oplus \sigma_{detector} = \alpha \quad (2)$$

We know that $\sigma_{detector} << \sigma_{misalignment}$. The results of previous study is $\sigma_{PV} << \sigma_{misalignment}$

- Multiple scattering depends on amount of material in detector and momentum of particle:

$$\sigma_{MS} = \beta/(p_T^2 \sin\theta)^{1/2} \quad (3)$$

Full Impact Parameter resolution (formula for the fit):

$$\sigma^2(d_0^{track}; z_0^{track}) = \alpha^2 + \beta^2/(p_T^2 \sin\theta) \quad (4)$$

Run2. IP resolution of d_0 with Nominal material: **Selected tracks**

IP resolution of d_0 for $|\eta|<1.2$

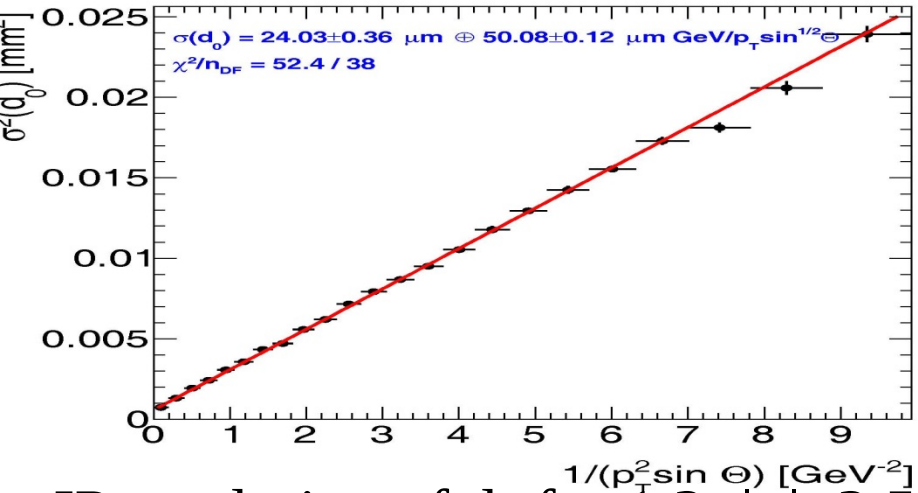

IP resolution of d_0 for $1.2<|\eta|<2.5$

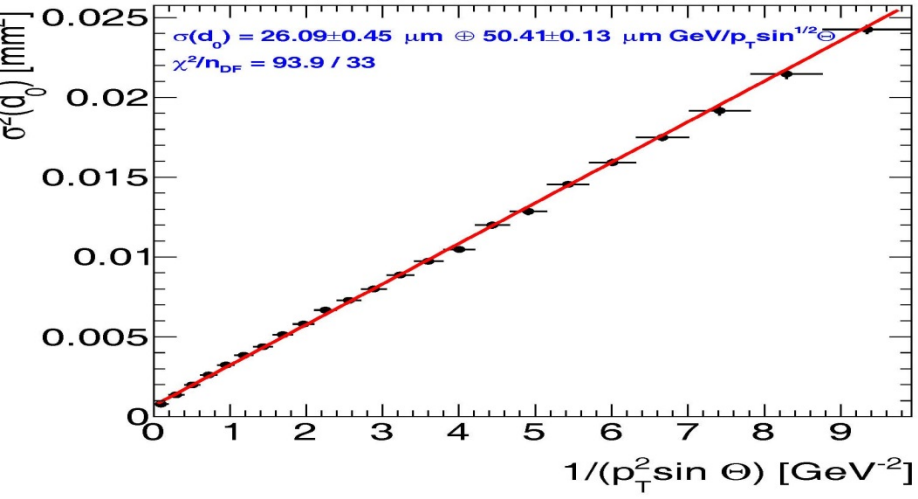

IP resolution of d_0 for $|\eta|<2.5$

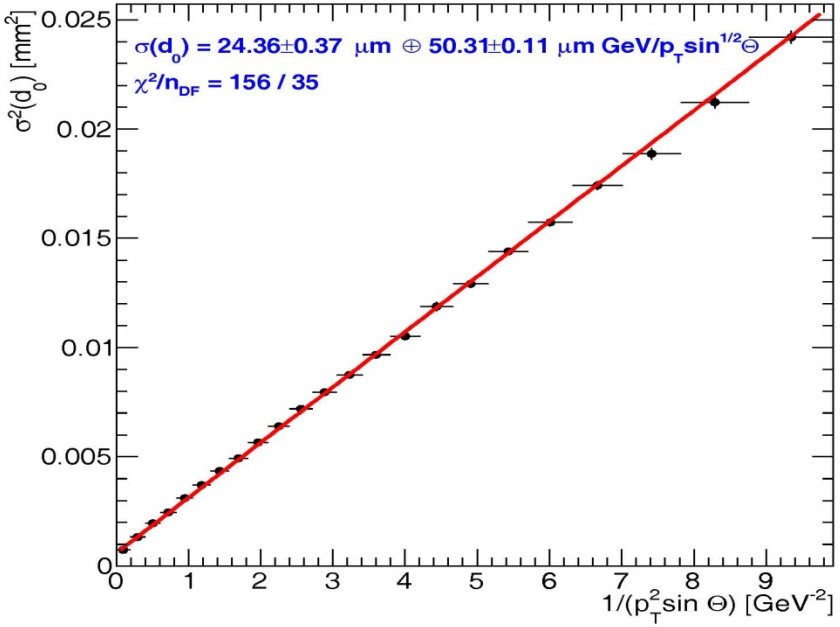

- Intercept of linear fit to resolution plot depends on alignment, and gradient depends on amount of multiple scattering (Material Budget)
- Parameter α increase on 8% from central to forward η-region.
- Parameter β does not depend from the η-region.

Impact Parameter resolution of $\mathbf{d_0}$, $z_0 \sin\Theta$ for Selected/Primary/Secondary tracks

Material *Type tracks*	η-region	$\alpha(d_0)$ [μm]	$\alpha(z_0\sin\Theta)$ [μm]	$\beta(d_0)$ [μm GeV]	$\beta(z_0\sin\Theta)$ [μm GeV]
ATLAS Run1	0.25<|η|<0.50	10	91	140	209
	1.50<|η|<1.75	12	71	240	263
Nominal *Run1 Selected*	|η|<2.5	27.7±0.8	80.8±2.4	108.3±0.2	115.4±1.1
	|η|<1.2	28.4±0.9	94.7±3.8	107.3±0.3	124.9±2.0
	1.2<|η|<2.5	29.1±0.8	33.5±0.9	108.6±0.2	106.0±0.4
Nominal *Selected*	|η|<2.5	24.4±0.4	72.1±2.8	50.3±0.1	71.7±1.6
	|η|<1.2	24.0±0.4	77.8±2.9	50.1±0.1	78.1±1.6
	1.2<|η|<2.5	26.1±0.5	50.2±2.8	50.4±0.1	66.8±1.5
Nominal *Primary*	|η|<2.5	24.5±0.4	71.3±2.9	49.8±0.1	70.7±1.6
	|η|<1.2	24.2±0.5	76.6±3.0	49.6±0.2	77.4±1.7
	1.2<|η|<2.5	26.2±0.7	50.0±2.6	49.9±0.2	66.3±1.4
Nominal *Secondary Non-electron*	|η|<2.5	302±15	379±17	314±11	190±19
	|η|<1.2	315±21	380±19	325±16	220±20
	1.2<|η|<2.5	224±16	319±18	298±10	177±17
Nominal *Secondary Electron*	|η|<2.5	40.8±2.3	54.0±4.5	98.5±0.9	63.1±2.4
	|η|<1.2	40.1±2.5	53.3±5.7	97.2±0.9	71.5±3.2
	1.2<|η|<2.5	34.2±4.7	35.2±5.8	77.8±1.3	56.2±2.5

Impact Parameter resolution of $\mathbf{d_0}$, $z_0\sin\Theta$ for additional material

Material *Type tracks*	η-region	$\alpha(d_0)$ [μm]	$\alpha(z_0\sin\Theta)$ [μm]	$\beta(d_0)$ [μm GeV]	$\beta(z_0\sin\Theta)$ [μm GeV]
Nominal *Selected*	|η|<2.5	24.4±0.5	72.5±2.9	50.3±0.2	71.5±1.7
	|η|<1.2	24.3±0.8	78.4±3.1	49.9±0.2	77.4±1.8
	1.2<|η|<2.5	26.0±0.7	50.6±2.7	50.4±0.2	66.9±1.5
+2.5% *Selected*	|η|<2.5	24.3±0.4	73.7±3.1	51.1±0.1	71.1±1.7
	|η|<1.2	24.7±0.6	79.3±3.2	50.5±0.2	78.1±1.8
	1.2<|η|<2.5	25.0±0.5	50.1±3.1	51.3±0.1	67.9±1.6
+5% *Selected*	|η|<2.5	24.3±0.5	73.9±3.2	51.8±0.1	72.6±1.8
	|η|<1.2	24.8±0.7	80.0±3.4	51.1±0.2	78.7±1.8
	1.2<|η|<2.5	25.0±0.5	49.9±3.1	52.0±0.1	69.2±1.6

1. The Alignment (α) for d_0 does not dependence from additional materials.
2. The Alignment (α) for $z_0\sin\Theta$ increase on 2% when additional materials is +5%.
3. The Material Budget (β) for d_0 increase on 3% when additional materials is +5%.
4. The Material Budget (β) for $z_0\sin\Theta$ increase on 1.5% when additional materials is +5%.

Misalignment — new constants

Use values for residual misalignment from post M8 error-scaling

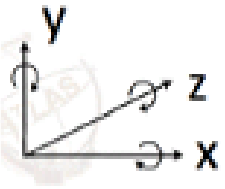

- Fixing all rotational DoF -> allowing no displacement
- Fixing local z for all modules (radial) -> allowing no displacement
- Max deviation of a single module 200 μm
- 4 new sets of constants using random misalignment by drawing from a Gaussian centred at the true module position with width σ:
  1. σ is equal to M8 residual misalignment (most conservative)
  2. σ (IBL) same as case 1, others scaled by 0.33
  3. σ scaled by 0.33 with respect to case 1
  4. σ scaled by 0.10 with respect to case 1

} realistic precision for low μ run

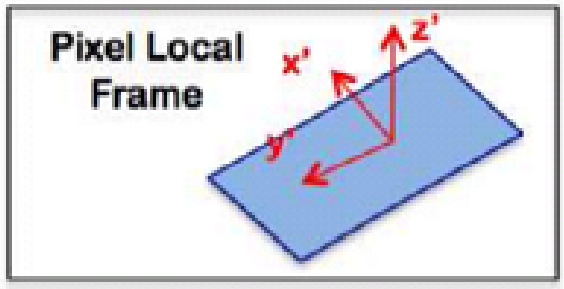

all numbers in μm

	local x	local y
IBL	40	50
PIX-barrel	15	60
PIX-EC	90	110
SCT-barrel	75	—
SCT-EC	125	—

Analysis of K_s^0

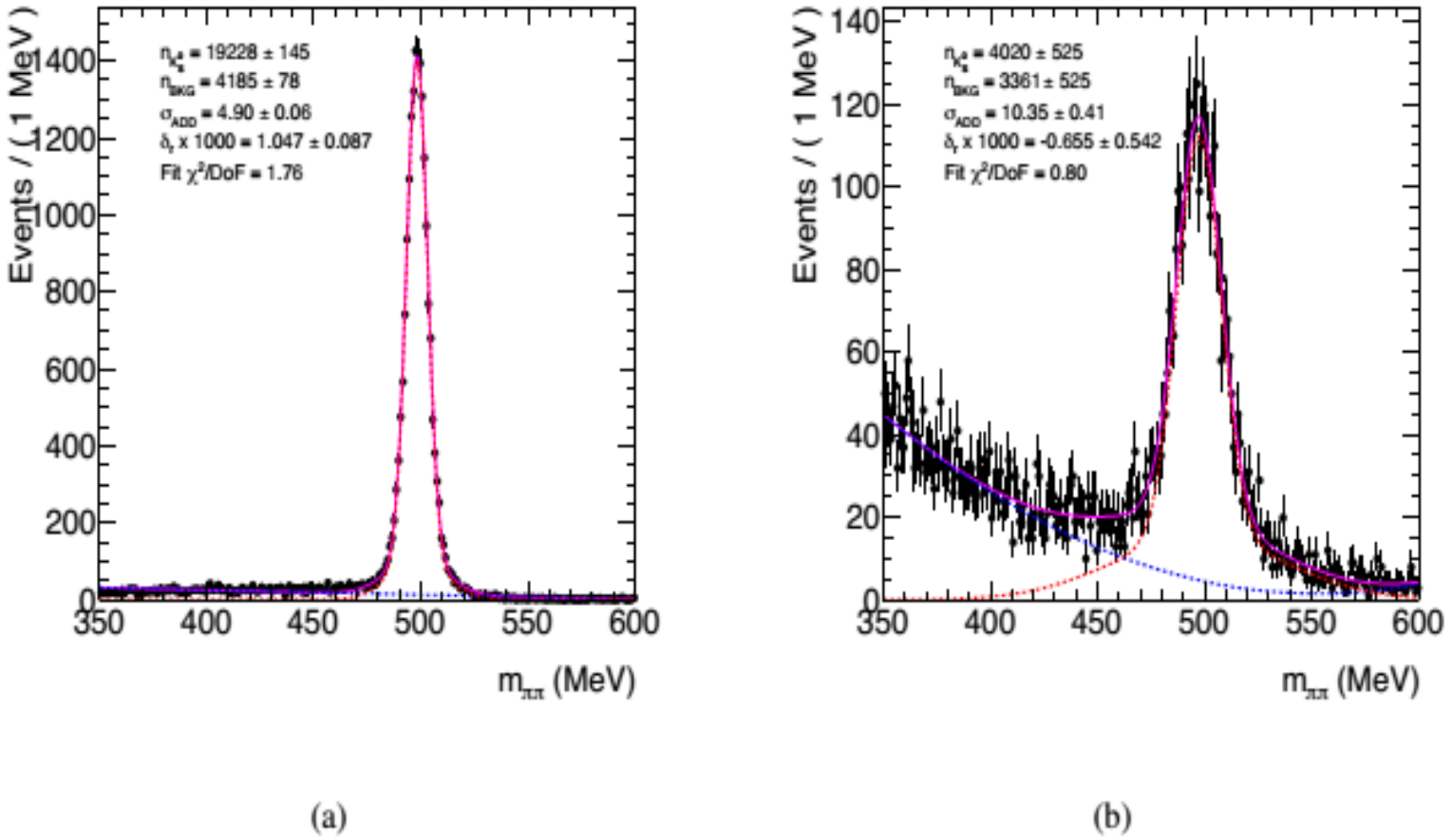

Figure 108: Sample fits to the reconstructed K_s^0 mass spectrum in a low background region and high background region

Analysis of K_s^0 vs φ

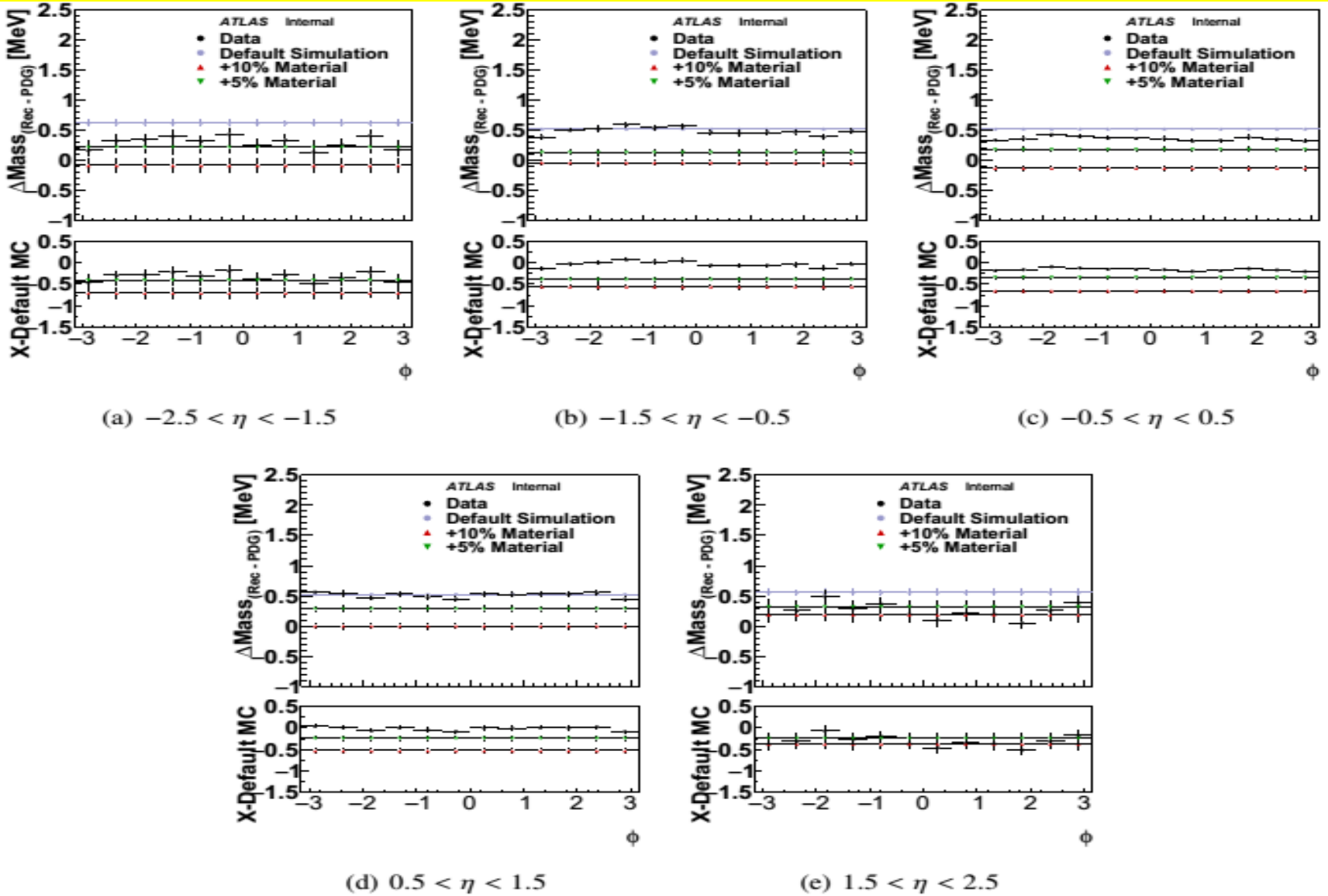

(a) $-2.5 < \eta < -1.5$ (b) $-1.5 < \eta < -0.5$ (c) $-0.5 < \eta < 0.5$

(d) $0.5 < \eta < 1.5$ (e) $1.5 < \eta < 2.5$

Figure 109: Reconstructed K_s^0 mass a function of ϕ in data and various MC samples. The directions are defined by the momentum vector of the K_s^0 candidate. The K_s^0 candidates are required to have a reconstructed decay radius of greater than 5 mm and $\cos\theta > 0.999$. For the MC samples the reconstructed mass is average across all ϕ. Only

Charged-particle multiplicities as a function of the η. I

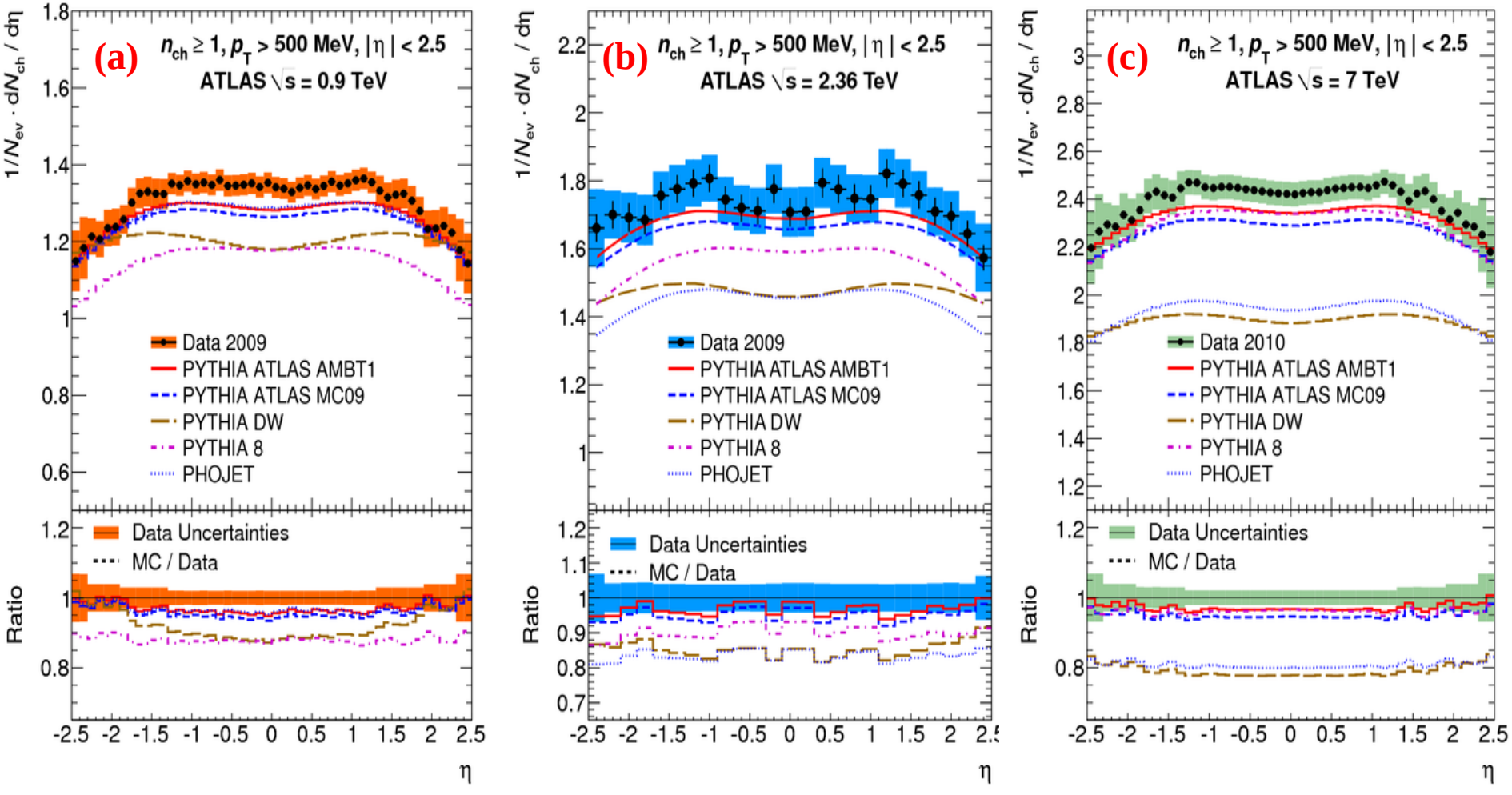

Charged-particle multiplicities as a function of the pseudorapidity for events with nch >=1, pt > 500 MeV and |eta| < 2.5 at √s = 0.9 (a), 2.36 (b) and 7 TeV (c). The dots represent the data and the curves the predictions from different MC models. The vertical bars represent the statistical uncertainties, while the shaded areas show statistical and systematic uncertainties added in quadrature. The bottom inserts show the ratio of the MC over the data.

Charged-particle multiplicities as a function of the η. II

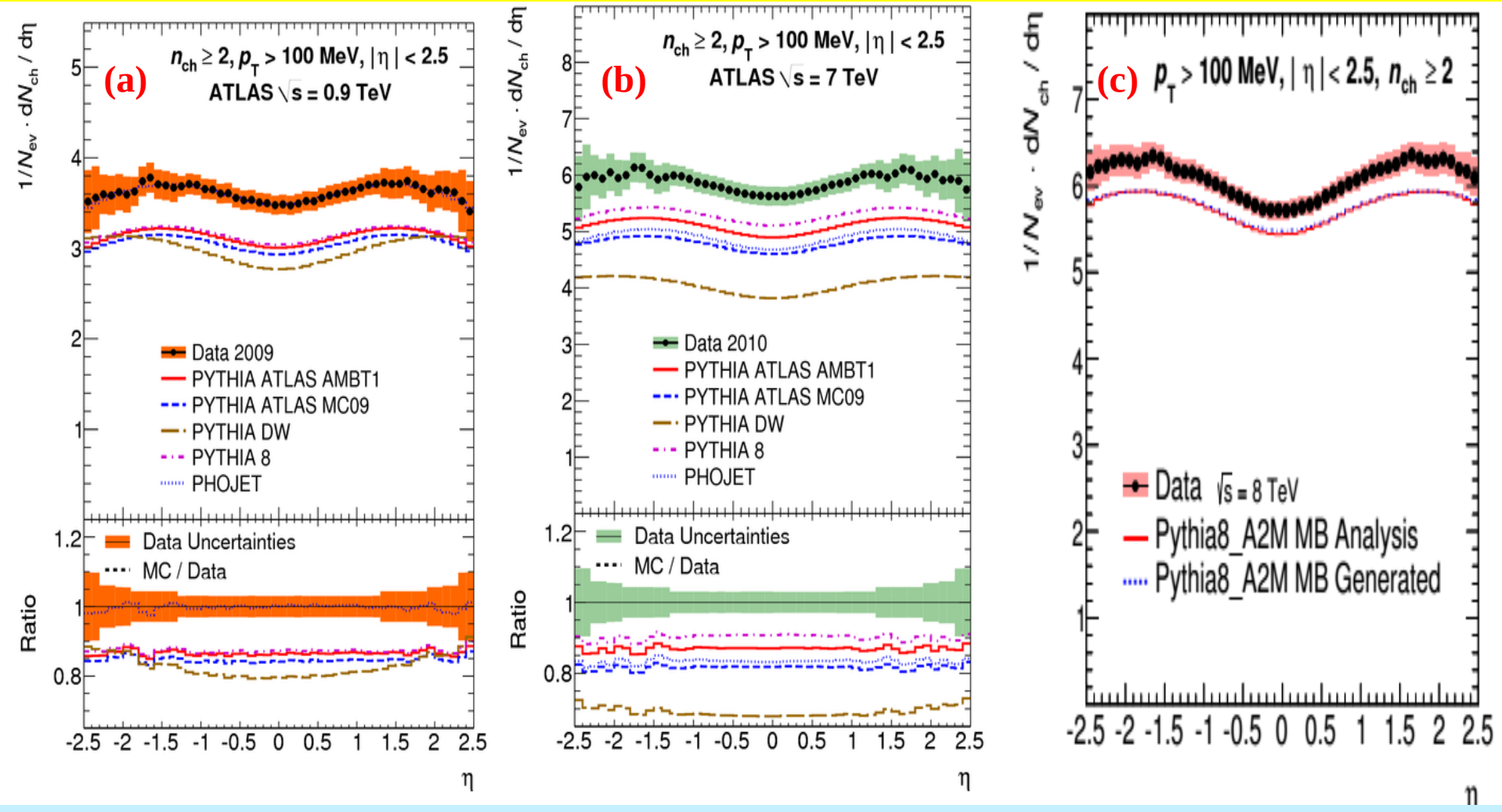

Charged-particle multiplicities as a function of the pseudorapidity for events with nch >=2, pt>100 MeV and |eta|<2.5 at √s = 0.9 (a), 7 (b) and 8 TeV (c). The dots represent the data and the curves the predictions from different MC models. The vertical bars represent the statistical uncertainties, while the shaded areas show statistical and systematic uncertainties added in quadrature. The bottom inserts show the ratio of the MC over the data.

Charged-particle multiplicities as a function of the p_T. I

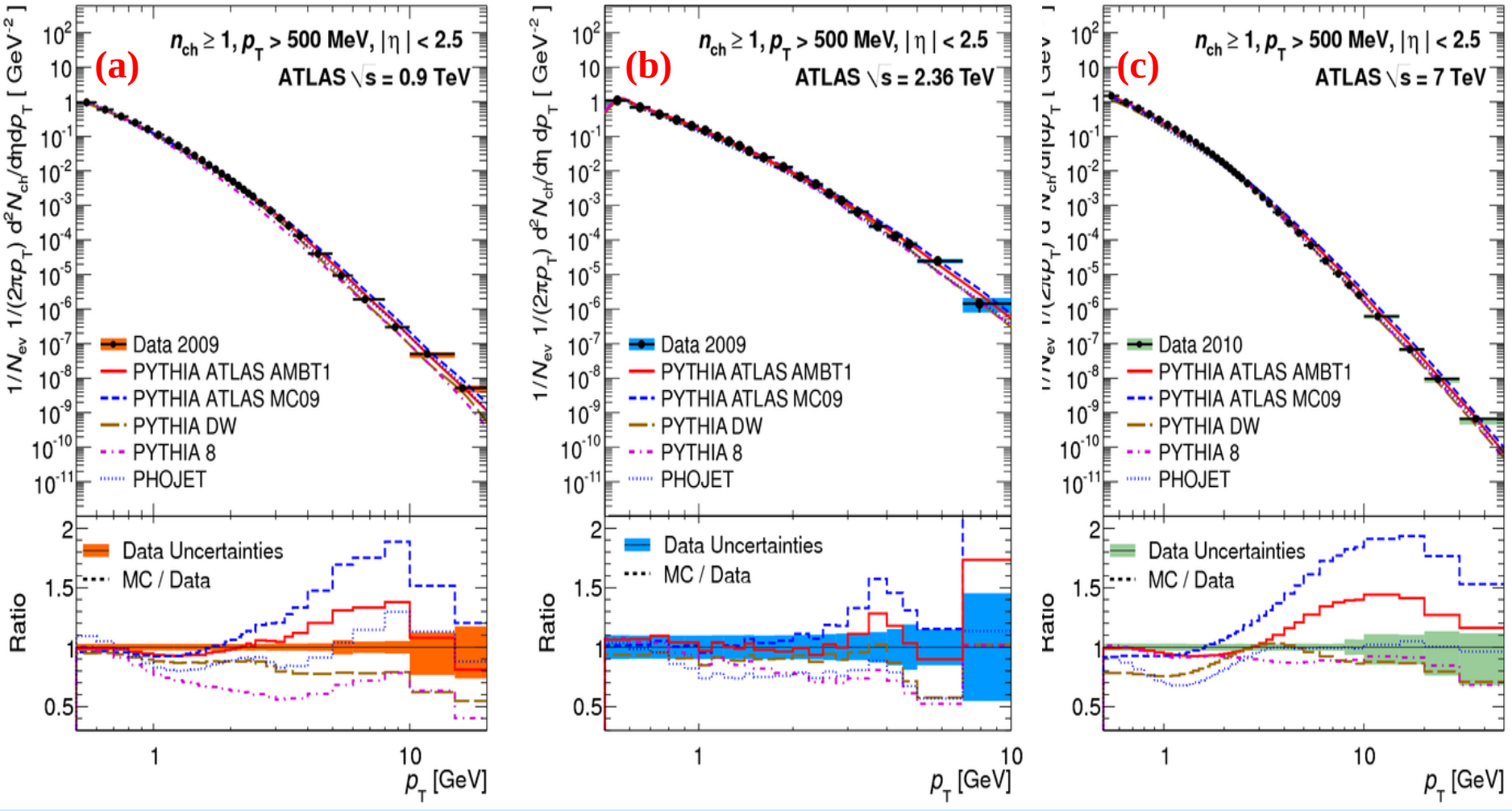

Charged-particle multiplicities as a function of the transverse momentum for events with nch >=1, pt>500 MeV and |eta| < 2.5 at √s = 0.9 (a), 2.36 (b) and 7 TeV (c). The dots represent the data and the curves the predictions from different MC models. The vertical bars represent the statistical uncertainties, while the shaded areas show statistical and systematic uncertainties added in quadrature. The bottom inserts show the ratio of the MC over the data.

Charged-particle multiplicities as a function of the p_T. II

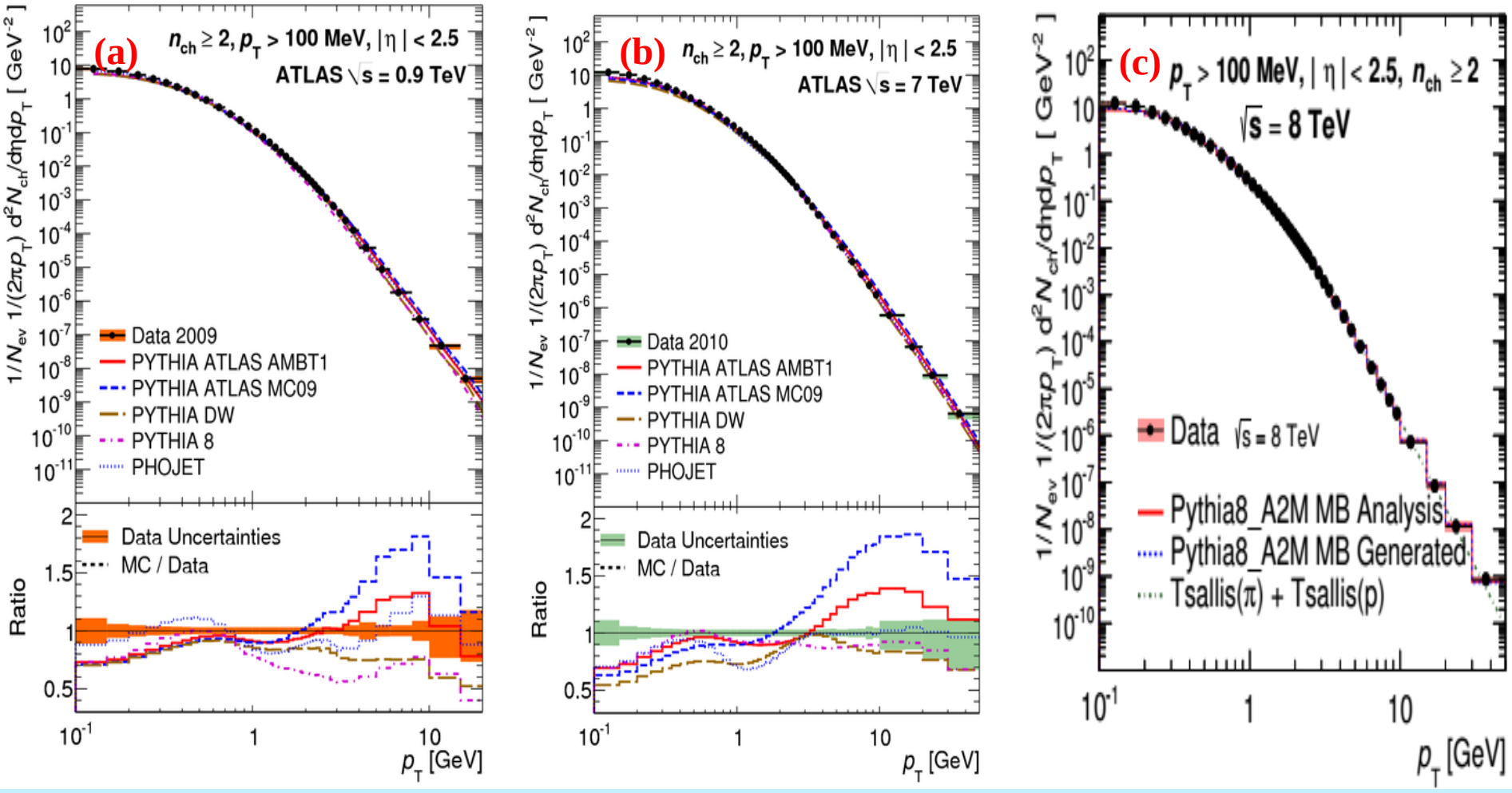

Charged-particle multiplicities as a function of the transverse momentum for events with nch >=2, pt > 100 MeV and |eta| < 2.5 at √s = 0.9 (a), 7 (b) and 8 TeV (c). The dots represent the data and the curves the predictions from different MC models. The vertical bars represent the statistical uncertainties, while the shaded areas show statistical and systematic uncertainties added in quadrature. The bottom inserts show the ratio of the MC over the data.

Charged-particle multiplicities distribution. I

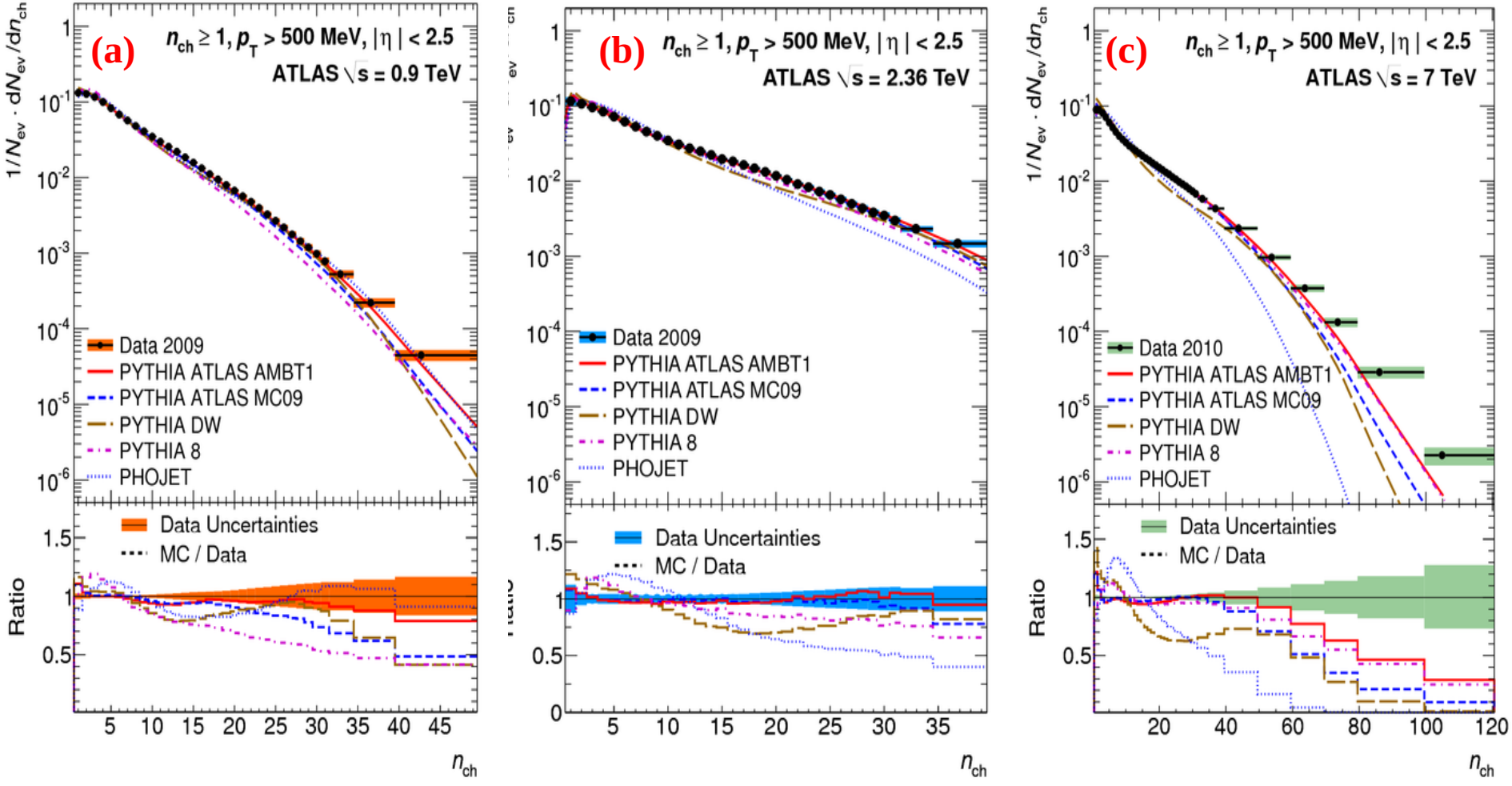

Charged-particle multiplicities distribution for events with nch>=1, pt>500 MeV and |eta|<2.5 at √s= 0.9 (a), 2.36 (b) and 7 TeV (c). The dots represent the data and the curves the predictions from different MC models. The vertical bars represent the statistical uncertainties, while the shaded areas show statistical and systematic uncertainties added in quadrature. The bottom inserts show the ratio of the MC over the data.

Charged-particle multiplicities distribution. II

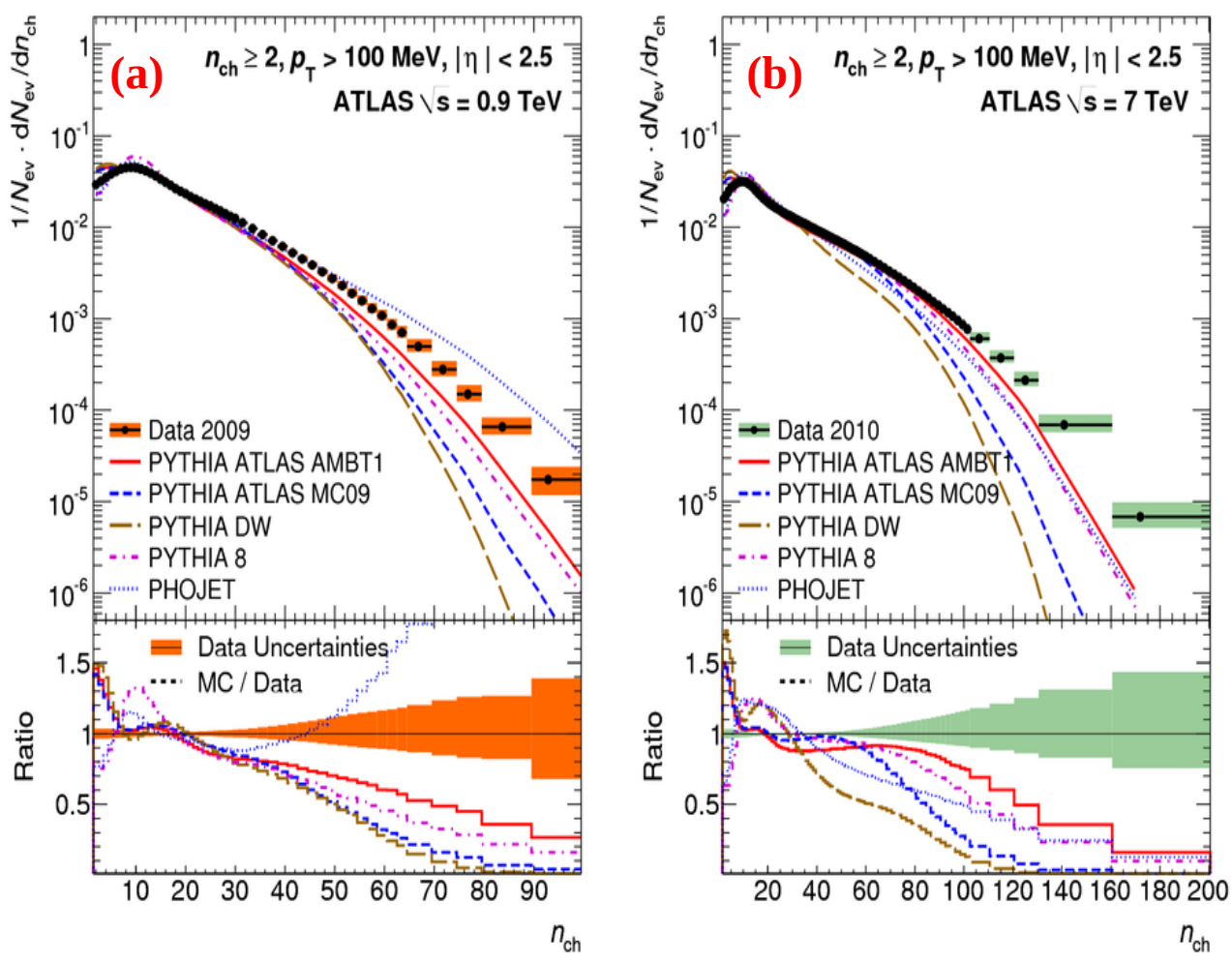

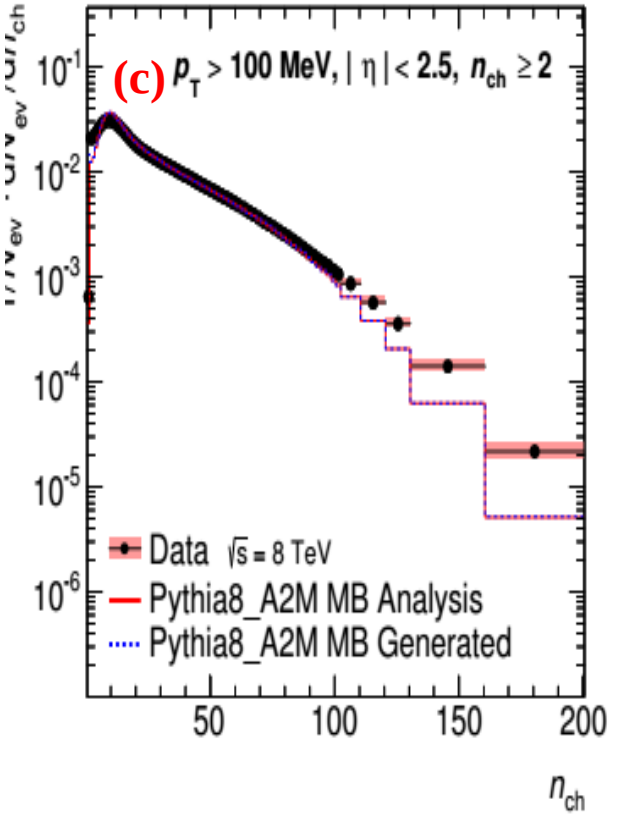

For increasing the multiplicity region at 13 TeV need to add HMT data

Charged-particle multiplicities distribution for events with nch>=2, pt>100 MeV and |eta|<2.5 at √s= 0.9 (a), 7 (b) and 8 TeV (c). The dots represent the data and the curves the predictions from different MC models. The vertical bars represent the statistical uncertainties, while the shaded areas show statistical and systematic uncertainties added in quadrature. The bottom inserts show the ratio of the MC over the data.

Average transverse momentum as a function multiplicities. I

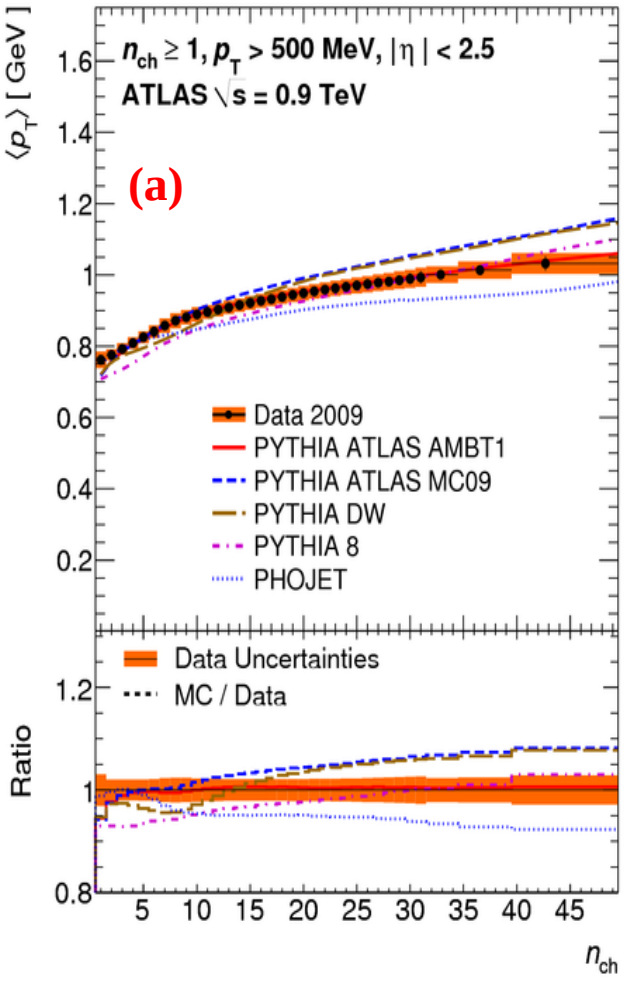

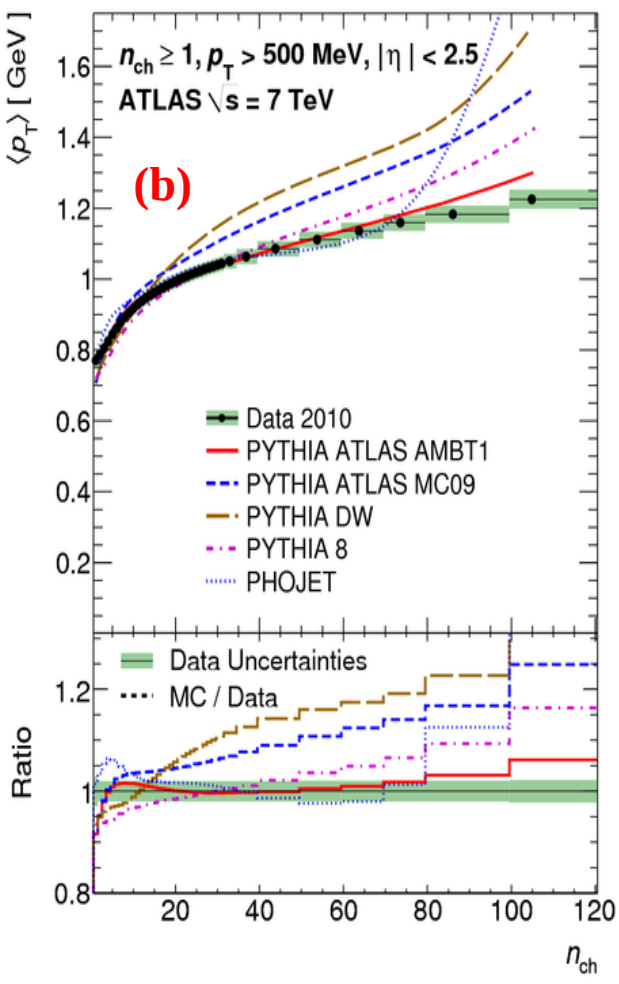

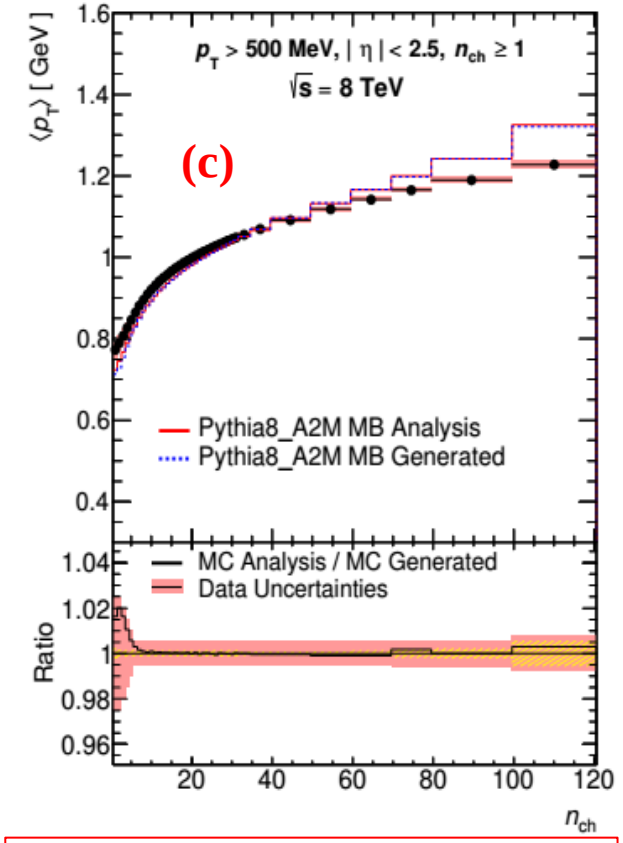

For increasing the multiplicity region at 13 TeV need to add HMT data

Average transverse momentum as a function of the number of charged particles in the event for events with nch>=1, pt>500 MeV and |eta|<2.5 at √s= 0.9 (a), 7 (b) and 8 TeV (c). The dots represent the data and the curves the predictions from different MC models. The vertical bars represent the statistical uncertainties, while the shaded areas show statistical and systematic uncertainties added in quadrature. The bottom inserts show the ratio of the MC over the data.

Average transverse momentum as a function multiplicities. II

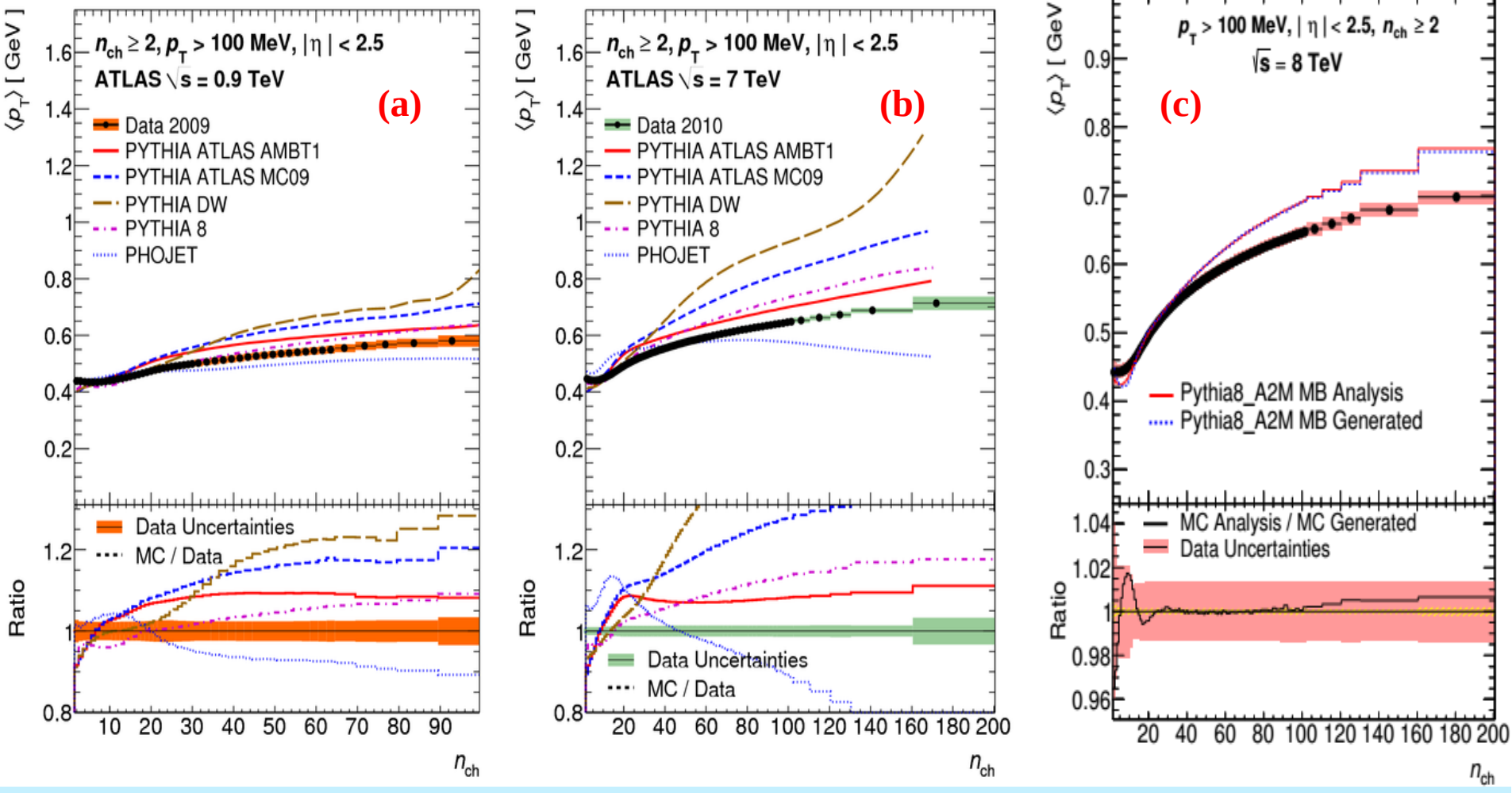

Average transverse momentum as a function of the number of charged particles in the event for events with nch>=2, pt>100 MeV and |eta|<2.5 at √s= 0.9 (a), 7 (b) and 8 TeV (c). The dots represent the data and the curves the predictions from different MC models. The vertical bars represent the statistical uncertainties, while the shaded areas show statistical and systematic uncertainties added in quadrature. The bottom inserts show the ratio of the MC over the data.

Average transverse momentum as a function multiplicities. III

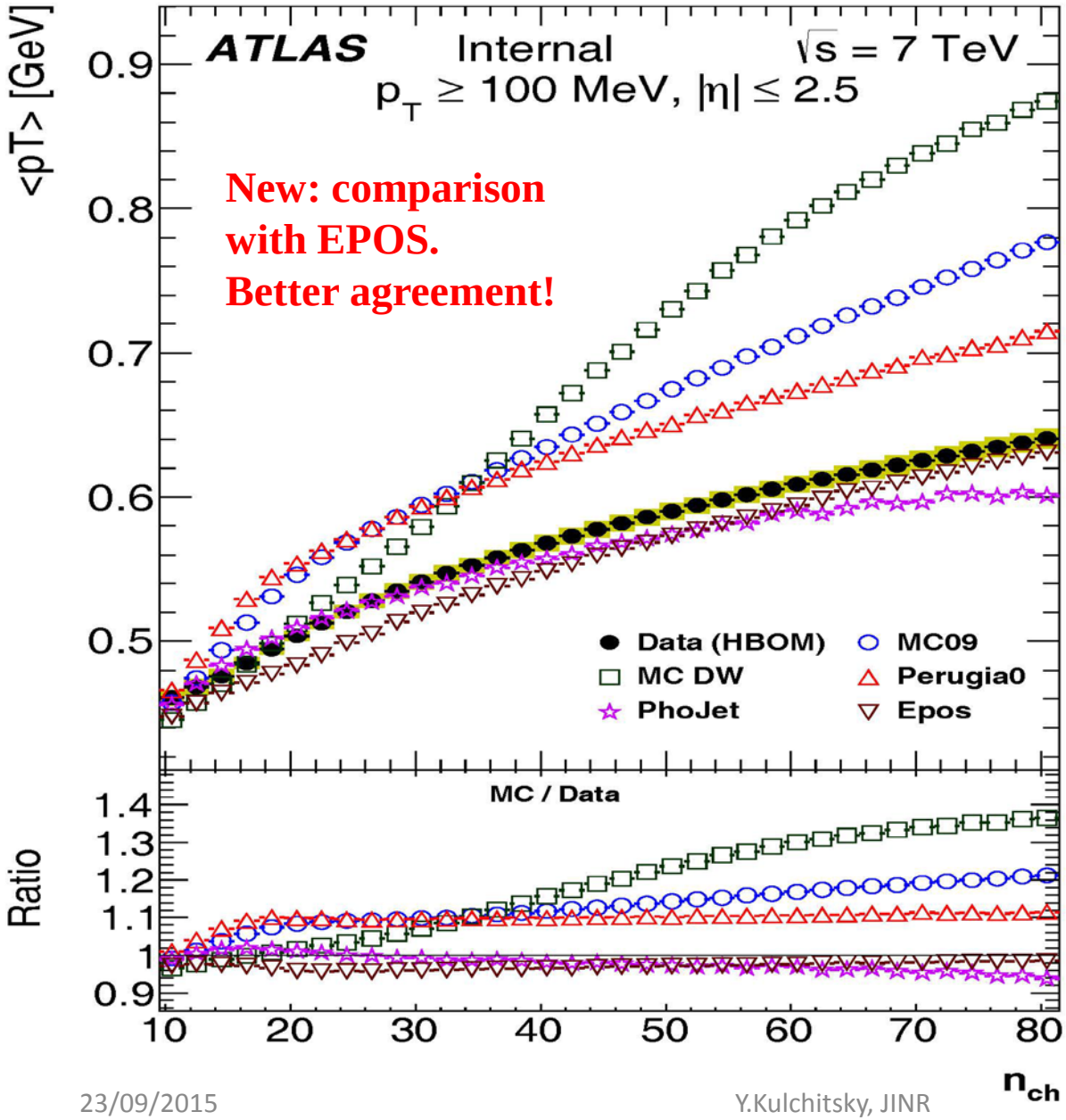

Average transverse momentum as a function of the number of charged particles in the event for events with nch>=2, pt>100 MeV and |eta|<2.5 at √s =7 TeV. In the first time we compare result with EPOS prediction. One can see the better agreement experimental result with EPOS prediction than for another MC predictions (except PhoJet).

Fraction of single and double diffraction

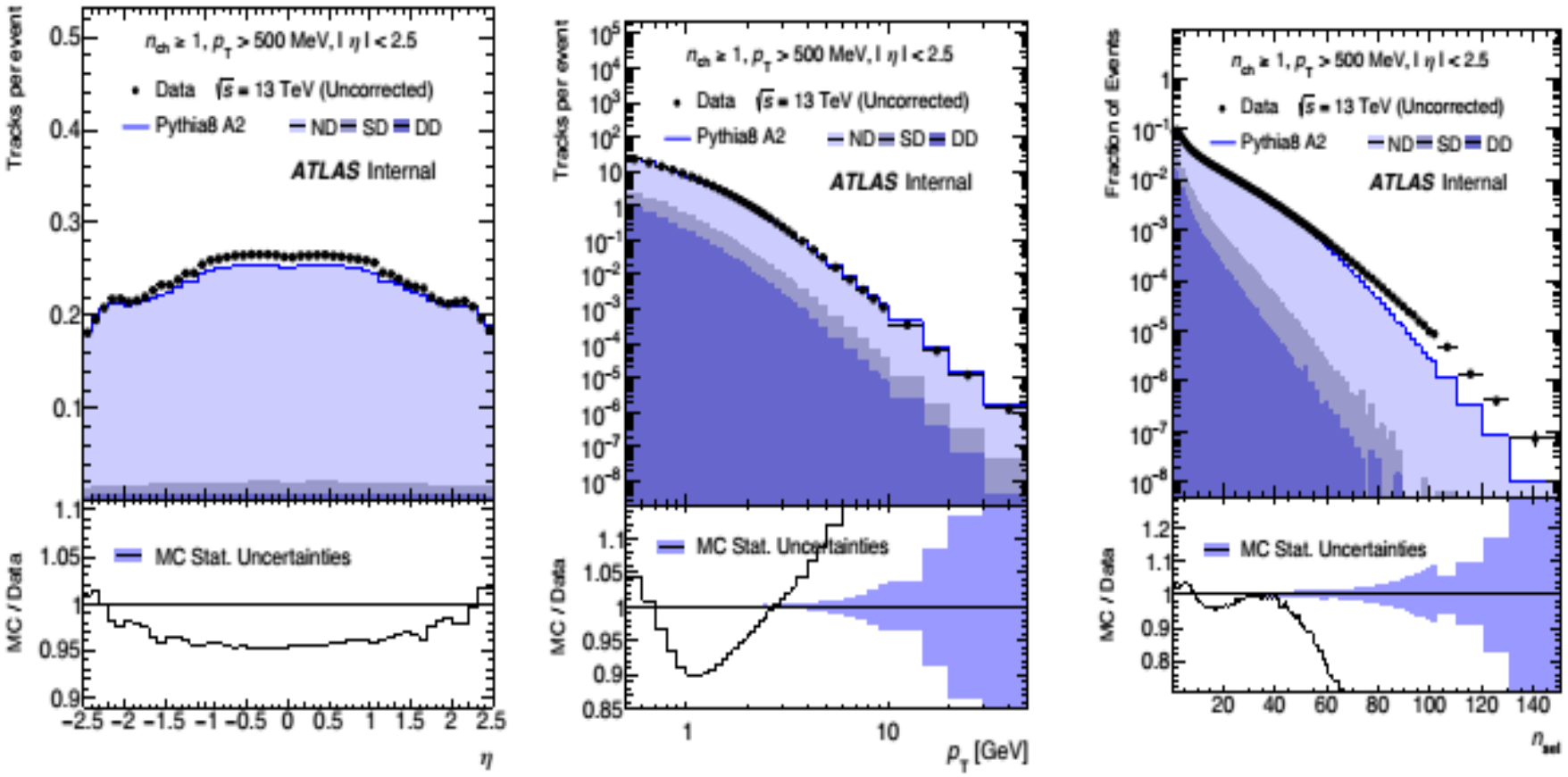

Comparison of the uncorrected data and PYTHIA8 A2 simulation for (a) the number of reconstructed tracks per event and the fraction of tracks versus (b) pseudorapidity, η and (c) transverse momentum, p_T. Each distribution is normalised on a per event basis for both data and simulation independently. The contributions to the simulation from non-diffractive (ND), single-diffractive dissociation (SD) and double-diffractive dissociation (DD) as predicted by PYTHIA8 A2 are also shown. The bottom inserts show the ratio of the MC over the data. The values of the ratio correspond to the averages of the bin content.

Minimum Bias Results

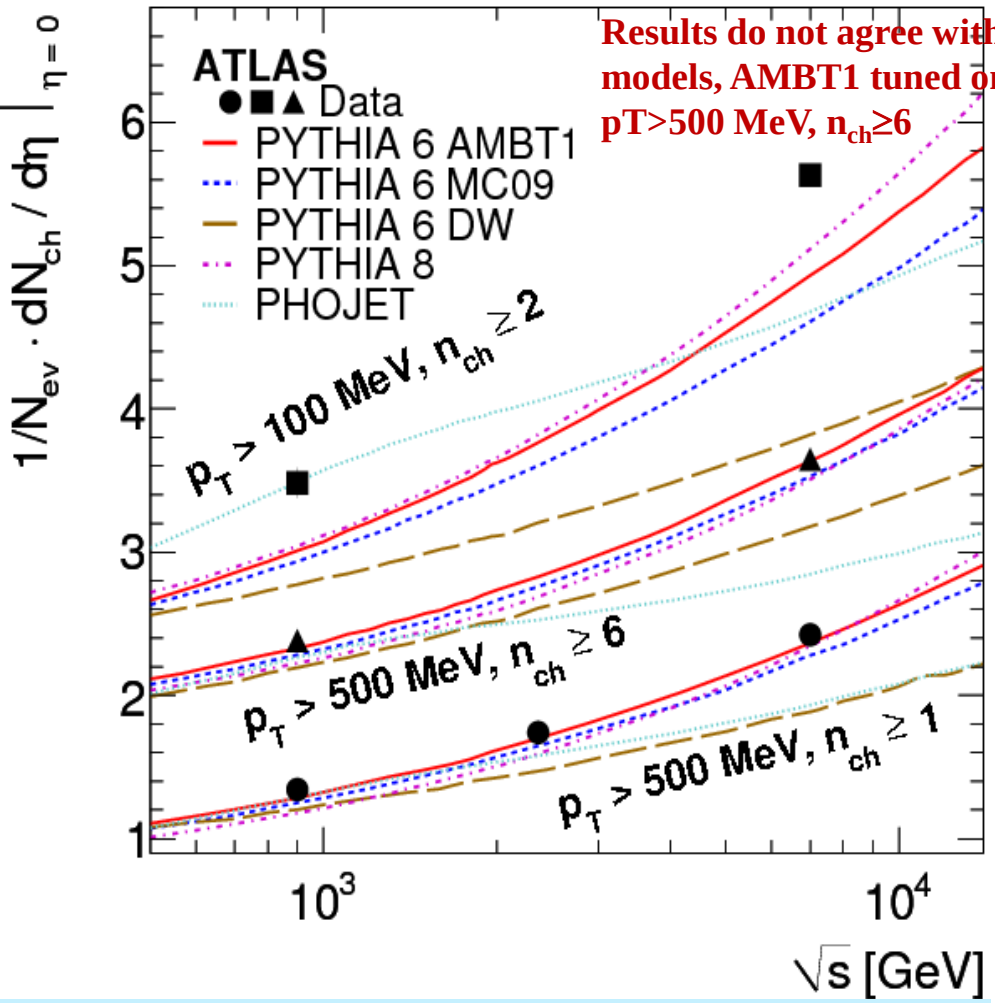

Results do not agree with models, AMBT1 tuned on pT>500 MeV, n_{ch}≥6

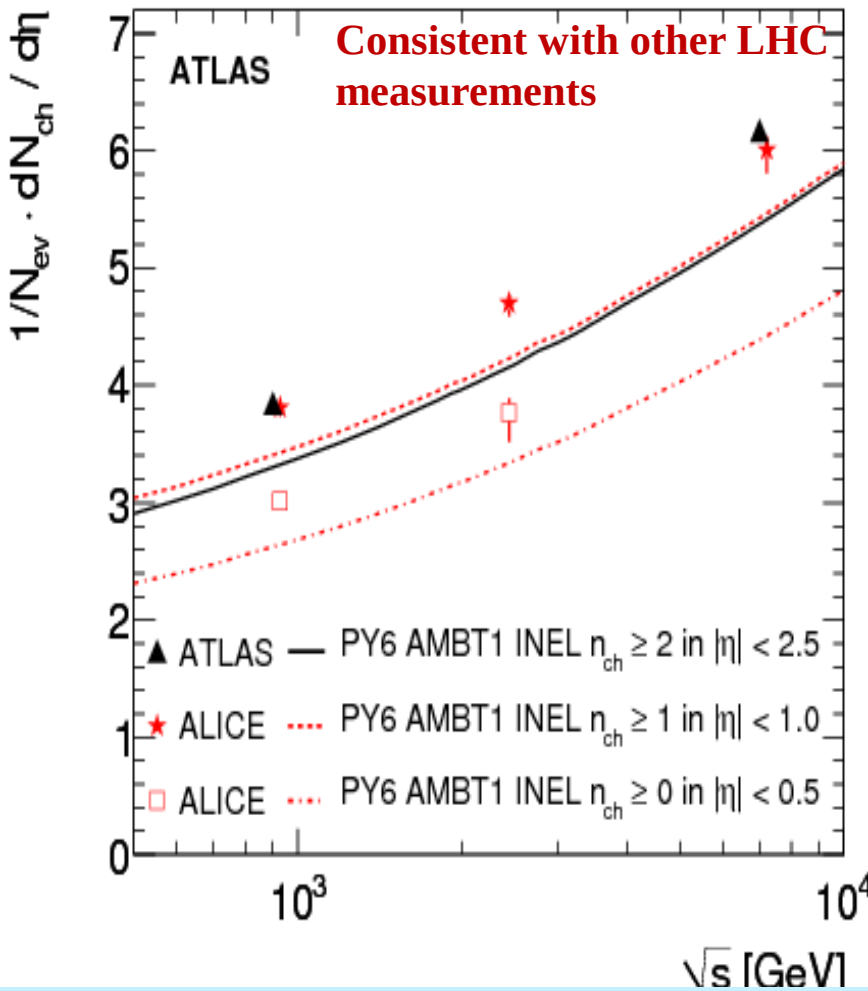

Consistent with other LHC measurements

Average charge multiplicity for η=0, for p_T>100 MeV, n_{ch}≥2; for p_T>500 MeV, n_{ch}≥1; for p_T>500 MeV, n_{ch}≥6; as function of √s. Plots are per unit of rapidity, and for |η|<2.5

Comparison of average charge multiplicity per unit of rapidity, phase spaces are indicated, (CMS uses diffraction corrected distributions), extrapolated to p_T>0